STUDIES ON HUMAN RIBONUCLEASE H1 AND ITS ACTION ON 2'-FLUOROARABINOSE OlIGONUCLEOTIDE HYBRID SUBSTRATES

A Dissertation
Submitted To
The Temple University Graduate Board

In Partial Fulfillment
Of The Requirements For The Degree Of
DOCTOR OF PHILOSOPHY
OF CHEMISTRY

BY
Nageswara Rao Alla
May 2012

Examining Committee Members:

Dr. Allen W. Nicholson, Advisory Chair, Department of Chemistry
Dr. Rodrigo B. Andrade, Department of Chemistry
Dr. Stephanie W. Wunder, Department Of Chemistry
Dr. George P. Tuszynski, External Member, School Of Medicine

ABSTRACT

Studies on human ribonuclease H1 and its action on 2'-fluoroarabinose oligonucleotide hybrid substrates

Nageswara R Alla

Doctor of Philosophy

Temple University, 2012

Advisor: Dr. Allen W. Nicholson

Ribonuclease H1 is a conserved enzyme that is localized in the nuclear and mitochondrial compartments of eukaryotic cells, and functions in DNA replication, repair, recombination and transcription. (Arunachandran *et al*., 2000; Cerritelli *et al*., 2003) Oligonucleotide binding to a complementary RNA sequence can provide a substrate for RNase H1, and provides the mechanistic basis for antisense oligonucleotide (AON)-directed gene silencing in cells (Opalinska *et al*., 2002). Effective evaluation of the therapeutic efficacy of next-generation AONs with novel structures requires an *in vitro* system involving, purified, highly active RNase H1 of human cells, and a full understanding of the catalytic mechanism of the enzyme. The goal of project 1 described in chapter 3, was to determine the involvement of a conserved Histidine (H264) in the catalytic mechanism of human RNase H1. Based on this analysis I was able to conclude that H264 has a dual role in phosphodiester hydrolysis and in product release.

The goal of project 2 (Chapter 4) was to examine the reactivities towards human RNase H1 of model hybrid substrates containing specific types of 2'-FANA substitutions (abbreviated as 'F', with 2'-deoxyribose abbreviated as 'D'), either at the "wings" of the molecule ("7-gapmer"; each wing=7 nt: FFFFFFF-DDDDDDD-FFFFFFF), or with 3 nt alternations ("3-altimer": FFF-DDD-FFF-DDD-FFF-DDD-FFF). The results of this study strongly support the continued examination of the potential therapeutic utility of the 2'-FANA modification in AONs. The highly efficient and selective inhibition of protein expression is a primary basis of action of most antisense therapeutic strategies. These data suggest that the 2'-FANA modification supports sustained silencing after a single administration, either by mRNA cleavage or by a translational block, and at substantially lower concentrations compared to the unmodified AON. The results of this project underscore the proposal that 2'-FANA-modified AONs will be important additions to the repertoire of rational antisense strategies for the effective treatment of disease.

ACKNOWLEDGEMENTS

I share the credit of my work with my supervisor, Dr . Allen W. Nicholson, who has supported me throughout my thesis with his patience and knowledge whilst allowing me the room to work in my own way. Without him this thesis, would not have been completed or written. One simply could not wish for a better knowledgeable supervisor. I sincerely thank Dr. George P. Tuszynski, Dr. Rodrigo B. Andrade, and Dr. Stephanie W. Wunder for serving on my doctoral committee, and for their constructive comments and feedback.

In my daily work I have been blessed with a cheerful group of fellow students especially Dr. Rhonda Nicholson for her advice. I would like to thank our collaborators, including the late Dr. Alan Gewirtz, and Dr. Anna Kalota for helping us with cell-based assays, and Dr. Masad J. Damha and Glenn Deleavey of McGill University for providing me with modified DNA oligonucleotides.

Above all I would like to thank my parents who raised me with a love of science and supported me in all my pursuits during the long years of my education. My Brother Vamsi for his words of advice and support when I needed the most. To my sisters Jyothsna and Padmaja and my wife Harika for their unconditional love. To my lovely nieces and naughty nephew whose beautiful smiles have helped me come out of many stressful situations.

I would like to dedicate this work to my dad who was my hero and if it wasn't for him I wouldn't be the person I am today.

TABLE OF CONTENTS

LIST OF TABLES

LIST OF FIGURES

LIST OF ABBREVIATIONS

Am	ampicillin
bp	base pair
BSA	bovine serum albumin
Cm	Chloramphenicol
dNTP	deoxynucleoside triphosphate
dsDNA	double-stranded DNA
dsRNA	double-stranded RNA
DTT	Dithiothreitol
EB	ethidium bromide
EDTA	Ethylenediaminetetraacetic acid
GST	Glutathione S-transferase
HBD	Hybrid binding domain
$(His)_6$	hexahistidine
IPTG	Isopropyl-β-D-galactopyranoside
LB	Luria-Bertani
LMP	low-melting point

MW	molecular weight
NEB	New England Bio Labs
nt	nucleotide
NTA	nitriloacetic acid
NTP	Ribonucleoside 5'-triphosphate
OD	optical density
PAGE	Polyacrylamide gel electrophoresis
PCR	Polymerase chain reaction
PNK	Polynucleotide kinase
PTGS	Post-transcriptional gene silencing
RNHD	RNase H domain
RNase H	Ribonuclease H
rRNA	Ribosomal RNA
SDS	Sodium dodecyl sulfate
ssRNA	single-stranded RNA
T7p	T7 Promoter
TAE	Tris-acetate-EDTA

TBE	Tris-borate-EDTA
Tc	tetracycline
TEMED	Tetramethylenediamine
tRNA	transfer RNA
UV	Ultraviolet

CHAPTER 1
INTRODUCTION

1.1. The Ribonucleases H and Their Classification

The Ribonucleases H (RNases H) are enzymes that specifically recognize RNA·DNA hybrid structures, and selectively cleave the RNA strand. The RNases H are universal cellular enzymes that play key roles in DNA replication, DNA repair, DNA recombination, and transcription (Stein and Hausen, 1969; Eder *et al*., 1993; Cerritelli *et al.,* 2003). Cells contain different forms of RNase H that have distinct functional roles. Ribonuclease H (RNase H; EC 3.1.26.4; H for hybrid) was first described by Hausen and coworkers in 1969 as an activity present in calf thymus tissue, and was termed a "Class 1" RNase H (Stein and Hausen, 1969). A second type of mammalian RNase H was subsequently characterized and named RNase HII (Itaya *et al.,* 1990). Biochemical studies on the gram negative bacterium *Escherichia coli* revealed a single RNase H activity (RNase HI); however, a less robust (and less abundant) RNase H was subsequently identified and named RNase HII (Itaya *et al*., 1990). The sequences of the two *E. coli* enzymes exhibit little similarity, but were later shown to share a common structural fold. Based on these and other studies, the RNases H have been classified into two major families, Type 1 and Type 2 (Ohtani *et al*., 1999), based on amino acid sequence (sequence homology) rather than similar biochemical attributes (Fig. 2). To make it easier to compare RNases H from various organisms and prokaryotic and eukaryotic organisms in particular, the names of the eukaryotic enzymes correspond to the nomenclature for *E. coli* RNase H enzymes, but use Arabic instead of Roman numerals (Ohtani *et al*., 1999; Crouch *et al*., 2000). Thus, Type 1 enzymes are designated RNase HI in prokaryotes, and RNase H1 in eukaryotes, while the Type 2 enzymes are called RNase HII and RNase H2, respectively.

The human RNases H1 and H2 are of particular interest, as RNase H1 also is an essential participant in antisense oligonucleotide gene silencing, and that mutations in RNase H2 are implicated in several important genetic diseases. Human RNase H1 (Hs-RNase H1) has 286 amino acids (molecular mass ~ 32.2 kDa) (or 260 amino acids if the mitochondrial targeting sequence (MTS) is excluded; ~ 29.4 kDa), compared to *E. coli* RNase HI (155 amino acids; ~ 17.6 kDa). Human RNase H2 has three subunits (H2A - 299 amino acids; ~ 33.4 kDa; H2B – 308 amino acids; ~ 34.8 kDa; H2C – 164 amino acids; 17.8 kDa). In contrast, *E. coli* RNase HII is active as a monomer (198 amino acids; ~ 21.5 kDa). RNase H1 and RNase H2 display distinct cleavage patterns on RNA/DNA hybrid substrates (Eder *et al*., 1993; Frank *et al*., 1994; Pileur *et al*., 2000; Haruki *et al*., 2002). While both enzymes cleave RNA/DNA hybrid duplexes, the major differences in specificity are that RNase H2 preferentially cleaves on the 5'-side of ribonucleotides at an RNA/DNA junction, and will also catalyze the cleavage of the phosphodiester adjacent to a single ribonucleotides within an otherwise perfect DNA duplex, while RNase H1 requires at least four consecutive ribonucleotides in one strand for recognition and cleavage (Fig. 1).

1.2. Biological function of RNase H

Ribonuclease H enzymes play vital functional roles in various biological processes in both eukaryotes and prokaryotes.. One function is to ensure the accurate replication or transcription of DNA. Thus, during prokaryotic and eukaryotic DNA replication, RNase H removes RNA primers involved in lagging strand DNA synthesis. RNases H1 and H2 also participate in DNA repair pathways (Eder *et al*., 1993; Kogma *et al*., 1998; Arunachandran *et al*., 2000; Cerritelli *et al*., 2003) and the processing of R-loops created during transcription (Qui *et al*., 1999; Chapados *et al*., 2001; Lin *et al*., 2010). In antisense oligonucleotide-based disease therapy, RNase H1 can be recruited to cleave disease-associated mRNAs (Dean *et al*., 2003). Deletions of RNase H1 display embryonic lethality in mice, due to failure to replicate mitochondrial DNA (Cerritelli *et al*., 2003). Mutations in human RNase H2 are implicated in a neurological disorder called

Figure 1. Substrate specificities of RNase H enzymes.

RNase H1 cleaves internal phosphodiesters within the RNA phosphodiesters in an RNA.DNA duplex, while RNase H2 preferentially cleaves the 5'-side of the ribonucleotide at an RNA•DNA junction of the chimeric strand within the hybrid substrate. Another major difference is that RNase H2 can hydrolyze a single ribonucleotide within a DNA duplex, while RNase H1 requires a minimum of four contiguous ribonucleotides for recognition and cleavage.

RNase H1

5'.**GUACCAUGCU**ATCGAGC.3'
3'.CATGGTACGATAGCTCG.5'

5'.GTACCATGC**U**CATCGAGC.3'
3'.CATGGTACGAGTAGCACG.5'

RNase H2

5'.**GUAUACUUGU**CTATATGC.3'
3'.CATATGAACAGATATACG.5'

5'.GTATACTTG**U**CTATATGC.3'
3'.CATATGAACAGATATACG.5'

Aicardi-Goutieres syndrome (Crow *et al*., 2006). Interestingly, some of these mutations do not affect the activity of the enzyme (Cohn *et al*., 2009). Deletions in RNase H1 and RNase H2 genes in the yeast *Saccharomyces cerevisiae* result in an increased sensitivity to the mutagenic effects of hydroxyurea, caffeine, and ethyl methanesulfonate (EMS) (Arunachandran *et al*., 2000). In contrast, deletion of the bacterial RNase HI gene does not affect cell growth. Many organisms contain both types of RNases H. However, some organisms contain only a single RNase H gene. Most archaeal genomes and some plants lack a gene for RNase H1, and therefore only express RNase H2 (Shultz *et al*., 2009; Todokoro *et al*., 2009). The biological significance of having single versus multiple RNase H genes is presently unclear. However, deletion of both the RNase HI and HII from bacteria is not lethal, but produces a temperature-sensitive growth phenotype. Also, the ability of RNase H2 to hydrolyze the phosphodiester adjacent to a single ribonucleotide incorporated in DNA is not observed with RNase H1, which supports the idea of differing biological functions for the two types of enzymes.

Retroviral RNases H are involved in removal of the (+)-strand RNA during the replication of the viral chromosome (Champoux *et al*., 1993). The RNase H activities of the Human Immunodeficiency virus, type 1 (HIV-1) and Moloney murine leukemia virus (M-MLV) reverse transcriptases have been heavily studied. These viral RNase H domains share strong structural homology to the bacterial RNase HI and human RNase H1 enzymes. Structural and biochemical studies on both the bacterial and M-MLV enzymes suggest a role for the positively charged C-terminal helix in substrate recognition (Kanaya *et al*., 1991; Lim *et al*., 2002). Although the corresponding helix is absent from the HIV-1 RNase H domain, positively-charged residues in the p66 connection domain may perform a similar function (Lima *et al*., 2006). Another important and unique feature defined for the viral RNase H domains is the primer grip region near the active site that contacts the DNA strand of the RNA·DNA hybrid substrate (Lim *et al*., 2006). Structural similarities between the bacterial and viral RNase H domains also indicate a two metal-ion mediated mechanism of catalysis for both types of enzyme (Shultz and Champoux 2008; Champoux and Schultz 2009). As with the bacterial enzyme, the RNase H domains of the reverse transcriptase of HIV-1 and M-MLV contain four highly conserved residues (DEDD) within the active site that coordinate the binding of the two catalytic Mg^{2+} ions. Although RNase H proteins are generally recognized as sequence-independent endonucleases, the retroviral RNases H exhibit a degree of sequence specificity (Champoux and Schultz 2009). In addition to the typical endoribonucleolytic activity on RNA·DNA hybrids, retroviral RNases H have two end-directed modes of cleavage that are unique. Several HIV strains contain acquired mutations in or near the RNase H domain that confer drug resistance (Deliviks-Frankberry *et al*., 2010). Consequently, anti-HIV drugs targeted to the RNase H domain of reverse transcriptase are being continuously pursued (Yu *et al*., 2008; Tramontano and Di Santo 2010).

1.3. Structure of Type 1 RNases H

1.3.1. Primary structure.

The structural organization of Type 1 RNases H from several representative organisms is shown in Fig. 1. All eukaryotic RNases HI, and orthologs from some prokaryotes, exhibit a highly-conserved N-terminal Hybrid-Binding Domain (HBD) and a C-terminal RNase H domain (RNHD), linked by a connection domain (CD) of variable length. This arrangement is seen in human and mouse proteins, but RNase H1 of *Saccharomyces cerevisiae* exhibits two tandem HBDs. The RNase H domain of prokaryotic RNases HI possesses a basic protrusion believed to be important in RNA/DNA recognition. The presence of basic protrusion may compensate for the lack of a HBD. RNase HI from the psychrophilic bacterium, *Shewanella* sp. SIB1, was the first bacterial RNase HI shown to contain an N-terminal HBD (Todokoro *et al*., 2007). The HBD also is present in other bacterial Type 1 RNases H, including *Thermotoga maritima* RNase HI (Tm-RNase HI) and *Bacillus halodurans* RNase HI (Bh-RNase HI) (Nowotny *et al*., 2005; Jongruja *et al*., 2010). The C-terminal RNase H domain of human RNase H1 has a strong structural similarity to *E. coli* RNase HI, although there is only 36% identity in amino acid sequence. Any additional functions of the Connecting Domain (CD) remain enigmatic. In *B. halodurans*, *T. maritime,* and *Shewanella SIB1* RNases HI, the CD is 16, 15 and 45 amino acids in length, respectively. In the human and mouse enzymes it is about 64 amino acids in length, and in the *Drosophila melanogaster* enzyme it is 150 amino acids. Thus, the smaller bacterial proteins have very short CDs, and also carry basic protrusions in the RNase H domain.

1.3.1.1 The Hybrid binding domain (HBD)

Initial studies of the N-terminal domain of the Type 1 RNases H demonstrated its ability to bind either RNA·RNA or RNA·DNA duplexes. The domain therefore was called the double-stranded RNA binding domain (dsRBD), or double-stranded RNA/hybrid binding domain (dsRHbd) (Cerritelli *et al*., 2003; Gaidamakov *et al*., 2005). It was subsequently renamed the Hybrid Binding Domain (HBD) as result of studies that showed a clear preference for RNA·DNA hybrids (Nowotny *et al*., 2008). The HBD of Human (Hs) RNase H1 (~50 amino acids) occupies the amino terminal one-fifth of the protein, and has a β1-β2-α1-β3-α2 secondary structure (Fig. 3A), which is a conserved structural feature. The Hs-RNase H1 HBD has 37% β-strand content and 39% α-helix content, and the three-stranded β-sheet is flanked by two α helices. The domain exhibits monomeric behavior in solution, and the fold is qualitatively different from known dsRNA- and dsDNA-binding modules. Although the catalytic activity resides in the C-terminal domain, the HBD significantly enhances enzyme affinity for

RNA·DNA hybrids, and confers processivity on mouse and human RNases H1. The HBD residues Tyr29, Trp43 and Phe58 are highly conserved, and interact with the DNA strand of hybrids (Nowotny *et al*., 2008). The conservation of these residues suggest that the HBDs of other Type 1 RNases H bind substrate in a manner similar to Hs-RNase H1. Deletion of the HBD in human and mouse RNases H1 yields a protein highly defective in catalytic activity (Nowotny *et al*., 2005; Jongruja *et al*., 2010). The HBD is essential for Hs-RNase H1 as it is the primary determinant of binding energy, RNA·DNA duplex recognition and processivity (Nowotny *et al* 2008). The HBD interacts with the minor groove of the RNA•DNA duplex.

1.3.1.2 The RNase H domain (RNHD)

The Hs-RNase H1 RNHD is composed of five β-strands and five α-helices (~150 amino acids; 21% β-strand, and 38% α-helix), and occupies the C-terminal three-fifths of the RNase H1 polypeptide (Fig. 3A). The Bh-RNase HI RNHD contains four α-helices (Nowotny *et a.,l* 2007). The central element of the Hs-RNase H1 RNHD is a mixed β-sheet, comprised of five β-strands. Four α-helices are on one side of the β-sheet, with the fifth α-helix on the opposite side (Fig. 4B). The overall folds of the RNHD of Ec-RNase HI and Bh-RNase H1 are similar. The central β-sheet, and α-helices A, B and D are present in all RNHDs, but differ from the Bh-RNHD, which possesses a basic protrusion consisting of helix C, followed by a loop (Nowotny *et al.,* 2007). The RNHD recognizes the RNA strand of RNA•DNA hybrids through extensive contacts with 2'-OH groups. The DNA strand is recognized by its ability to adopt a B-form conformation, and an ability to form a kink at a specific phosphodiester linkage. Based on sequence homology, residues D145, E186, D210 and D274 are predicted to be components of the active site (Fig. 3B) (Wu *et al*., 2001).

1.3.1.3 Connection Domain (CD)

The connection domain links the HBD and RNHD, and varies in length among different species. The CD is proposed to be important for providing flexibility, allowing the N- and C-terminal regions to move freely in and around the substrates. Dramatic differences in length and composition of the connection domain suggest that this region might interact with additional proteins in the cell (Cerritelli *et al*., 2009). For Hs-RNase H1 the CD is ~64 amino acids, and if fully extended in flexible form, it would permit the HBD and RNHD to be separated by >20 nm. If the conformation of the CD is stretched to the maximum, the RNHD could be separated from the HBD on a hybrid substrate by up to ~60 nt (Cerritelli *et al*., 2009).

1.3.1.4 The mitochondrial targeting sequence (MTS)

There are two in-frame methionine codons at the 5'-end of the RNase H1 mRNA of higher eukaryotes. Translation from the first methionine codon produces a protein with the MTS, allowing localization to the mitochondria. Proteins targeted to the mitochondria lose the MTS upon import. Not all eukaryotic RNases H have an MTS upstream of the HBD. *S. cerevisiae* and *C. elegans* RNases H1 have no MTS. *C. elegans* has an additional Type 1 RNase H (Ce-RNase H1.1), in addition to the enzyme with the HBD-CD-RNHD structural composition (Arunachandran *et al*., 2002). The Ce-RNase H1.1 mRNA has two potential start codons, with the first codon directing synthesis of a protein with a MTS (Kochiwa *et al*., 2006).

1.3.2 Crystal structure of RNase H

From a biochemical, structural, and genetic standpoint the prokaryotic RNases H (Fig. 3) are the best characterized members of the RNase H family. Crystal structures of Ec-RNase HI

Figure 2. Primary structures of Type 1 RNases H isolated from different species, and the percent identity of amino acid sequence of the RNase H domains compared to that of Ec-RNase HI (adapted from Ohtani *et al.,* 1999). The figure shows the typical organization of RNases H in prokaryotes and eukaryotes. Shown are the numbering of the residues, and positions of the catalytic domain (black shading), hybrid binding domain (HBD) (gray shading) and variable connection domain (CD) (solid line). Additional domains include the mitochondrial targeting sequence (MTS) in mammals (no shading) and the tandem HBD in *S. cerevisiae* RNase H1 (white box). The percent identity of RNase H domain with respect to the *E. coli* RNase HI is indicated on the right.

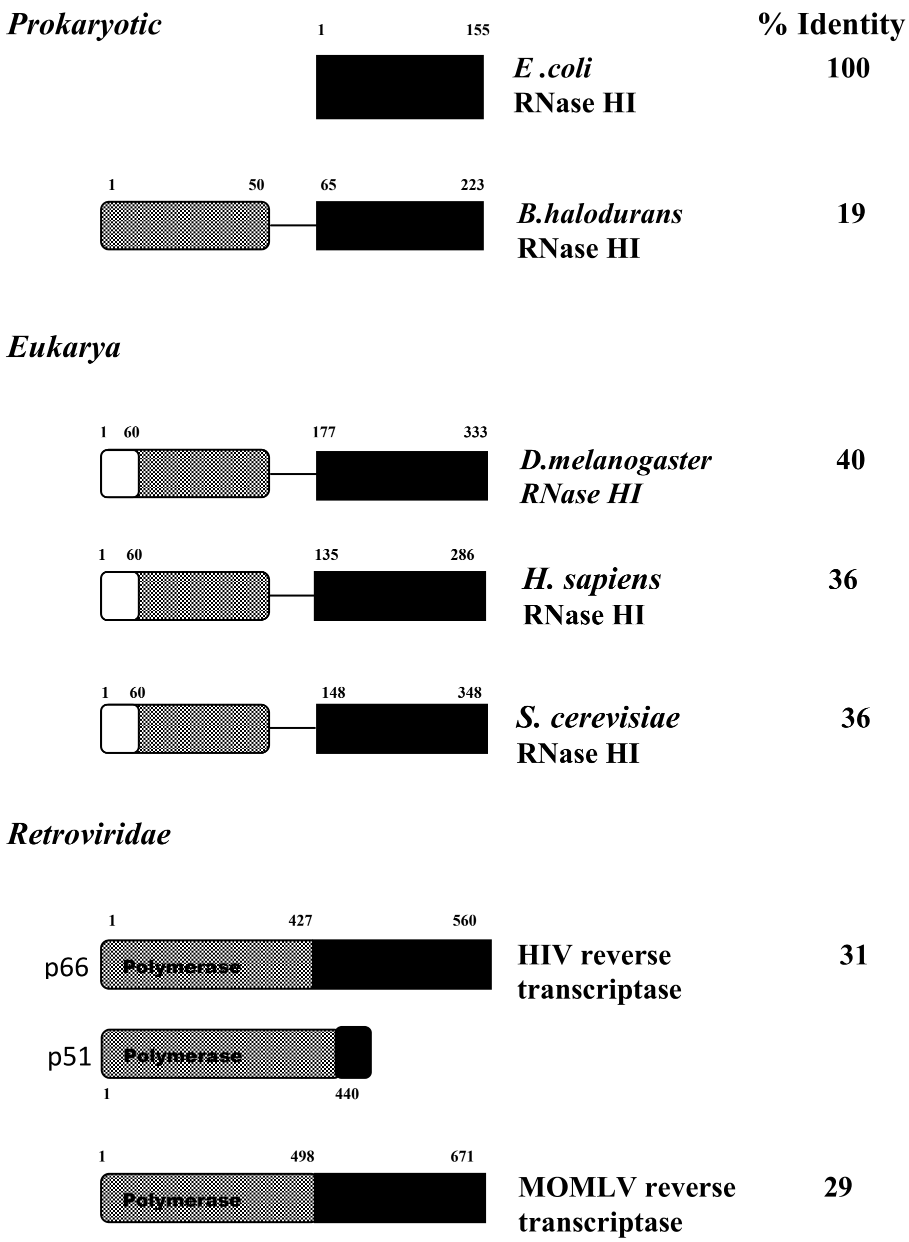
Prokaryotic
% Identity
1
155
E .coli
RNase HI
100
1
50
65
223
B.halodurans
RNase HI
19
Eukarya
1
60
177
333
D.melanogaster
RNase HI
40
1
60
135
286
H. sapiens
RNase HI
36
1
60
148
348
S. cerevisiae
RNase HI
36
Retroviridae
1
427
560
p66
Polymerase
HIV reverse
transcriptase
31
p51
Polymerase
1
440
1
498
671
Polymerase
MOMLV reverse
transcriptase
29

were the first to be determined, and revealed a novel fold consisting of a five-stranded β sheet, flanked on both sides by α helices (Kanayagi *et al*., 1990; Kochiwa *et al*., 2006). The active site contains four highly conserved carboxylic acid residues: D10, E48, D70, and D134. RNase H1 enzymes require a minimum of four ribonucleotides within an RNA·DNA hybrid for recognition (Ohtani *et al*., 1999) suggesting that the enzyme recognizes a unique feature of the hybrid established by four contiguous ribonucleotides on one strand. The first crystal structures of an RNA•DNA substrate-enzyme complex were determined for the catalytic domain of Bh-RNase H (Fig. 4).

The structures revealed that the protein specifically binds a hybrid with the RNA strand in the A form and DNA strand in the B form helix (Nowotny *et al*., 2005). Because of the helical differences, the minor groove width of the RNA•DNA hybrid is narrowed to about 8.4 Å, which is larger than the A form RNA (4 Å), but significantly less than B form DNA (11.5 Å) helix. Altering the conformation and flexibility of RNA·DNA hybrid reduces the cleavage activity of RNase H (Lima *et al*., 2004; Lima *et al*., 2007), suggesting that the enzyme contacts both the RNA and DNA strand. The active site face of the RNase H1 exhibits two grooves, separated by a ridge by about 8.5 Å, into which fits the backbone of the RNA•DNA heteroduplex (Fig. 6). The RNA strand is recognized through extensive contacts of 2'-OH groups by the protein. The DNA strand is recognized by its ability to adopt a B-form conformation. Attempts to crystallize full-length human RNase H1 were not successful, but Nowotny coworkers succeeded in crystallizing the catalytic domain (HC) of Hs-RNase H1 bound to an RNA•DNA hybrid (Nowotny *et al*., 2007). The central element of RNase HC is a mixed β sheet composed of five strands. On one side of the β sheet there are 4 α-helices, and the fifth and last helix is on the opposite face. (Nowotny *et al*., 2007) (Fig. 6). D145, E186, D120 and D274 are in the active site of the enzyme. The overall folds of RNases H of *E. coli, B. halodurans*, human, and the HIV/MO-MLV reverse transcriptases are similar, and the superimposed human and *E. coli* proteins exhibit remarkably similar folds (Nowotny *et al*., 2007). In addition to the two surface grooves for RNA•DNA hybrid binding, the human protein exhibits a basic protrusion that also is present in *E. coli* RNase HI and MO-MLV RNase H. The basic protrusion contributes to the formation of a DNA-binding channel (Fig. 4) by providing additional van der Waals and hydrogen bonding interactions with the DNA strand, and as such contributes to substrate specificity. The majority of the enzyme-hybrid substrate interactions occur along the minor groove of the hybrid. The RNA is in the regular A form conformation, with a C3'-endo sugar pucker. The active site interacts with the 2'-OH groups of four consecutive ribonucleotides, two on each side of the scissile phosphodiester. The Hs-RNase RNHD interacts with seven nucleotides of the DNA strand, with the most prominent contacts made between a phosphate group that is two base pairs from the scissile bond and a phosphate-binding "pocket", formed by R179, T181 and N240 (Fig. 6). A similar phosphate-binding pocket is present in the Bh-RNase H structure (Nowotny *et al*., 2005) Placement of the phosphate in the pocket requires a significant distortion of the DNA backbone torsional angles. Since only a DNA strand can assume such a conformation, this structural distortion prevents binding of an RNA•RNA duplex structure to the RNHD. Chemical modifications of the DNA strand that induce an A-form sugar pucker prevent the cleavage of the opposing RNA phosphodiester, as well as two ribonucleotides downstream, which confirms the importance of basic protrusion in substrate recognition, and specificity for the B-form of the DNA strand (Nowotny *et al*., 2007). The second DNA-binding site in RNHD is a channel formed by W221, W225 and S233 in the basic protrusion (Fig 6D). The DNA snugly fits in this channel, making van der Waals contacts and hydrogen bonds. The 2'-OH groups of the RNA would

Figure 3. Human RNase H1 secondary structure.

A. Domain structure as of human RNase H1. The human RNase H1 polypeptide contains 286 amino acids. The HBD is located is located at the N-terminus, and the RNase H domain (RNHD) occupies the C-terminal portion of the polypeptide. The two domains are joined by a connection domain (CD). The mitochondrial targeting sequence (MTS) is indicated, but its sequence is not included in panel B. The HBD has three β-strands (1, 2 and 3; gray lines) and two α-helices (A and B; curled lines). The RNHD has a β-β-β-α-β-α-α-α-β-α structural arrangement.

B. Sequence alignment of HBDs of RNases H1 of human (Hs), mouse (Mm), chicken (Gg), fruitfly (Dm), yeast (Sc) and *B. halodurans* (Bh). Conserved residues are highlighted in blue for DNA phosphate interaction, green for deoxyribose interaction, yellow for the hydrophobic core, and purple for arginines that stabilize the helices and the RNA-binding loop. The RNA-binding loop is shown in boldface (adapted from Nowotny *et al.*, 2008).

C. Sequence alignment of catalytic domains (RNHD) of RNases H. Conserved residues in the active site are highlighted in yellow; those interacting with the RNA strand are in red, and those interacting with the DNA in cyan. Conserved hydrophobic core residues are highlighted in gray. The basic protrusion region is colored in pink, and its sequence is boxed. Hs, human; Mm, mouse; Gg, chicken; Dm, *D. melanogaster*; Sc, *S. cerevisiae*; Ec, *E. coli*; HIV, human immunodeficiency virus RT; Bh, *B. halodurans*. H264 and E188 of human and Bh RNHD respectively are indicated in blue bold letters (adapted from Nowotny *et al.,* 2007).

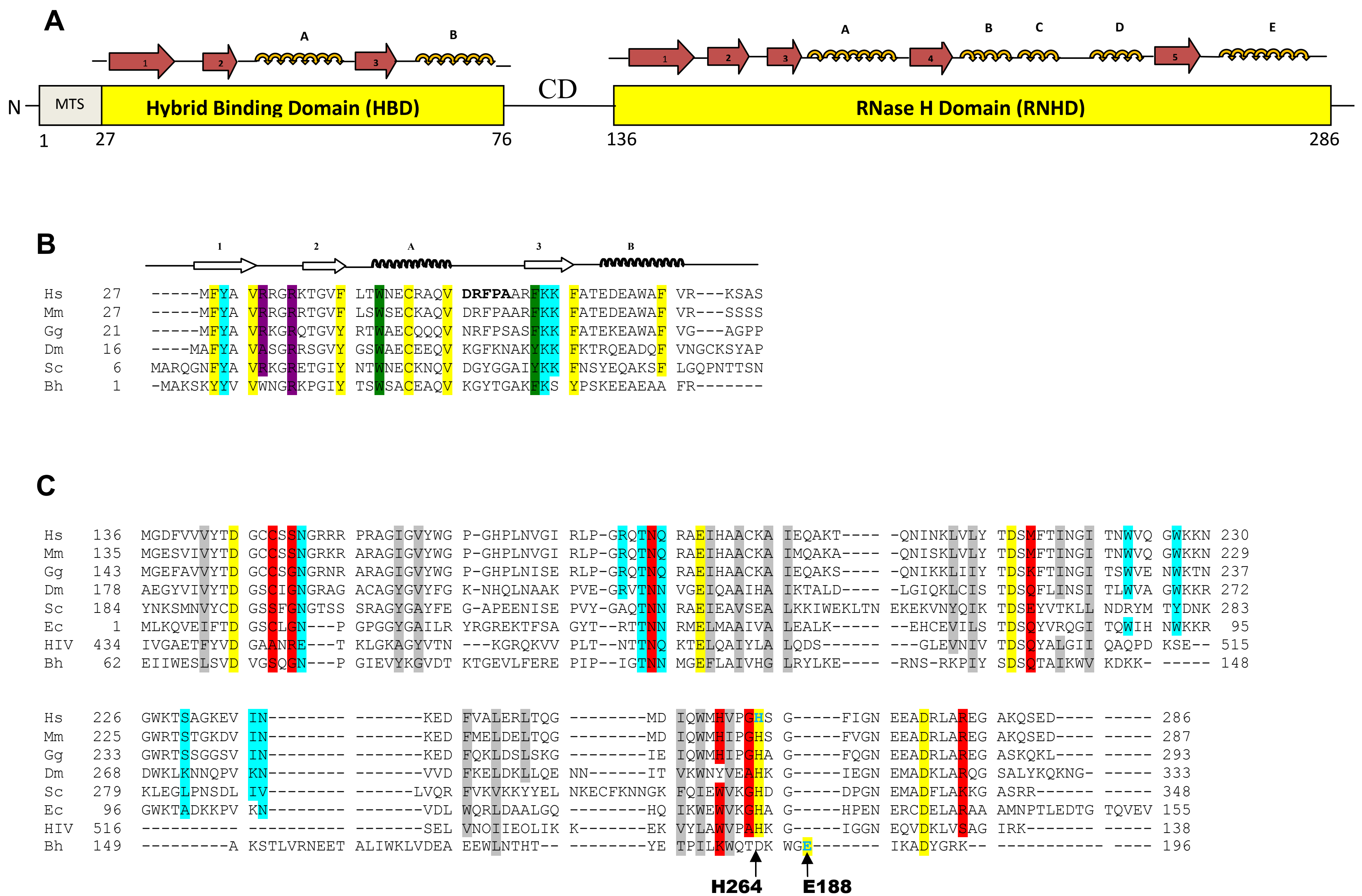
A
N
MTS
Hybrid Binding Domain (HBD)
CD
RNase H Domain (RNHD)
C
1
27
76
136
286
B
Hs 27 -----MFYA VRRGRKTGVF LTWNECRAQV DRFPAARFKK FATEDEAWAF VR---KSAS
Mm 27 -----MFYA VRRGRRTGVF LSWSECKAQV DRFPAARFKK FATEDEAWAF VR---SSSS
Gg 21 -----MFYA VRKGRQTGVY RTWAECQQQV NRFPSASFKK FATEKEAWAF VG---AGPP
Dm 16 ----MAFYA VASGRRSGVY GSWAECEEQV KGFKNAKYKK FKTRQEADQF VNGCKSYAP
Sc 6 MARQGNFYA VRKGRETGIY NTWNECKNQV DGYGGAIYKK FNSYEQAKSF LGQPNTTSN
Bh 1 -MAKSKYYV VWNGRKPGIY TSWSACEAQV KGYTGAKFKS YPSKEEAEAA FR-------
C
Hs 136 MGDFVVVYTD GCCSSNGRRR PRAGIGVYWG P-GHPLNVGI RLP-GRQTNQ RAEIHAACKA IEQAKT---- -QNINKLVLY TDSMFTINGI TNWVQ GWKKN 230
Mm 135 MGESVIVYTD GCCSSNGRKR ARAGIGVYWG P-GHPLNVGI RLP-GRQTNQ RAEIHAACKA IMQAKA---- -QNISKLVLY TDSMFTINGI TNWVQ GWKKN 229
Gg 143 MGEFAVVYTD GCCSGNGRNR ARAGIGVYWG P-GHPLNISE RLP-GRQTNQ RAEIHAACKA IEQAKS---- -QNIKKLIIY TDSKFTINGI TSWVE NWKTN 237
Dm 178 AEGYVIVYTD GSCIGNGRAG ACAGYGVYFG K-NHQLNAAK PVE-GRVTNN VGEIQAAIHA IKTALD---- -LGIQKLCIS TDSQFLINSI TLWVA GWKKR 272
Sc 184 YNKSMNVYCD GSSFGNGTSS SRAGYGAYFE G-APEENISE PVY-GAQTNN RAEIEAVSEA LKKIWEKLTN EKEKVNYQIK TDSEYVTKLL NDRYM TYDNK 283
Ec 1 MLKQVEIFTD GSCLGN---P GPGGYGAILR YRGREKTFSA GYT--RTTNN RMELMAAIVA LEALK----- --EHCEVILS TDSQYVRQGI TQWIH NWKKR 95
HIV 434 IVGAETFYVD GAANRE---T KLGKAGYVTN ---KGRQKVV PLT--NTTNQ KTELQAIYLA LQDS------ ---GLEVNIV TDSQYALGII QAQPD KSE-- 515
Bh 62 EIIWESLSVD VGSQGN---P GIEVYKGVDT KTGEVLFERE PIP--IGTNN MGEFLAIVHG LRYLKE---- -RNS-RKPIY SDSQTAIKWV KDKK- ----- 148
Hs 226 GWKTSAGKEV IN-------- -------KED FVALERLTQG --------MD IQWMHVPGHS G-----FIGN EEADRLAREG AKQSED---- ----- 286
Mm 225 GWRTSTGKDV IN-------- -------KED FMELDELTQG --------MD IQWMHIPGHS G-----FVGN EEADRLAREG AKQSED---- ----- 287
Gg 233 GWRTSSGGSV IN-------- -------KED FQKLDSLSKG --------IE IQWMHIPGHA G-----FQGN EEADRLAREG ASKQKL---- ----- 293
Dm 268 DWKLKNNQPV KN-------- -------VVD FKELDKLLQE NN------IT VKWNYVEAHK G-----IEGN EMADKLARQG SALYKQKNG- ----- 333
Sc 279 KLEGLPNSDL IV-------- ------LVQR FVKVKKYYEL NKECFKNNGK FQIEWVKGHD G-----DPGN EMADFLAKKG ASRR------ ----- 348
Ec 96 GWKTADKKPV KN-------- -------VDL WQRLDAALGQ --------HQ IKWEWVKGHA G-----HPEN ERCDELARAA AMNPTLEDTG TQVEV 155
HIV 516 ---------- ---------- -------SEL VNOIIEOLIK K-------EK VYLAWVPAHK G-----IGGN EQVDKLVSAG IRK------- ----- 138
Bh 149 ---------A KSTLVRNEET ALIWKLVDEA EEWLNTHT-- --------YE TPILKWQTDK WGE------- IKADYGRK-- ---------- ---- 196
H264
E188

sterically clash with the W221 side chain, thereby preventing RNA binding. As a result of the distortion of the DNA strand in the phosphate binding pocket, the minor groove width decreases to 7 Å compared to 11.7 Å at the DNA binding channel. These variations are not seen in Bh-RNase H which lacks the basic protrusion. Thus, Hs-RNase RNHD most likely recognizes the DNA strand by the absence of 2'-OH and the flexibility of the B form helix (Nowotny *et al*., 2007).

The HBD has approximately a 25-fold greater affinity for RNA·DNA hybrids compared to dsRNA (Nowotny *et al*., 2008). Deletion of the HBD in the human and mouse RNases H1 severely reduces catalytic activity and processivity *in vitro* (Gaidakamov *et al*., 2005; Nowotny *et al*., 2008). The domain functions as a monomer, and consists of three α-helices and two β-sheets (β1β2αAβ3αB) (Fig. 5A). The Hs-RNase H1 HBD interacts primarily with the backbone of an RNA·DNA hybrid along the minor groove. The HBD recognizes the hybrid mainly through αA and β3 (Fig. 5C), and also interacts with two consecutive 2'-OH groups of the RNA strand, using the loop connecting αA and β3. This loop is also termed the RNA-binding loop, and consists of D51-A56 (Nowotny *et al.,* 2008). The RNA-binding loop is stabilized by the conserved residue Arg35 that forms a hydrogen bond with the carbonyl oxygen of Asp51. Arg52 and Arg55 form hydrogen bonds with ribose 2'-OH groups (Fig. 5D). The phosphodiester groups of the RNA strand are not involved in direct contacts with protein side chains (Nowotny *et al*., 2008). The DNA-binding surface of the HBD is composed of a shallow, positively-charged groove that interacts with three consecutive phosphodeoxyribose units of the DNA strand, and with aromatic side chain stacking on deoxyribose residues (Fig. 5C,D,E). The side chain hydroxyl group of Tyr29 (in β1), the side chain amine and backbone amide of Lys60 (in β3) and the guanidinium group of Arg57 interact

Figure 4. Crystal structures of *B. halodurans*, *E. coli,* and H. sapiens (Hs) RNase H.

A. Crystal structure of *E. coli* RNase HI, using a ribbon representation of the secondary structure. The β-strands are labeled with Arabic numbers, and the helices are labeled alphabetically.

B. Crystal structure of Hs-RNase H1 RNHD, using a ribbon representation of the secondary structure.

C. Ribbon representation of the crystal structure of the RNHD of *Bacillus halodurans*.

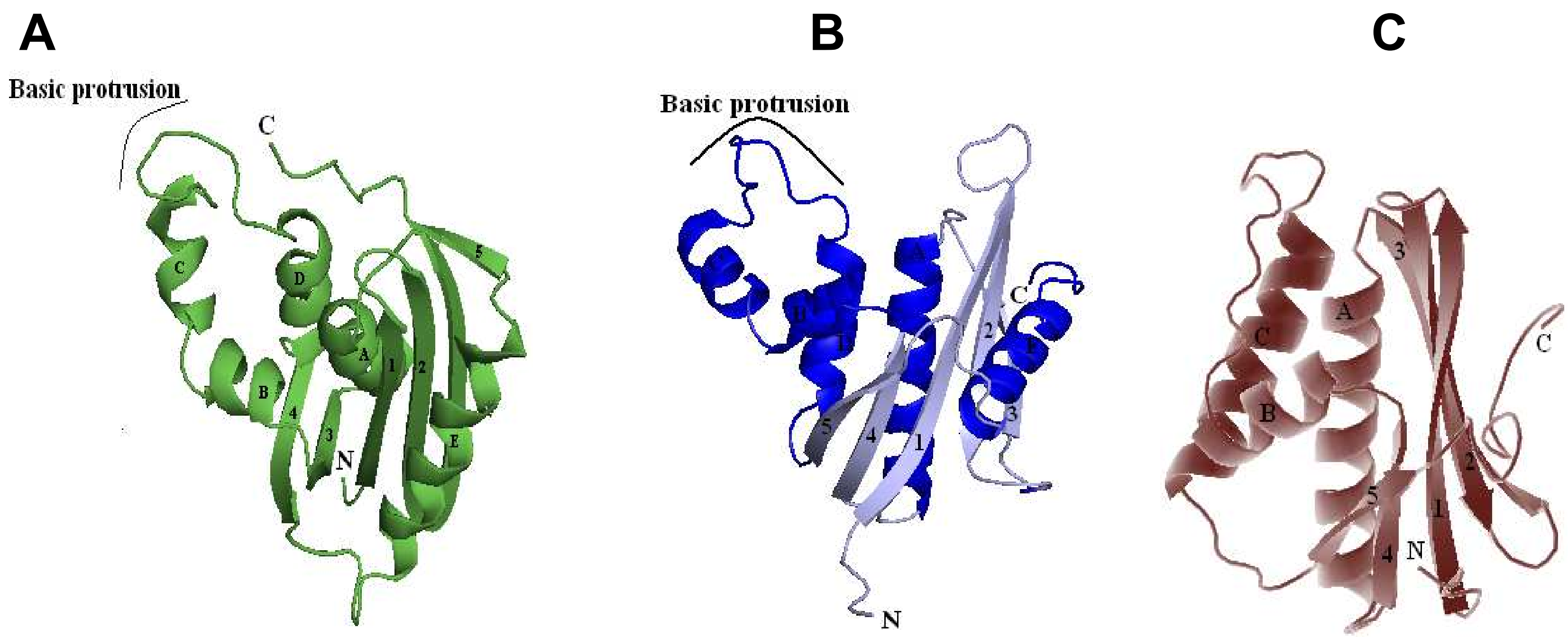

E. coli *H. sapiens* *B. halodurans*

with three consecutive DNA phosphodiesters (Nowotny et al., 2008). The aromatic rings of Trp43 (in αA) and Phe58 (in β3) together form a hydrophobic patch and stack on two adjacent deoxyribose sugars. An attempt modeling to substitute deoxyribose for ribose at the aromatic patch indicates that the 2'-OH groups would sterically clash with Trp43 and Phe58 (Fig. 5E) (Nowotny *et al*., 2008). A similar type of mechanism for recognition of A-form DNA was also observed in basic protrusion of Hs-RNHC (Nowotny *et al*., 2008).

1.3.2.1 **Two metal ion catalytic mechanism of RNases H.**

The conserved structures of RNases H indicate a common catalytic mechanism (Todokoro *et al*., 2007; Nowotny *et al*., 2007). RNase H enzymes utilize a two metal-ion catalytic mechanism for phosphodiester hydrolysis (Todokoro *et al*., 2007; Nowotny *et al*., 2007). This mechanism also involves four conserved acidic residues in the active site (Fig. 7A, B) (Todokoro *et al*., 2007; Nowotny *et al*., 2007). The two Mg^{2+} ions are jointly coordinated to a nonbonding oxygen of the scissile phosphodiester of the substrate RNA strand, and also are coordinated with the four conserved carboxylates (Asp71, Glu109, Asp132 and Asp192 in Bh-RNase H, and Asp145, Glu186, Asp210 and Asp274 in Hs-RNase H), as well as several water molecules (Fig. 7A). The positions of the two divalent metal ions are designated A and B (Fig. 7A, B). A stereochemical analyis of phosphodiester hydrolysis has established an S_N2-like nucleophilic attack on the scissile phosphorus atom by the water nucleophile. The nucleophillic attack is accompanied by inversion of configuration at phosphorus, followed by formation of the 5'-phosphate and 3'-hydroxy ends of the cleaved RNA products. The catalytic mechanism includes deprotonation of a metal bound water molecule to form a hydroxide nucleophile that carries out in-line attack on the scissile phosphodiester (Fig. 7C). In the two-metal-ion mechanism, metal ion A is proposed

Figure 5. Structure of the HBD of Hs-RNase H1 and its interaction with RNA·DNA hybrid.

A. The Structure of the HBD of Hs-RNase H1. Shown in stick form are the side chains forming the hydrophobic core (mainly aromatic), and two the Arginine side chains (R32 and R35) that cap the C-termini of helices B and A, respectively.

B. Electrostatic surface potential of Hs-HBD, calculated using GRASP (Nicholls *et al*. 1991). The positively-charged residues (blue) in a cluster are labeled.

C. HBD residues interacting with the DNA strand, and the Arg35 side chain that stabilizes the RNA-binding loop are shown in ball-and-sticks. Base-pairs interacting with the HBD are numbered 1–5.

D. Close-up view of the RNA-binding loop. The 2'-OH groups interacting with the loop are shown as red spheres. The dashed lines indicate hydrogen bonds.

E. W43 and F58, shown in green ball-and-stick form under the molecular surface, contact deoxyribose residues of the DNA (blue). These side chains would sterically clash with the 2'-OH groups (red) of a modeled RNA (light pink). Ribonucleotides (R1 and R2) and deoxyribonucleotides (D3-D5) are numbered.

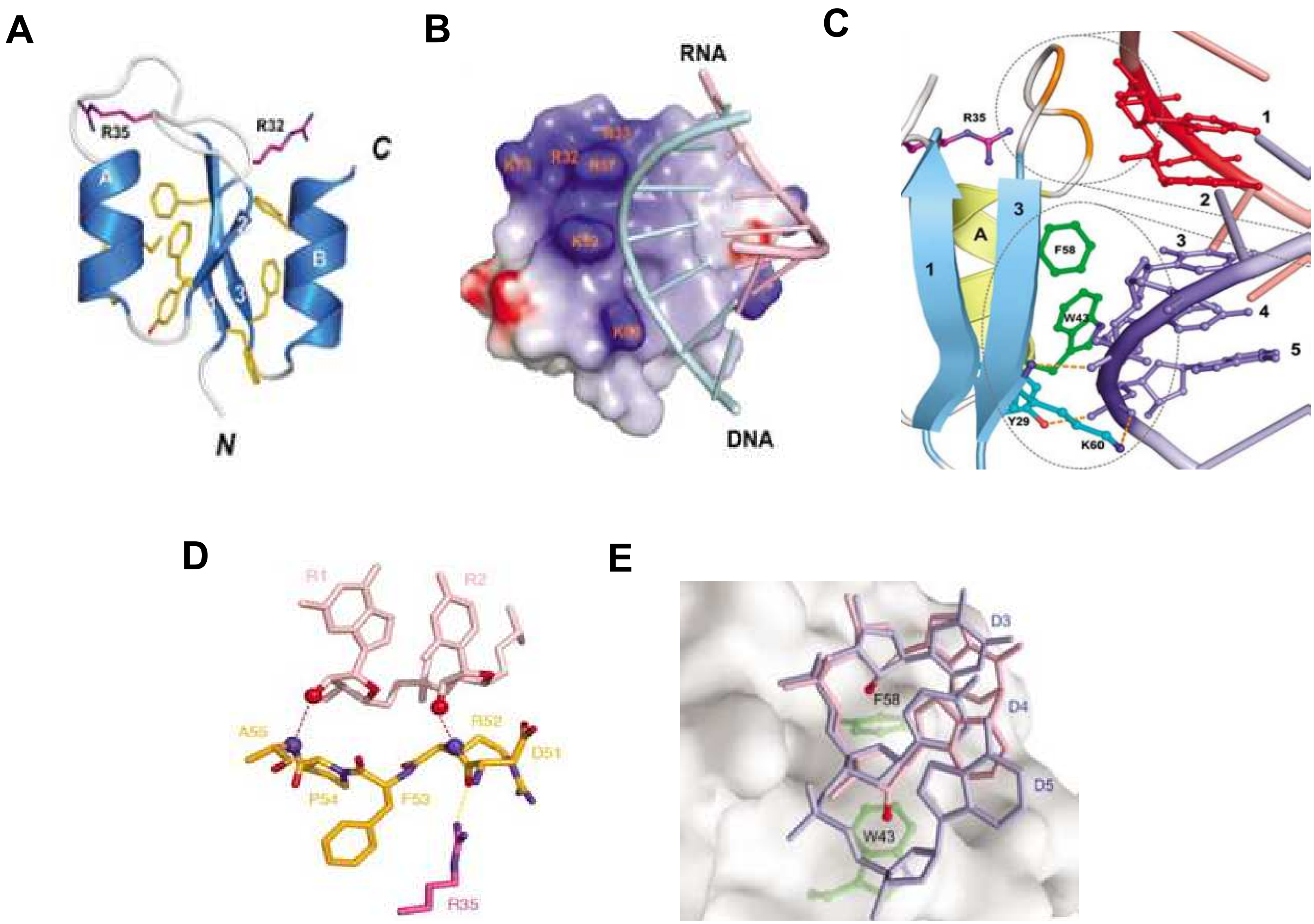
A
R35
R32
C
A
B
N
B
RNA
R32
DNA
C
R35
1
3
A
F58
W43
Y29
K60
1
2
3
4
5
D
R1
R2
A55
R52
D51
P54
F53
R35
E
D3
F58
D4
D5
W43

Figure 6. Structure of the RNHD of Hs-RNase H1, and its interaction with an RNA·DNA hybrid.

A. Ssurface potential representation of Hs-RNase RNHD and an 18 bp RNA·DNA hybrid, displayed using a tube-and-stick model (RNA in magenta/pink; DNA in cyan). The nucleotides interacting with the protein are highlighted in darker color. The arr ows indicate the positions of the mobile loops.

B. Diagram of the protein-nucleic acid interactions. Yellow highlighting indicates residues interacting with the backbone of the substrate, and green highlighting indicates residues interacting with sugars and bases. Cyan and black lines indicate interactions mediated by the backbone or side chains of the protein, respectively. Water-mediated interactions are indicated by ‘‘W.’’ Scissors indicates the scissile phosphodiester.

C. DNA binding in the phosph ate-binding pocket. A 2Fo-Fc simulated annealing omit map contoured at 1.5 σ is superimposed over the model.

D. Interaction of substrate with the DNA-binding channel formed by the basic protrusion.

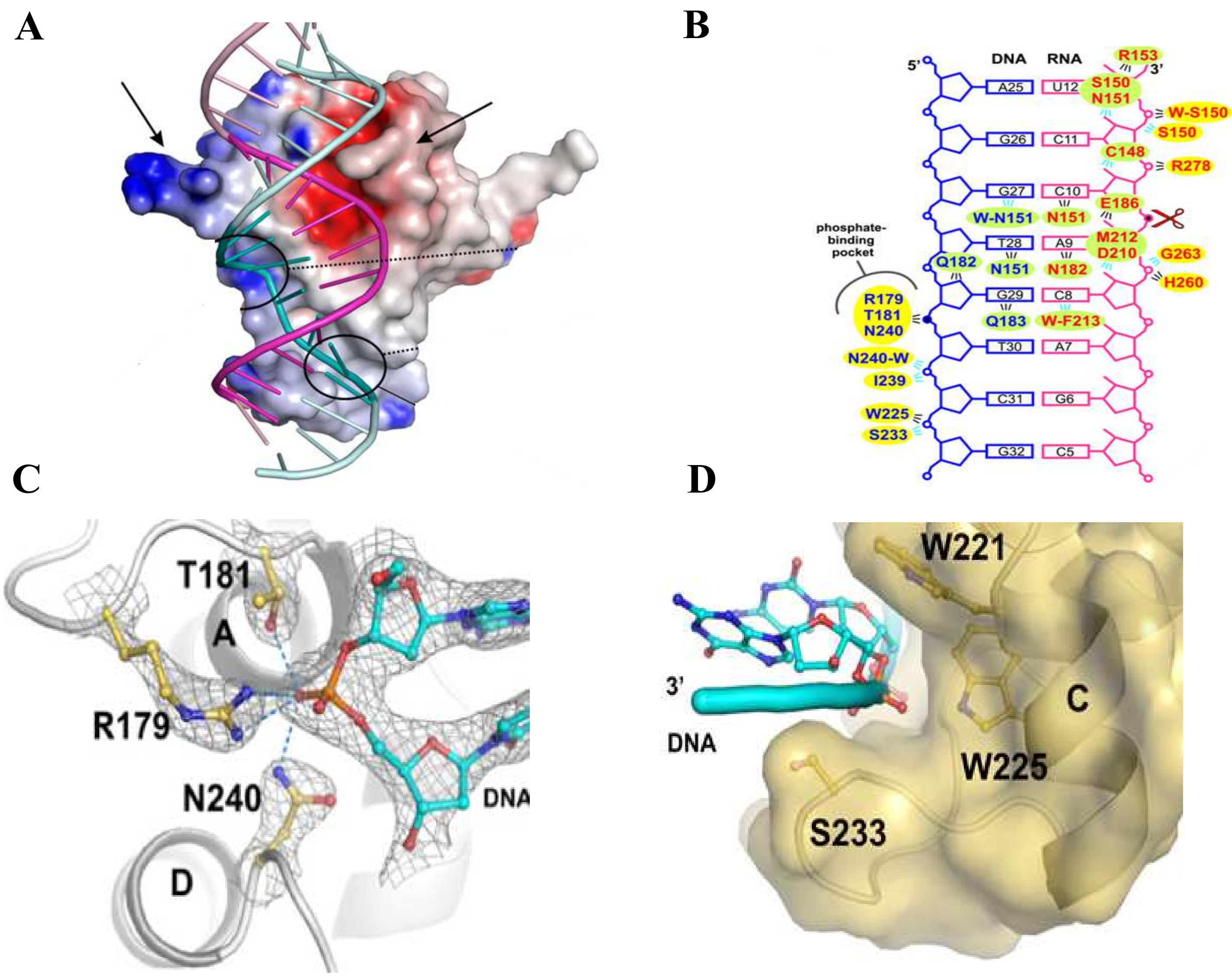
A
B
C
D
DNA
RNA
5'
3'
A25
U12
G26
C11
G27
C10
T28
A9
G29
C8
T30
A7
C31
G6
G32
C5
R153
S150
N151
W-S150
S150
C148
R278
E186
W-N151
N151
M212
D210
G263
H260
phosphate-binding pocket
Q182
N151
N182
R179
T181
N240
Q183
W-F213
N240-W
I239
W225
S233
T181
A
R179
N240
D
DNA
W221
3'
DNA
C
W225
S233

to play an essential role in generation of the nucleophile. Structural and biochemical analysis of bacterial RNase HI and archaeal RNase HII enzymes also suggest an involvement of the pro-R_p nonbonding oxygen atom of the phosphodiester immediately 3' of the scissile bond in orienting the water molecule for optimal in-line attack (Todokoro *et al*., 2007). The role of metal ion B is to stabilize the transition state (TS) intermediate, and facilitate the departure of the 3'-oxygen leaving group. Upon binding an RNA•DNA hybrid, the two metal ions are separated by 4 Å in the active site, and are positioned for catalysis. Metal ion A is coordinated with octahedral geometry, and binds and activates the water nucleophile (Fig. 7C) (Nowotny *et al*., 2006). Metal ion B is coordinated in an irregular geometry, and as such may destabilize the enzyme-substrate complex, effectively lowering the transition state energy barrier. In the next step, movement of two metal ions towards each other brings the water nucleophile closer to the phosphorus atom of the scissile bond, forming a pentacovalent transition state. The transition state is then converted into products (Fig. 7C) (Nowotny *et al*., 2005; Nowotny *et al*., 2006). After hydrolysis, the cleaved 5'-phosphomonoester product end cannot coordinate with both metal ions, and one of the metal ions may displaced from the active site, leading to release of cleavage products (Nowotny *et al*., 2007; Todokoro *et al*., 2007). Many RNase H enzymes, including human RNase H1, *E. coli* RNase HI and HIV RNase H, also have a conserved histidine residue located on a conformationally flexible loop. It has been proposed that the histidine side chain contributes to substrate release by dislodging the 5'-phosphate from the active site (Todokoro *et al*., 2007). However, other functions are possible. This proposed model is examined in this project.

1.3.2.2. Functional roles of conserved amino acids in RNase H1 catalytic action.

The conserved amino acid residues in the RNHD of Hs-RNase H1 that contacts with

RNA·DNA are: D145, E186, D210, D274, H264, N151, N182, Q183, T181, W221, W225 and S233 (Fig. 3C and Fig. 6). Of these, W225, S233 and Q183 vary. The Hs-RNase H1 HBD has 14 highly conserved amino acid residues: F28, Y29, V31, R32, R35, F40, W43, C46, V50, F58, K60, F61 and F70. The RNHD residues are discussed first.

D145, E186, D210, D274 and H264: Based on sequence homology, the residues D145, E186, D210, and D274 were originally predicted to participate in the catalytic site (Fig. 3C). Mutagenesis studies confirmed that D145, E186, and D210 are essential for catalytic activity (22). The D145 side chain binds metal ions A and B, with one of the carboxylate oxygens coordinating to MgA, and the other oxygen with MgB (Fig. 7A). D145 is required for catalysis, but the mutant enzyme retains the ability to bind substrate (Wu *et al*., 2001; Nowotny *et al*., 2007). The side chain of E186 coordinates only with MgA (Nowotny *et al*., 2007), and the E186A mutant is defective in catalytic activity (Nowotny *et al*., 2007). There is a stringent requirement for D210 in catalysis, and the D210 side chain coordinates with MgA and MgB *via* a bridging water molecule (Fig. 7A). The D210N mutant lacks Mg^{2+} as well as Mn^{2+} dependent catalytic activity (Nowotny *et al*., 2007). The D274 side chain coordinates with MgA. However, the D274N mutant retains catalytic activity, so there is no stringent functional requirement for this side chain Residue H264 is conserved in many RNases H1 (for example, H124 in *E. coli* RNase HI, H539 in HIV RNase H) and is required for optimal catalytic activity. E188 in Bh-RNase H occupies the same position in the loop as H264 in Hs-RNase H1. When the Hs-RNase RNHD is superimposed onto the Bh-RNase RNHD bound to a cleaved DNA·RNA hybrid, the histidine side chain clashes with the 5'-phosphomonoester group. Based on this observation, a proposed role of H124/E188 is to promote product release (Nowotny *et al*., 2006). This project shows that H264 also might play a role in positioning the metal ion A, perhaps through an interaction with a third metal ion, and participate in the catalytic step in addition to product release.

N151, N182, Q183 and T181. N151, N182 and Q183 form a ridge that separates the two valleys that accommodate the hybrid substrate. The minor groove of the hybrid “saddles” on the ridge, and the RNA and DNA backbones fit in each valley. The catalytic site is located in the RNA-binding groove, which also interacts with the 2’-OH groups of four consecutive ribonucleotides. T181, along with R179 and N240, form a phosphate-binding pocket that interacts with the DNA strand (Nowotny *et al*., 2007). W221, W225 and S233 form a second DNA-binding channel in the basic protrusion (Fig. 4B and 6D). The DNA backbone fits snugly into this channel, and forms van der Waals contacts and hydrogen bonds (Nowotny *et al*., 2007). When an RNA backbone is modeled into this channel, the 2’-OH of the RNA clashes with the indole ring of W221. It can therefore be concluded that RNase H likely recognizes the DNA strand of the hybrid by (i) the absence of 2’-OH groups and (ii) a B-form conformation.

Conserved groups in the HBD: F28, Y29, V31, R32, R35, F40, W43, C46, V50, F58, K59, K60, F61 and F70. The hydroxyl group of Y29, the amino and amide groups of K59 and K60, and the guanidium group of R57 interact with three consecutive phosphates of DNA. The aromatic rings of W43 and F58 form an aromatic patch that closely approach two consecutive 2’-deoxyribose rings of the DNA (Fig. 6). R35 bolsters the RNA-binding loop (D51-A56) (Fig. 3B). The R32 side chain provides a positive charge that enhances DNA binding, and F61 and F70 interact with 2’-deoxyribose rings.

1.3.2.3 Proposed Reaction Pathway.

A proposed reaction pathway of Hs-RNase H1 is shown in Fig. 8. The pathway involves recognition of the RNA·DNA hybrid by the HBD, followed by engagement of the RNHD that stabilizes the catalytically-competent complex (Fig. 8A). Phosphodiester hydrolysis then occurs, and the products are released. The HBD remains engaged with the hybrid, and the catalytic domain can therefore engage in subsequent multiple rounds of cleavage during a single binding event. Hs-RNase H1 action conforms to Michaelis-Menten kinetics. During catalysis of Hs-RNase H1 it is not known precisely how the two Mg^{2+} ions are positioned appropriately at the scissile phosphate for cleavage. It is also unclear how the enzyme-substrate complex is destabilized and product release occurs. H124 in *E. coli*, H539 in HIV RT and E188 in *B. halodurans* are proposed to promote the product release. In this study we have examined the functional role of the conserved H264, corresponding to H124 (*E. coli* RNase H1) and E188 (Bh-RNase H1) in the catalytic mechanism of Hs-RNase H1.

Figure 7. RNase H1 catalytic site metal ion coordination and schematic representation of proposed reaction steps for RNase H1.

A. The catalytic site of Bh-RNase H. The conserved carboxylates, metal ions, scissile phosphate, and nucleophile are highlighted and labeled**.** RNA is in pink, metal ions are small yellow spheres, and the water molecule is a red sphere (adapted from Nowotny *et al.,* 2005).

B. View of the Hs-RNase H1 catalytic site. Catalytic residues are orange, the RNA is pink, and Ca^{2+} ions as yellow spheres. Metal ion coordination is represented by blue dashed lines. Water molecules are shown as small red spheres. The attacking water nucleophile is indicated by an arrow (adapted from Nowotny *et al*., 2007).

C. Schematic representation of the reaction steps proposed for RNase H1. The substrate RNA is shown in pink, and the products in purple. Coordination of metal ions is highlighted in dark blue, and scissile phosphate in red. Selected hydrogen bonds are shown as blue lines. Black circles represent water molecules. The distance (in Å) between the two metal ions in the enzyme–substrate, enzyme–intermediate and enzyme–product complexes are given (adapted from Nowotny *et al.,* 2006).

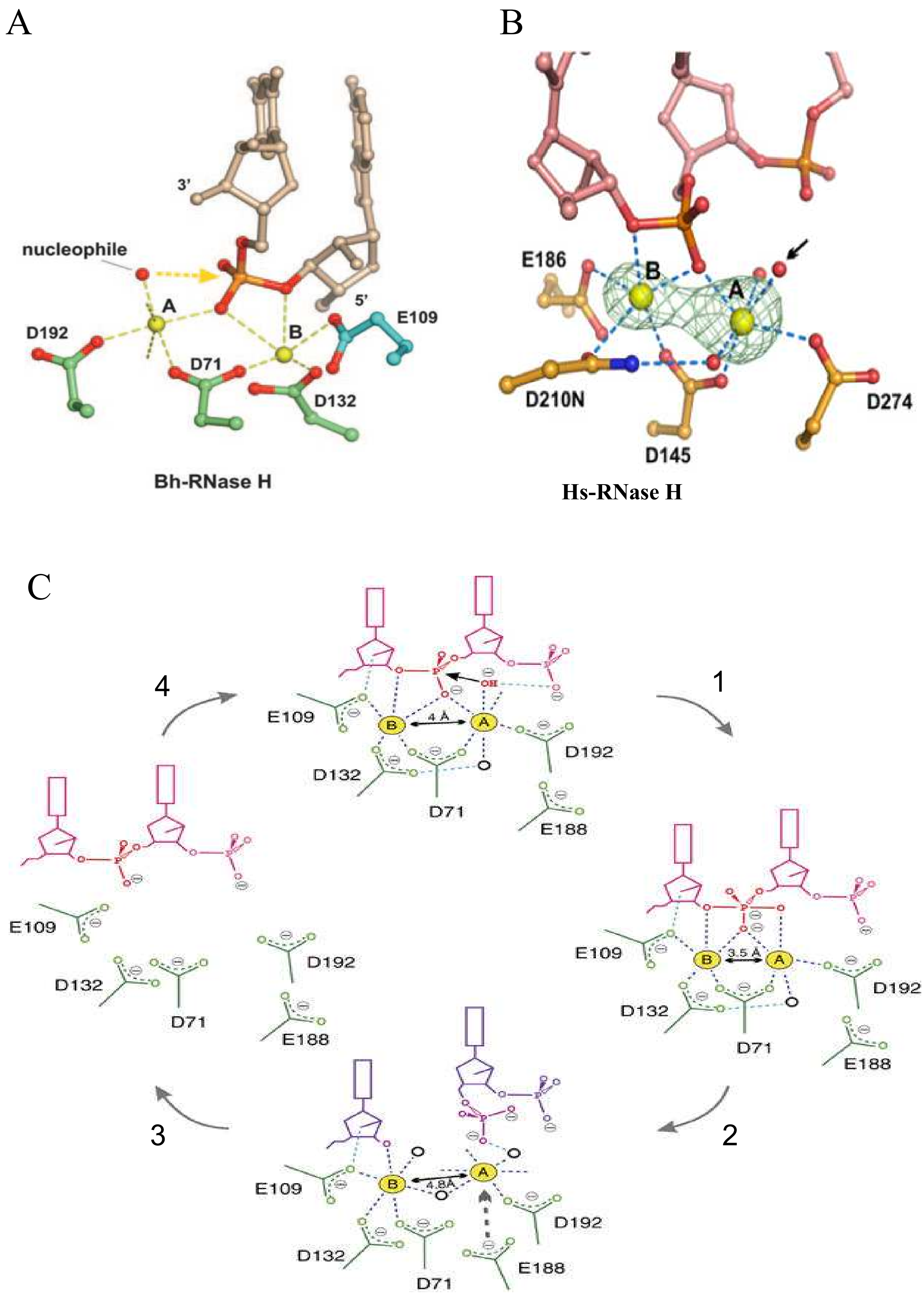
A
B
3'
5'
nucleophile
D192
D71
D132
E109
Bh-RNase H
E186
D210N
D145
D274
Hs-RNase H
C
1
2
3
4
4 Å
3.5 Å
4.8Å
E109
D132
D71
D192
E188

Figure 8. Proposed reaction pathway for Hs-RNase H1.

A. A proposed model for the catalytic cycle for Hs- RNase H1. The HBD is shown in blue and the RNHD in light green.

B. Kinetic scheme for Hs-RNase H1 cleavage of an RNA•DNA hybrid. k_1 is the association rate constant, k_{-1} is the dissociation rate constant, k_2 is the rate constant for the chemical step, and k_p is the product release rate constant.

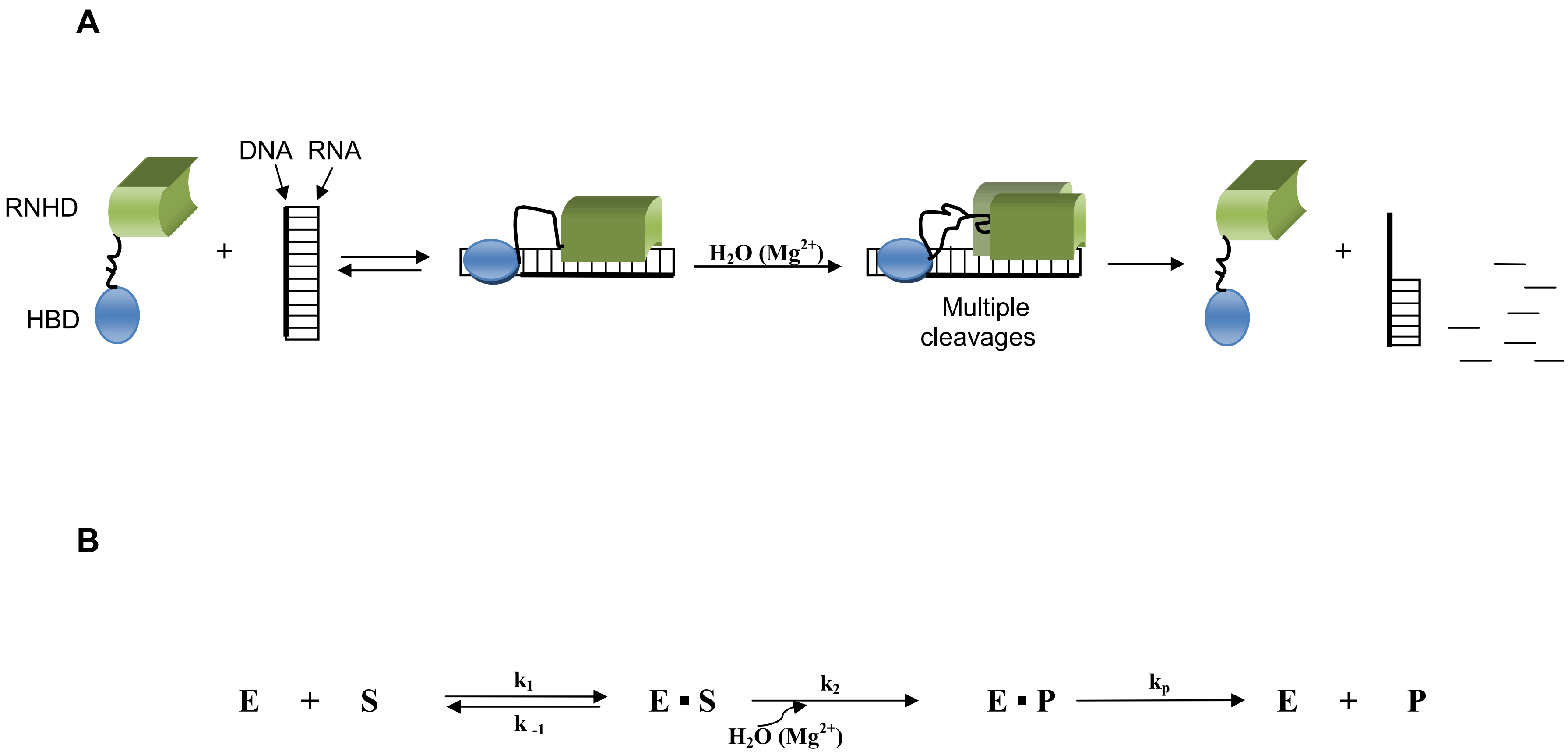
A
RNHD
HBD
DNA
RNA
+
H2O (Mg2+)
Multiple cleavages
+
B
E + S
k1
k -1
E ▪ S
k2
H2O (Mg2+)
E ▪ P
kp
E + P

CHAPTER 2
MATERILAS AND METHODS

2.1 Materials and Reagents

2.1.1 Materials

Water was deionized and distilled, Chemicals and reagents were molecular biology grade and were purchased from Sigma-Aldrich (St. Louis, MO) or Fisher Scientific (Chicago, IL). Pipet tips and microcentrifuge tubes were purchased from ISC Bioexpress (Kaysville, UT). Fuji Super RX film, Whatman 3M filter paper, dialysis membranes (Spectra-Por CE, 10,000 MWCO) were purchased from Fisher Scientific. Glass plates, spacers, combs and microelectroporation chambers were purchased from LabRepCo (Horsham, PA). Standardized 1M solutions of $MgCl_2$, $MnCl_2$ and $CaCl_2$ were obtained from Sigma. Ni^{2+}-NTA chromatography resin and restriction grade thrombin was purchased from Novagen (Madison, WI). Ni^{2+} His-Trap (1 ml) chromatography columns for AKTA FPLC were purchased from GE Lifesciences (Piscataway, NJ). Protein assay kits and protein MW standards (low MW range) for SDS-PAGE were purchased from Bio-Rad Laboratories (Hercules, CA). Amicon spin concentrators were purchased from Millipore (Billerica, MA). UltraPure buffer-saturated phenol, silver staining kit, agarose and low melting point agarose were obtained from Invitrogen (Carlsbad, CA). Gene Ruler™ DNA ladder mix was purchased from MBI Fermentas (Amherst, NY). Plasmid Mini Kits, QiaQuick gel extraction kits and QiaQuick PCR purification kits were purchased from Qiagen (Valencia, CA). Ribonucleoside 5'-triphosphates (rNTPs) were obtained from Amersham-Pharmacia Biotech (Piscataway, NJ). [γ-^{32}P]ATP (3000 Ci/mmol) and [α-^{32}P]UTP (3000 Ci/mmol) were purchased from Perkin-Elmer (Boston, MA). *E. coli* bulk stripped tRNA was purchased from Sigma and was further purified by repeated phenol extraction, followed by ethanol precipitation. T4 DNA ligase, Vent DNA polymerase, and T4 polynucleotide kinase were purchased from New England Biolabs (NEB) (Beverly, MA).

Restriction enzymes EcoRV, Sphl, BamH1, Nde1, HindIII and BglI also were purchased from NEB. Calf intestine alkaline phosphatase and shrimp alkaline phosphatase and 2'-deoxynucleoside 5'-triphosphates (dNTPs) were obtained from Roche Molecular Biochemicals (Indianapolis, IN). T7 RNA polymerase was purified in-house as described (He*et al*., 1997; Studier *et al*., 1990). Oligodeoxynucleotide transcription templates and mutagenic oligodeoxynucleotides were synthesized by Invitrogen, and the deprotected forms were purified by denaturing gel electrophoresis. Purified DNAs were stored at -20^{o}C in TE buffer (pH 8.0). RNA storage solution was obtained from Ambion (NY, USA).

2.1.2 Reagents

In general, the pH of the buffer needs to be adjusted when the value is specified. Tris buffers were adjusted to the specified pH by concentrated (12 N) HCl. Acrylamide gel stock solutions were stored in the dark at 4 ˚C. Tris buffer and salt solutions are usually autoclaved.

TE buffer (10X) [(pH 8.2-8.3 at room temperature (RT)]

890 mM Tris base

890 mM Boric acid

2 mM EDTA (disodium salt)*

TAE Buffer (10X) (pH 8.1-8.2 at RT)

400 mM Tris base

200 mM Acetic acid

10 mM EDTA (disodium salt)

TE Buffer (1X)

10 mM Tris.HCl (pH 6.5)

1 mM EDTA (disodium salt)

RNA/DNA extraction Buffer [pH adjusted to 6.5 with NH_4OH to stabilize the RNA]

0.5 M Ammonium acetate

10 mM EDTA (Disodium salt)

Human RNase H1 dilution buffer (1X)

25 mM Tris·HCl (pH 7 at 30^{o}C)

50 mM KCl

10 mM DTT

T7 RNA Polymerase Transcription Buffer (1X)

40 mM Tris·HCl (pH8.2)

20 mM $MgCl_2$

10 mM Spermidine·3HCl

5 mM DTT

0.01% (v/v) Triton X-100

80mg/mL PEG 8000

Reaction Stop Solution/Denaturing gel loading buffer (2X)

40 mM EDTA (disodium salt)

95% (v/v) Formamide

0.04% (w/v) Xylene cyanol

0.04% (w/v) Bromophenol Blue

RNase H1 Substrate Cleavage Assay Buffer (1X)

25 mM Tris·HCl (pH 7 at 30^{o}C)

150 mM KCl

10 mM DTT

RNase H1 Gel Shift Assay Buffer (1X)

1X RNase H1 Substrate Cleavage Assay Buffer

10% (v/v) Glycerol

RNA·DNA Annealing buffer (1X)

10 mM Tris·HCl

50 mM KCl

0.1 mM EDTA (disodium Salt)

30% Acrylamide Stock Solution (29:1 acrylamide:bisacrylamide)

[For Denaturing polyacrylamide gels]

29% (w/v) Acrylamide

1% (w/v) N,N-methylenebisacrylamide

30% Acrylamide Stock Solution (80:1 acrylamide:bisacrylamide)

[For non-denaturing polyacrylamide gels]

29.63% (w/v) Acrylamide

0.375% (w/v) N,N'-methylene-bisacrylamide

15% Denaturing Polyacrylamide Gel/7M Urea

21 g Urea

5 ml 10X TBE

15 ml 30% Acrylamide Stock Solution (29:1)

0.5 ml 10% (w/v) Ammonium persulfate

0.05 ml TEMED

[50 ml total volume]

8% Non-denaturing Polyacrylamide Gel [for Gel Shift assays]

13.33 ml 30% Acrylamide Stock Solution (80:1)

2.5 ml 10XTBE

0.5 ml 10% (w/v) Ammonium persulfate

0.05 ml TEMED

5 ml Glycerol

[50ml total volume]

SDS-PAGE Electrophoresis Buffer (5X) (pH 8.3, no need to adjust)

72 g Glycine

15 g Tris base

5 g SDS

[1000 ml total Volume]

SDS-PAGE Gel Loading Buffer (2X)

100 mM Tris·HCl (pH 6.8)

4% (w/v) SDS

0.2% (w/v) Bromophenol Blue

20% (v/v) Glycerol

200 mM DTT (added last for fresh use)

SDS-PAGE Sample Buffer/ Cell Cracking Buffer

50 mM Tris·HCl (pH 6.8)

20 mM EDTA (disodium salt)

10% (v/v) Glycerol

1% (v/v) 2-mercaptoethanol

1% (v/v) SDS

12% SDS-PAGE

Separation Gel

3.8 ml	Tris·HCl (1.5 M, pH 8.8 at RT)
0.15 ml	10% (w/v) SDS
6.0 ml	30% Acrylamide stock solution (29:1)
0.15 ml	10% (w/v) Ammonium persulfate
0.006 ml	TEMED

[15 ml total volume]

Stacking Gel

1.25 ml	Tris·HCl (1M pH 6.8 at RT)
0.1 ml	10% (w/v) SDS
1.7 ml	30% Acrylamide stock solution (29:1)
0.1 ml	10% (w/v) Ammonium persulfate
0.01 ml	TEMED

[10 ml total Volume]

Tricine-SDS-PAGE Buffer System

Anode (+) Buffer

24.22 g Tris base

[1000 ml total volume. Adjust to pH 8.1 (at RT) with HCl]

Cathode (-) Buffer

12.11 g Tris base

10 ml 10% (w/v) SDS

17.92 g   Tricine

[1000 ml total volume. Adjust to pH 8.1 with HCl]

Separation Gel Stock Solution (Tricine-SDS-Page)

13.95 g   Acrylamide

0.45 g   N,N'-Methylene-bisacrylamide

[30 ml total Volume]

Stacking Gel Stock Solution (Tricine-SDS-PAGE)

14.4 g   Acrylamide

0.45 g   N,N'-methylene-bisacrylamide

[30 ml total volume]

Gel Buffer (Tricine-SDS-PAGE)

36.33 g   Tris base

3 ml   10% (w/v) SDS

[100 ml total Volume, Adjust to pH 8.45 with HCl)

Coomassie Blue Gel Staining Buffer

0.1% (w/v)   Coomassie Brilliant Blue R-250

45% (v/v)   Methanol

10% (v/v)   Glacial acetic acid

Coomassie Blue Gel Destaining Buffer

45% (v/v)   Methanol

10% (v/v)   Glacial acetic acid

Ni^{2+} -NTA-Column Binding Buffer

25 mM   HEPES (pH 7.4)

500 mM NaCl

5 mM Imidazole

10% (v/v) Glycerol

2 mM β-Mercaptoethanol

Ni^{2+} -NTA-Column Washing Buffer

25 mM HEPES (pH 7.4)

500 mM NaCl

40 mM Imidazole

10% (v/v) Glycerol

2 mM β-Mercaptoethanol

Ni^{2+}-NTA-Column Elution Buffer

25 mM HEPES (pH 7.4)

500 mM NaCl

400 mM Imidazole

10% (v/v) Glycerol

2 mM β -Mercaptoethanol

Ni^{2+}-NTA-Column Dialysis Buffer 1 (Dialysis buffer A)

50 mM HEPES (pH 7.4)

500 mM NaCl

200 mM Imidazole

10% (v/v) Glycerol

2 mM β-Mercaptoethanol

Ni^{2+}-NTA-Column Dialysis Buffer 2 (Dialysis Buffer B)

50 mM	HEPES (pH 7.4)
500 mM	NaCl
100 mM	Imidazole
10% (v/v)	Glycerol
2 mM	β -Mercaptoethanol

Ni^{2+}-NTA Column Dialysis Buffer 3 (Dialysis Buffer C)

50 mM	HEPES (pH 7.4)
500 mM	NaCl
1 mM	EDTA (disodium salt)
2 mM	β -Mercaptoethanol
10% (v/v)	Glycerol

His-Trap Ni^{2+}-NTA Column Binding Buffer

25 mM	HEPES (pH 7.4 at RT)
500 mM	NaCl
5 mM	Imidazole
2 mM	β -Mercaptoethanol
10% (v/v)	Glycerol

His-Trap Ni^{2+}-NTA Column Elution Buffer

25 mM	HEPES (pH 7.4 at RT)
500 mM	NaCl
5 mM	Imidazole
2 mM	β -Mercaptoethanol
10% (v/v)	Glycerol

2.2 Methods

2.2.1 Protein overexpression and purification

Human RNase H1, and the corresponding RNHD and HBD with N-terminal Hexahistidine affinity tags were expressed in *E. coli* BL21(DE3) CodonPlus cells (Stratagene) and purified using a Ni^{2+}-NTA column (either gravity flow, or FPLC column).

2.2.1.1 Protein overexpression

Bl21(DE3) CodonPlus cells were transformed with pET15b-rnh (wild-type or mutant gene) plasmid by heat shock at 42°C for 30 sec, then cooled on ice for 2 min (a fresh transformation was required for each expression and purification procedure). 0.9 ml of preheated (42°C) SOC medium was added to each transformation reaction. The reactions were incubated at 37°C for 1 hr with shaking at 225–250 rpm. Using a sterile spreader, ~≤200 µl of the cells transformed with the experimental DNA were spread onto LB-Amp agar plates. The plates were incubated overnight at 37°C. A single colony was picked up and inoculated into 500 ml LB medium containing 100µg/ml Ampicillin and was grown at 30°C until the culture reached an OD of 0.5 (595nm). Then, IPTG was added (1 mM final concentration) and incubation continued for 3 hr at 30°C. Cells were collected by low-speed centrifugation (6000 rpm, 4°C, 20 min) in a Sorvall SLA-3000 rotor, and stored at -20°C. A 1ml aliquot was removed immediately before IPTG addition, and another 1ml aliquot was removed 4 hr after IPTG addition. These samples were analyzed using 12% SDS-PAGE (Fig. 9A). The gel was run at 120 V until the bromophenol blue reached the bottom of the gel.

2.2.1.2 Protein Purification

Ni^{2+}-NTA Affinity chromatography (gravity flow)

The *E. coli* cell pellet obtained from 500 ml of culture was thoroughly resuspended in 30 ml of Ni^{2+}-NTA column binding buffer and subjected to repeated sonication on ice. The ultrasonic cell disrupter (Misonix Inc) was used at "4-5" setting for 1 min, with 1 min intervals between bursts. The process was repeated 10-12 times. The lysate was clarified by low speed centrifugation (6000 rpm, 4^{o}C for 20 min) in a Sorvall SS-34 rotor. The supernatant was loaded directly onto the prepared purification column (see further steps below). The pellet fraction was stored at 20^{o}C for future protein purification from inclusion bodies, if necessary, also as described below.

A 1.5 ml Ni^{2+}-NTA column (His-Bind resin, Novagen) was used to purify protein from a 500 ml culture. The column is prepared using a 10ml disposable plastic pipette, with a small amount of sterile glass wool as the column support, a short piece of Tygon tubing to direct the eluent, and a screw clamp to control the flow rate. The purification was operated in a 4^{o}C cabinet refrigerator. Prior to loading the sample the resin was washed with 10 column volumes of Ni^{2+}-NTA column binding buffer, then charged with 10 ml of 50 mM $NiSO_4$. The clarified sonicate (~25 ml; see above) was loaded onto the column at a rate of ~1 ml per min. The column was washed with 20 column volumes of Ni^{2+}-NTA column binding buffer, followed by 10 column volumes of Ni^{2+}-NTA column washing buffer, or until protein could not be detected by the Bio-Rad protein assay (Bio-Rad). The protein was eluted with ten 1 ml volumes of Ni^{2+}-NTA column elution buffer. The protein was present mainly in the first five eluted volumes. If the protein contains the hexahistidine tag, it was then subjected to three serial dialyses at 4^{o}C, using Spectra-Por CE tubing (10,000 MWCO). The first dialysis step used Ni^{2+}-NTA-column dialysis buffer A for 3 hr, followed by a 3 hr dialysis against Ni^{2+}-NTA-column dialysis buffer B, then an extensive overnight dialysis in Ni^{2+}-NTA-column dialysis buffer C. Protein concentrations were determined by Bradford assay (Bio-Rad Laboratories) using BSA as standard. A small aliquot also was analyzed by SDS-PAGE (Fig. 9B). The protein was stored at -20°C in 50% (v/v) glycerol, 500 mM NaCl, 25 mM HEPES (pH 7.4), 0.5 mM EDTA, and 2 mM EDTA.

Ni^{2+}-NTA Affinity chromatography using AKTA FPLC

All buffers were sterilized and particulate matter removed by passage through a 0.2 μm filter. The chromatographic column used was a 1 ml His-Trap HP column (GE Healthcare). The clarified, sonicated cell lysate prepared as described above was loaded onto a sample loop that enables loading of the lysate onto the column. Pumps A and B, tubing, and His-Trap column were washed with distilled water (from the in-house distillation unit) followed by a wash with FPLC binding buffer. The column was equilibrated with 5 column volumes of FPLC binding buffer, using a flow rate of 1 ml/min. The pretreated protein sample was loaded using a syringe onto the sample loop (10 ml Superloop from GE Healthcare). The position of the injection valve of the AKTA should be changed to "load" from the default inject position, in order to fill the sample loop. The pump will then load the protein sample onto the column by changing the valve position back to inject. The flow-through should be collected in a clean tube for electrophoretic analysis. The column was washed with 10 column volumes of binding buffer (or until the UV absorbance reaches baseline).

The protein is eluted with FPLC elution buffer, using a linear gradient over 20-30 column volumes. The protein usually elutes at ~250-300 mM imidazole in the gradient (Fig. 10). The eluted protein was dialyzed and stored at -20˚C as described above. Once the run is complete, the column, tubing and pumps should be washed with distilled water, followed by 20% (v/v) ethanol. The His-Trap also should be stored in 20% (v/v) ethanol at room temperature in order to prevent bacterial growth in the column. The column can be reused, if purifying the same protein, up to 10-15 times. The pumps should also be flushed and stored in 20% (v/v) ethanol

Figure 9. Overexpression of His_6-RNase H1, and gel electrophoretic analysis of the purified protein.

A. Protein expression was induced with IPTG as described in Materials and Methods. Aliquots were taken and were analyzed by 12% SDS-PAGE, and protein visualized by Coomassie Blue staining. The molecular mass of overexpressed RNase H1 is indicated to the right. Wild-type RNase H1 with $(His)_6$-tag has molecular mass of approximately 32 kDa. Lane 1: protein markers (molecular masses are indicated to the left); Lane 2: protein profile prior to addition of IPTG; Lanes 3,4: protein profiles 2 and 4 hours after addition of IPTG, respectively.

B. Gel electrophoretic analysis of purified His_6-RNase H1. Protein (~1 μg), purified by affinity chromatography, was analyzed by 12% SDS-PAGE, followed by Coomassie Blue staining.

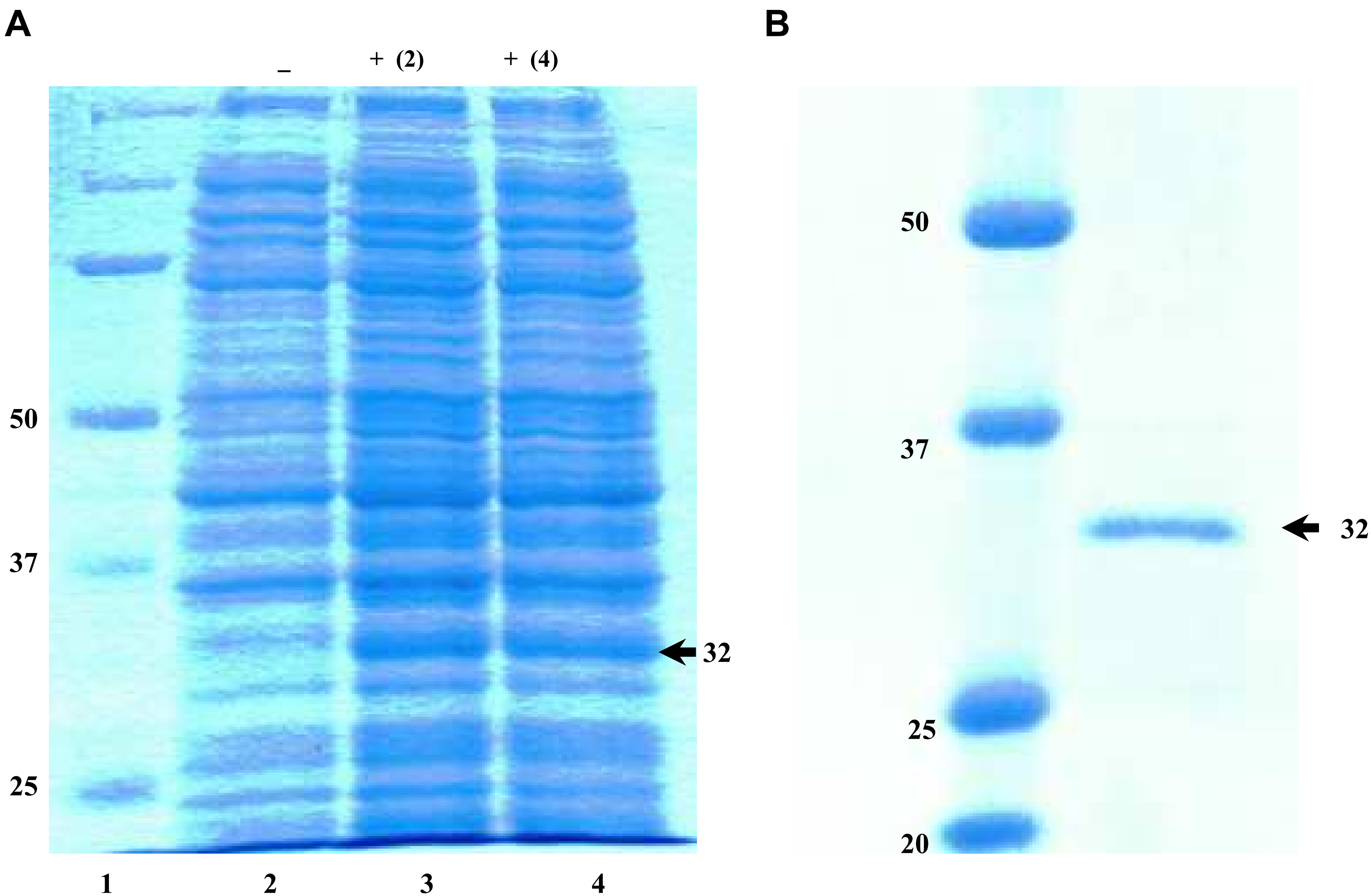
A
B
–
+ (2)
+ (4)
50
37
25
32
1
2
3
4
50
37
32
25
20

when not in use.

Protein Purification from inclusion bodies

RNase H1 can also be purified from inclusion bodies by using 6M urea-containing buffer, as follows. The pellet collected after centrifugation following sonication (see also above) was resupended in 5 ml Ni^{2+}-NTA column binding buffer containing 6 M urea for 1 hr on ice, and a supernatant generated by low speed centrifugation (6000 rpm, $4^{o}C$, 20 min) in a Sorvall SLA 1500 rotor. The supernatant was diluted into 25 ml of Ni^{2+}-NTA column binding buffer and loaded on to a Ni^{2+}-NTA column. This was followed by the steps described above for the purification of the enzyme from the soluble portion of the sonicated cell lysate.

2.2.2. Substrate synthesis and purification

Purification of oligodeoxynucleotides

The sequences of oligodeoxynucleotides used in the project are listed in Table 1. Deprotected synthetic oligodeoxynucleotides (obtained from Invitrogen) were resuspended in 100 µl TE buffer, and a 50 µl aliquot was combined with an equal volume of denaturing gel loading solution. The sample was electrophoresed (25 V/cm) at room temperature in a 15% polyacrylamide gel (1.5 mm thick) containing 7M urea in TBE buffer. The oligodeoxynucleotides were visualized by UV shadowing (Hassur and Whitlock, 1974). UV shadowing is a technique for visualizing nucleic acids separated on polyacrylamide/urea gels. The technique utilizes short wavelength UV light (254 nm) and a fluor-coated TLC plate. The nucleic acid will appear as a dark band when exposed to UV light, while the TLC plate will appear green. Gel bands containing the DNA were located and excised with a clean scalpel. Gel slices were crushed using 1 ml pipet tips into small pieces (~1 mm diameter), and soaked in 500 µl RNA/DNA extraction buffer at room temperature overnight for oligodeoxynucleotides, or 3

Figure 10. FPLC chromatographic purification of Hs-RNase H1 on a His-TRAP column. Purification was performed as described in Materials and Methods. Fraction numbers are given as red Arabic numbers at the bottom. Fractions 12-16 contain pure $(His)_6$-Hs-RNase H1.

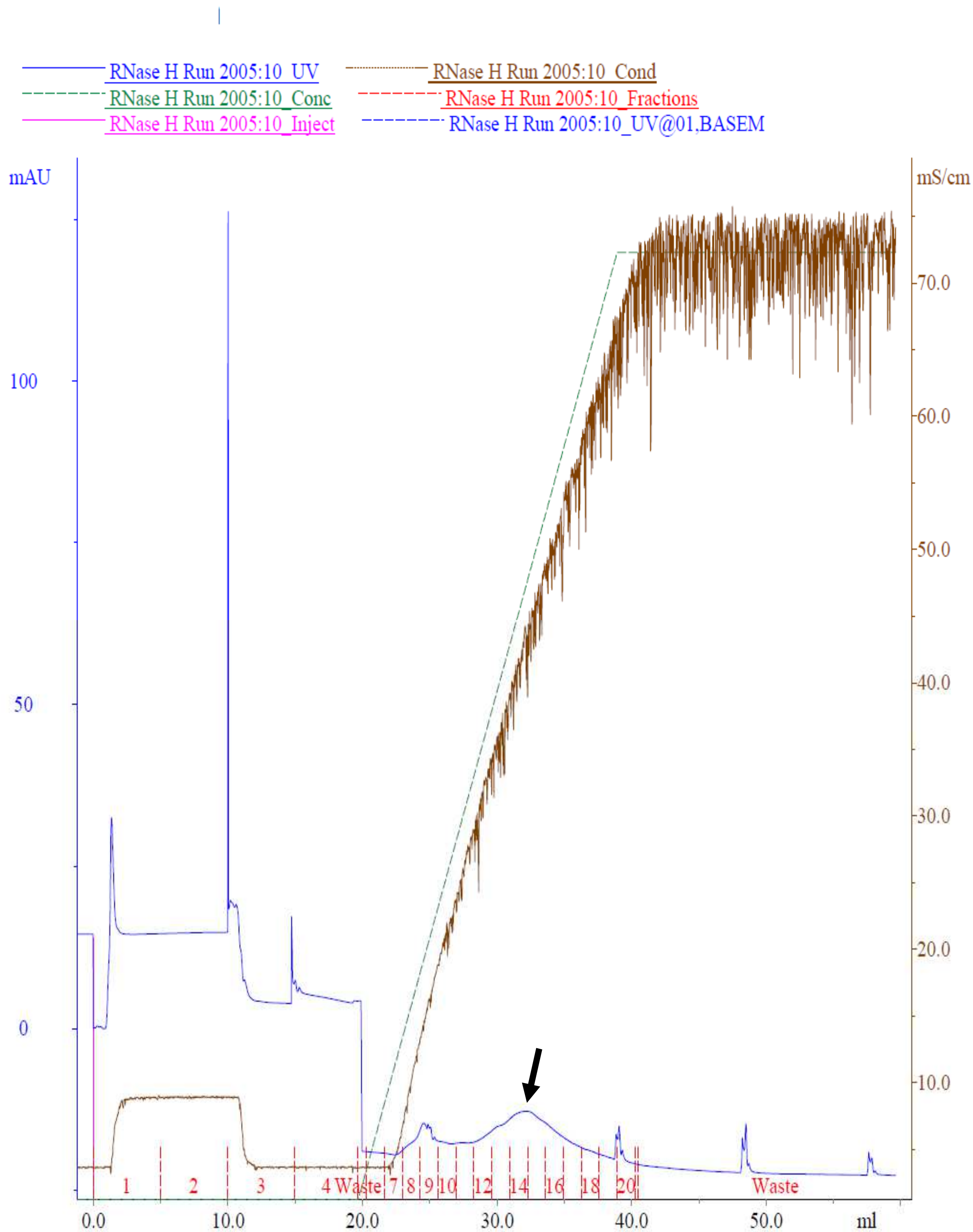
RNase H Run 2005:10_UV
RNase H Run 2005:10_Cond
RNase H Run 2005:10_Conc
RNase H Run 2005:10_Fractions
RNase H Run 2005:10_Inject
RNase H Run 2005:10_UV@01,BASEM
mAU
mS/cm
100
50
0
70.0
60.0
50.0
40.0
30.0
20.0
10.0
1
2
3
4 Waste
7
8
9
10
12
14
16
18
20
Waste
0.0
10.0
20.0
30.0
40.0
50.0
ml

hr for oligoribonucleotides. After centrifugation at maximum speed (14,000 rpm, 5 min), the supernatant was transferred into a clean tube and the DNA precipitated by adding 1/10 volume of 3M NaOAc (pH 5.2) and 2.5 volumes of 95% ethanol, then kept at -20^{o}C overnight. After centrifugation at maximum speed (14000 rpm, 4^{o}C) for 30 min, the DNA pellets were washed with cold 70% ethanol, then centrifuged at maximum speed (14000 rpm, 4^{o}C) for 30 min. The DNA pellets were briefly dried using a Vacufuge Concentrator (Eppendorf Model 5301) and resuspended in an appropriate volume of TE buffer (~50 µl). The DNA concentration was determined by UV spectrophotometry, and molar concentrations were calculated using Equation 1.

Equation 1

$$\text{Molarity } (\mu\text{M}) = \frac{\text{OD}_{260} \text{ (1 cm path length) X dilution factor X 1000}}{\text{MilliMolar Extinction Coefficient}}$$

The millimolar extinction coefficients of oligodeoxynucleotides can be obtained from the supplier's (Invitrogen) product information sheet. Alternatively, they can be calculated as follows. Millimolar extinction coefficients of long (>30 nt) oligonucleotides in units of OD_{260}.l/µmol.cm are: A, 15.4; C, 7.2; G, 11.5; U, 9.9.

The DNA concentration also can be calculated in µg/ml of dsDNA, ~40 µg/ml of ssDNA or RNA, and ~20-33 µg/ml of oligodeoxynucleotide. To convert from g/ml to molarity, the molecular mass of DNA/RNA can be calculated as below. The molecular mass of oligodeoxynucleotide (g/mol): A, 313.2; C, 289.2; G, 329.2; T, 304.2 (average, 308.95). The molecular mass of oligoribonucleotide (g/mol): A, 329.2; C, 305.2; G, 345.2; U, 306.2 (average, 321.45). The OD_{260}/OD_{260} ratio assesses the purity of nucleotides, with a value of 2.0 representing essential pure RNA, 1.8 representing essentially pure DNA, and ≤ 1.8

indicative of the presence of contaminants.

Synthesis of Internally ^{32}P-labeled RNA

In vitro transcription reactions employed a PCR-amplified 200 bp segment of full-length human c-myb cDNA cloned into pET-15b plasmid. The DNA also encodes a T7 class III promoter (Milligan *et al*., 1987). 500-1000 µg of the PCR product was added to a transcription reaction (100 µl) containing 1xT7 transcription buffer supplemented with the four rNTPs (1 mM each), 10 µCi [α-^{32}P]UTP, and ~400 units of T7 RNA polymerase. Reactions were incubated at 37˚C for 3-4 hr, then stopped by adding one-half volume of Reaction Stop solution. The sample was electrophoresed (25 V/cm) at room temperature in a 15% denaturing polyacrylamide gel. The position of the radioactive RNA was determined by autoradiography using Fuji RX film. The film was exposed to the gel for 20 min, then developed in developing buffer (GBX, Sigma) for 2 min, stopped in stopping buffer (GBX, Sigma) for 30 sec, then fixed in fixing buffer (GBX, Sigma) for 2 min. If the RNA is nonradioactive, the gel band was visualized by UV shadowing (see above). The radioactive (or nonradioactive) RNA-containing gel band was excised, crushed and soaked in RNA/DNA extraction buffer (~500 µl). RNA was recovered by ethanol precipitation and resuspended in RNA storage solution (Ambion) (~50 µl). The amount of internally ^{32}P-labeled substrate was determined by counting 1 µl in 6 ml of Scintiverse E cocktail, using an LS6500 Liquid scintillation counter (Beckman Coulter). To calculate the amount in mmol, Equation 2 was used to convert from cpm to mmol:

Equation 2

$$\frac{\text{cpm/counting efficiency (0.99)}}{\text{Number of U residues in strand} \times \dfrac{\mu\text{Ci of hot UTP used} \times 2.2 \times 106\ \text{dpm}/\mu\text{Ci}}{\text{Total mmol of cold UTP used}}}$$

5'-^{32}P-labeling of RNA

To 5-^{32}P-label RNA, the 5'-triphosphate group of enzymatically synthesized (nonradioactive) RNA (~100 pmol) was removed by treatment with calf intestinal alkaline phosphatase (4 units) at 37^{o}C for 1 hr using the supplied buffer. The RNA was purified by phenol-chloroform extraction followed by ethanol precipitation. Dephosphorylated RNA (~5 pmol) was incubated (30 µl reaction volume) at 37^{o}C for ~1 hr with 10 µCi of [γ-^{32}P]ATP (3000 Ci/mmol) and T4 polynucleotide kinase (10 units), using the supplied buffer. Radioactive RNA was purified by electrophoresis in a 15% denaturing polyacrylamide gel (1.5 mm thick) in TBE buffer containing 7M urea as described above. The RNA was recovered by ethanol precipitation and stored at -20^{o}C in RNA storage solution (Ambion) (~50 µl). The amount of 5-^{32}P-labeled RNA was determined by counting an aliquot (1 µl) in Scintiverse E (6 ml), using a LS6500 Liquid Scintillation Counter. To calculate the amount in mmol, Equation 3 was used to convert cpm to mmol:

Equation 3

$$\frac{\text{cpm/counting efficiency (0.99)}}{\text{Specific activity of isotope } (3\text{X}10^6\ \mu\text{Ci/mmol})\ \text{X}\ 2.2\ \text{X}\ 10^6\ \text{dpm}/\mu\text{Ci}}$$

2.2.3 Substrate cleavage assay

RNase H1 cleavage assays were performed using internally ^{32}P-labeled or 5'-^{32}P-labeled RNA. Specific conditions of the cleavage assays are given in appropriate Figure or Table legend. RNA/DNA hybridization is accomplished by combining 1 molar equivalent of RNA with 4 or 5 molar equivalents of DNA, then heating the mixture at 90^{o}C for 2 min in annealing buffer, followed by slow cooling to room temperature. The RNA is incubated with the specified amount of RNase H1 for 1 min at 30^{o}C in RNase H1 reaction buffer lacking Mg^{2+}. RNase H1 was then added at the specific concentration, followed by incubation at 30^{o}C for 1 minute. The reaction was initiated by adding Mg^{2+} (10 mM final concentration unless otherwise specified). Reactions (10 µl reaction volume) were stopped by adding an equal volume of reaction stop solution, then analyzed by electrophoresis in a 15% denaturing polyacrylamide gel containing 7 M urea in TBE buffer. The gel was exposed to a phosphorimager screen overnight at 4^{o}C. The results were visualized by phosphorimaging (Typhoon 9400 System, Amersham Biosciences) and quantified by ImageQuant software (v.5.2). Curve fitting for determination of the kinetic parameters was performed using Kaleidagraph software (v.4.1).

Determination of initial rates, and the kinetic parameters K_m and k_{cat}.

The kinetic constants, V_{max} and K_m, were determined by Michaelis-Menten based analysis of the dependence of the initial velocity (V_o) on substrate concentration. Different substrate concentrations, ranging from 10 nM to 400 nM were used in order to provide reliable estimates of the kinetic constants. Short reaction times were used to limit the amount of substrate cleaved to <20%. Substrates were incubated with human RNase H1, quenched at specific times, and aliquots electrophoresed in a polyacylamide gel as described above. The amount of substrate cleaved was measured, and the initial rates and Michaelis-Menten parameters K_m and V_{max} were calculated using Kaleidagraph software (v.3.5). Under steady-state conditions, the relationship between V_{max} and K_m can be presented as the Michaelis-Menton equation (Equation 4)

Equation 4

$$V_o = \frac{V_{max}[S]}{K_m + [S]}$$

Since substrate is in large excess over enzyme, the free substrate concentration is essentially the same as the total substrate concentration. Therefore, [S] essentially represents the total substrate concentration. V_o represents the initial velocity. The K_m value corresponds to the substrate concentration in which the initial velocity is half the maximal initial velocity. The turnover number (k_{cat}) can be calculated using Equation 5, where $[E]_T$ is the total enzyme concentration.

Equation 5

$$V_{max} = \frac{k_{cat}}{[E]_T}$$

The K_m and k_{cat} values also can be determined by the Lineweaver-Burk equation (Equation 6), using Kaleidagraph software (v.4.1).

Equation 6

$$\frac{1}{V_o} = \left[\frac{K_m}{V_{max}[S]}\right] + \frac{1}{V_{max}}$$

2.2.3 Electrophoretic mobility shift assay (EMSA)

EMSAs were performed with the substrate used in the cleavage assays, which is the 5'-^{32}P-labeled 21 bp hybrid that corresponds to a portion of the c-myb mRNA sequence. ^{32}P-labeled hybrid (10,000 cpm) was combined with the indicated amount of enzyme in binding buffer (20 µl final volume), and incubated at room temperature for 10 min, followed by 20 min on ice. Electrophoresis was then performed at 4^{o}C in a 1.5 mm thick, 8% nondenaturing polyacrylamide gel containing 0.5xTBE buffer at 150 V for 3 hr. Binding reactions were visualized by phosphorimaging (Typhoon 9400 system). The K'_d values were calculated using equation 7, where $[E]_f$ and $[S]_f$ are the concentration of unbound enzyme and substrate, respectively, and [ES] is the concentration of the enzyme-substrate complex.

Equation 7

$$K'_d = \frac{[E]_f X [S]_f}{[ES]}$$

Since it is not possible to accurately know the concentration of the substrate, an alternative procedure involves measuring the radioactive signal, then calculating the fraction of RNA bound (B) using Equation 8, where $[S]_T$ is the concentration of total substrate, and [ES] is the concentration of the enzyme-substrate complex. Here, the amount of free RNA is measured in order to calculate the fraction of RNA that is bound by enzyme, since some dissociation of the RNA-protein complex usually occurs during electrophoresis.

Equation 8

$$B = \frac{[ES]}{[S]_T}$$

Equation 8 can then be presented as follows:

Equation 9

$$B = \frac{1}{1 + K\,[E]_f} \quad \text{or}$$

Equation 10

$$1/B = 1 + \frac{K'_d}{[E]_f}$$

Since the enzyme concentration (in the nM range) is in large excess over the substrate (in fM range), the free enzyme concentration is essentially equal to the total enzyme concentration, $[E]_T$. Equation 12 can then be presented as:

Equation 11

$$1/B = 1 + \frac{K'_d}{[E]_T}$$

Therefore, the double reciprocal plot, generated by plotting 1/B vs $1/[E]_T$, provides a slope that is equal to the K'_d value.

CHAPTER 3

EVIDENCE FOR A DUAL FUNCTIONAL ROLE OF A CONSERVED HISTIDINE IN ANTISENSE OLIGONUCLEOTIDE-DIRECTED CLEAVAGE OF RNA BY RNASE H1

3.1 Introduction and Project Overview

Ribonuclease H1 is a conserved enzyme that is localized in the nuclear and mitochondrial compartments of eukaryotic cells, and functions in DNA replication, repair, recombination and transcription (Arunachandran *et al*., 2000; Cerritelli *et al*., 2003). Oligonucleotide binding to a complementary RNA sequence provides a substrate for RNase H1, and represents the mechanistic basis for antisense oligonucleotide (AON)-directed gene silencing in cells (Opalinska *et al*., 2002). The effective evaluation of the therapeutic efficacy of next generation AONs with novel structures requires an *in vitro* system involving purified, highly active RNase H1, and an understanding of the catalytic mechanism of the enzyme. This chapter describes the purification of the mature form of human RNase H1 from bacterial cells, and the analysis of its basic biochemical properties in assays that use a hybrid substrate whose RNA sequence represents a clinically important target. Hs-RNase H1 exhibits optimal catalytic activity at a monovalent (K^+) salt concentration of ~50 mM, and a pH of 8. Catalytic activity is best supported by either Mg^{2+} or Mn^{2+} as the catalytic cofactor. Co^{2+} and Ni^{2+} support lower levels of activity, while Ca^{2+} is inactive. In assays where addition of the AON to initiates the reaction, the processivity of Hs-RNase H1 is demonstrated,as well as ability of the AON to engage in multiple rounds of substrate turnover at low AON/RNA ratios. Mutation to alanine of the conserved histidine at position 264 causes a significant reduction in the catalytic activity of Hs-RNase H1. The V_{max} for the H264A mutant, determined under steady-state conditions, is 100-fold lower than the V_{max} for wild type enzyme. Under single-turnover conditions, the half-life of the hydrolysis step is ~10-fold lower for the H264A mutant than that for the wild-type enzyme. These results indicate an involvement of the H264 side chain in product release step, as predicted from the crystal structures by Nowotny and coworkers, and also in the catalytic step as indictaed by molecular modeling studies of Klein and coworkers. A model for H264 side chain function is presented.

3.2 RESULTS

3.2.1 Purification of Hs-RNase H1 and the salt and pH dependence of catalytic activity.

Hs-RNase H1 was purified in its mature nuclear/mitochondrial form using two different routes, both of which took advantage of an N-terminal hexahistidine affinity tag. The protein was purified to ~95% electrophoretic homogeneity using either conventional gravity flow affinity chromatography, or by FPLC. In the latter procedure, the protein eluted at 300 mM imidazole (see Materials and Methods)*. The hexahistidine tag has only a minor influence on the catalytic activity, since time course assays of cleavage of a radiolabeled RNA•DNA hybrid revealed no significant difference in either cleavage rate or cleavage pattern (Fig. 11). The substrate is a 21 bp oligodeoxynucleotide-RNA hybrid, with the RNA sequence corresponding to a sequence within the human c-myb mRNA coding sequence. The oligodeoxynucleotide was originally synthesized in phosphorothioate form, and further substituted at selected positions with 2'-fluoroarabinose. This modification to provides efficient and persistent silencing of c-Myb expression in leukemia cell lines (Kalota *et al*., 2004).Oligonucleotides containing phosphodiester groups used retained in this study, since phosphorothioate groups has been shown to inhibit RNase H1 *in vitro* (Gao *et al*., 1992), and that the fluoroarabinose sugars also can perturb RNase H1 action (see chapter 4).

To assess the effect of salt concentration on hs-RNase H1 activity, substrate cleavage assays were performed using a range of concentrations of K^+ (as the chloride salt), and in the presence of 10 mM Mg^{2+}. The results are summarized in Fig. 13, where it is observed that Hs-RNase H1 activity increases with increasing salt concentration, reaching a maximum at ~150 mM KCl

(Fig. 13A). Higher salt concentrations cause a progressive reduction in activity. The pH dependence of Hs-RNase H1 catalytic activity was determined by measuring substrate cleavage at pH values between 5.5 and 11.5, and in the presence of 10 mM Mg^{2+} and 150 mM KCl. The fraction of substrate cleaved as function of pH is shown in Figure 13B, which shows a transition to maximal activity between pH 6 and 7.5. Based on these results, a pH of 7.5 and a KCl concentration of 150 mM were used as standard reaction components.

3.2.2 Divalent metal ion dependence of RNase H1 catalytic activity.

Structural and biochemical studies of Hs-RNase H1and *B. halodurans* (Bh) RNase H1, have identified a two metal ion catalytic mechanism (Nowotny *et al*., 2005; Yang *et al*., 2006). It has also been shown that Tm-RNase H1 can utilize several different divalent metal ions (Todokoro *et al*., 2007). It therefore was of interest to determine the metal ion dependence of Hs-RNase H1. Ca^{2+}, Co^{2+}. Ni^{2+}, Mg^{2+}, Mn^{2+}, and Zn^{2+} were tested for their ability to support Hs-RNase H1 activity. Quantitative analysis (Fig. 12) shows that maximal activity is achieved at a ~10 mM concentration of Mg^{2+} or Mn^{2+}, while Co^{2+}, Ni^{2+} and Zn^{2+} support only minor levels of activity. Ca^{2+} does not support catalytic activity over the concentration range examined (data not shown). Based on these results, Mg^{2+} (10 mM) was used as a standard reaction component.

3.2.3 Sustained action of sub-stoichiometric levels of an antisense oligodeoxynucleotide in directing RNA cleavage by Hs-RNase H1 *in vitro*.

Having established optimal *in vitro* reaction conditions for Hs-RNase H1, we investigated whether this assay was capable of demonstrating the sustained action of an oligodeoxynucleotide in directing RNA cleavage, as would be required for an efficient RNase H1-dependent gene silencing pathway *in vivo*. Sub-stoichiometric amounts of the oligodeoxynucleotide, ranging down to hundred-fold less than the complementary RNA, were added to initiate cleavage and, the fraction RNA cleaved was measured. The ability of the AON to engage in multiple rounds of substrate cleavage is shown in Table 1.

3.2.4 A conserved histidine in the Hs-RNase H1 catalytic center is important for both phosphodiester hydrolysis and product release.

Based on crystallographic studies by Nowotny, Yang and coworkers (Nowotny *et al*., 2005; Yang *et al*., 2006), and computational analyses by Klein and coworkers (Ho *et al*., 2010), two key functional roles were proposed for the H264 side chain in the human (Hs)-RNase H1 catalytic mechanism (note: E188 of *B. halodurans* (Bh) RNase H1 and H124 of *E. coli* (Ec) RNase HI, are equivalent to H264 of Hs-RNase H1). Nowotny and coworkers showed that H264 (E188/H124) is in a flexible loop, and is positioned near the catalytic metal ions MgA and MgB (Nowotny *et al*., 2005). They proposed a role of the H264 side chain in product release, perhaps through an interaction of the side chain with the 5'-phosphomonoester group of the cleaved product. The type of interaction is unclear, but it was proposed that a steric clash of the H264 side chain and the 5'-phosphomonoester group would facilitate departure of the product, through relief of steric strain (Nowotny *et al*., 2007). However, it is also possible that the H264 side chain is directly or indirectly involved in an attractive interaction with the 5'-phosphomonoester group, and thus would act as a chaperone in the product release pathway. To examine the function of H264 in the Hs-RNase H1 catalytic mechanism, H264 was changed to alanine, and the Hs-RNase H1 H264A mutant protein was purified from the soluble fraction of sonicated cell lysates. Time-course cleavage assays (Fig. 14A) reveal that the H264A mutant exhibits a significant defect in catalytic activity, under conditions where Hs-RNase H1 efficiently processes the RNA·DNA heteroduplex. The steady-state kinetic parameters K_m, V_{max}, and k_{cat} were determined (Fig. 14B). The H264A mutation causes a significant reduction in the turnover number (k_{cat}) (>100-fold) compared to wild-type enzyme. In contrast, the H264A mutant exhibits a K_m comparable to wild-type enzyme (Fig. 14D). A time-course reaction under single-turnover conditions (enzyme excess) showed that the $t_{1/2}$ for phosphoester hydrolysis cleavage by the H264A mutant is 10-fold lower than the wild-type enzyme (Fig. 15A and 15B). Thus, the H264A mutation slows the rate of reaction, independent of its involvement in product release. Taken together, the data from these analyses strongly suggest that the H264 side chain is involved in the catalytic step as well as in product release, but plays only a minor role in substrate binding.

3.3 Discussion

The basic experimental parameters that influence the activity of the mature (i.e. nuclear/mitochondrial) form of Hs-RNase H1 have been assessed in assays that use a model 21bp RNA·DNA hybrid as substrate. The optimal salt concentration is ~150 mM KCl, and the optimal pH is 7.5. Hs-RNase H1 activity is supported by the divalent metal ions Mg^{2+}, Mn^{2+}, Co^{2+}, Ni^{2+} and Zn^{2+}, with Mg^{2+} or Mn^{2+} providing optimal and comparable levels of activity. In contrast, Ni^{2+}, Co^{2+} and Zn^{2+} support only nominal levels of activity. Mg^{2+} is presumably is the physiologically relevant species *in vivo*. However, higher concentrations of the metal are inhibitory, while higher concentrations of Mn^{2+} are not inhibitory. The salt (KCl) concentration optimum occurs in the range of ~150 mM, with a progressive decrease in enzyme activity at higher concentrations. The inhibition may reflect an ionic competition with the RNA·DNA hybrid for enzyme binding.

3.3.1 Possible functions of H264 in the Hs-RNase H1 catalytic mechanism.

The biochemical behavior of the H264A mutant indicates an important involvement of the

H264 side chain in the catalytic mechanism. Based on this study and previous investigations, two functional roles can be proposed for the H264 side chain in the Hs-RNase H1 catalytic mechanism: one role is associated with product release, and the other role is in phosphodiester hydrolysis. H264 is on a flexible loop and is positioned near the the two catalytic metal ions, MgA and MgB. Based on this positioning, and on a molecular modeling analysis of a putative product complex, Nowotny and coworkers proposed how the H264 side chain might promote product release. Specifically, the side chain would facilitate product release through the relief of "steric clash" with the newly-formed 5'-phosphomonoester group (Nowotny *et al*., 2005). However, it is also possible that the H264 side chain may have an affinity for the 5'-phosphomonoester group, thereby enabling an efficient product release pathway. Evidence that product release pathway also might involve a third divalent metal ion, is described below.

The behavior of the mutant enzyme under single-turnover conditions indicates an involvement of the H264 side chain in the chemical (phosphodiester hydrolysis) step. The kinetic data do not provide insight on how the H264 side chain may be involved in this event, but molecular dynamics (MD) modeling studies of Bh-RNase H1 by Klein and coworkers (Ho *et al*., 2010) suggest a mechanism for the side chain. The MD modeling included Mg^{2+} ions in the solvent, and revealed the presence of a third Mg^{2+} ion near the catalytic site that interacts with the E188 side chain (and by inference, also the H264 side chain of Hs-RNase H1). The calculations show that the binding of the third Mg^{2+} ion is stabilized by outer-sphere coordination to the E188 side chain. This novel interaction does not alter the positions of MgA and MgB, or their ligand coordination patterns (Ho *et al*., 2010). Thus, a primary function of the H264 side chain role may be to bind a third Mg^{2+} ion (hereafter called MgC). If this is indeed the case, the inhibitory effect of the H264A mutation on hydrolysis and product release may reflect the lack of MgC in these steps. Since H264 is contained in a flexible loop, the MgC ion may be able to shift its position, therefore permitting its participation in both steps.

Proposed Function #1 for MgC coordinated to H264: *Optimizing the rate of the chemical step.* A single-turnover kinetic analysis (see above) has shown that the H264A mutation slows the rate of hydrolysis by ~10-fold. Assuming that the H264A mutation abolishes binding of MgC (see above) this result shows that MgC is involved in the chemical step, since this is the rate-determining event under single-turnover conditions. According to Klein and coworkers (Ho *et al.*, 2010), at physiologically relevant Mg^{2+} concentrations, H264-enabled Mg^{2+} binding to site C creates an electrostatic environment optimal for phosphodiester hydrolysis catalyzed by MgA and MgB. However, the specific features of an optimal electrostatic environment was not precisely defined. One possibility is that MgC may provide optimal geometric positioning of the water nucleophile bound to MgA, thereby maximizing the rate of in-line attack on phosphorus. This proposal has not been critically tested, and would require additional MD simulations.

Proposed Function #2 for MgC coordinated to H264: *Optimizing the rate of product release.* Based on their crystallographic studies of Hs-RNase H1 and Bh-RNase H1, Nowotny, Yang and coworkers proposed a role for MgC in product release (Nowotny *et al.*, 2005; Yang *et al.,* 2006). Specifically, the product 5'-phosphomonoester engages with MgC as part of a pathway of assisted product release. A shift in coordination of Mg from site A to site C may also would shift the position of the cleaved RNA product, *via* the coordinated 5'-phosphomonoester group, which is then released to solution. A subsequent proposal from the same group omits an involvement of MgC, and instead proposes that the relief of a steric clash of the H264 side chain with the newly-formed 5'-phosphomonoester group allows efficient release of the product (Nowotny *et al.*, 2007). Crystal structures show that His264 is on a flexible loop (Nowotny *et* *al*., 2007). The flexibility of the loop may allow movement of the Mg^{2+} ion in concert with product release.

Studies on *E. coli* RNase HI, which contains the conserved histidine at position 124, support the dual functional role of this residue, and provide additional insight on the proposed third metal binding site. Similar to the H264A mutation of Hs-RNase H1, the H124A mutation reduces the V_{max} >90-fold with Mg^{2+} as the catalytic cofactor (Kanaya *et al*., 2000). While Mn^{2+} also supports Ec-RNase HI catalytic activity, higher concentrations are inhibitory (Keck *et al*., 1998). However, the Mn^{2+} inhibition is not observed with the H124A mutant (Haruki *et al*., 1994; Oda *et al*., 1993). The inhibitory effect of the H124 mutation and Mn^{2+} support the proposed interaction of the Histidine side chain with a divalent metal ion at site C. How Mn^{2+} inhibits Ec-RNase HI at higher concentrations is not known. However, one possibility is that metal site C is unoccupied in the initial steps of the catalytic pathway but receives the metal ion from site A upon phosphodiester hydrolysis as part of the product release pathway. The inhibitory action of Mn^{2+} may reflect a higher affinity for site C, compared to Mg^{2+}. If release of metal from site C is required to release the product RNA and complete the catalytic cycle, then an impaired ability of Mn^{2+} to be released from site C (and therefore also the product RNA) would reduce the steady-state V_{max} value. In summary, the H264A, H124A, and E188A mutations are predicted to abolish metal binding to site C, thus disrupting the product release pathway, causing a reduction in V_{max}.

Figure 11. Effect of N-terminal Hexahistidne tag on Hs-RNase H1 cleavage of substrate

Shown is a phosphorimage of a sequencing gel, comparing reaction time course of cleavage of an RNA-DNA hybrid by His_6-Hs-RNase H1 and Hs-RNase H1. Reactions were carried out essentially as described in Materials and Methods. Reaction times are given at the top of the gel image. "P1" refers to P1 nuclease reaction. Arrows indicate the main (and final) products of cleavage (5 and 6 nt in length) in the 2'-deoxy P(O) AON reactions. "0" indicates a control where RNA was combined with enzyme in the absence of Mg^{2+}, then 95% formamide/20 mM EDTA immediately added and the samples analyzed as described. The asterisks next to the P1 lane indicate nonenzymatic RNA cleavage products.

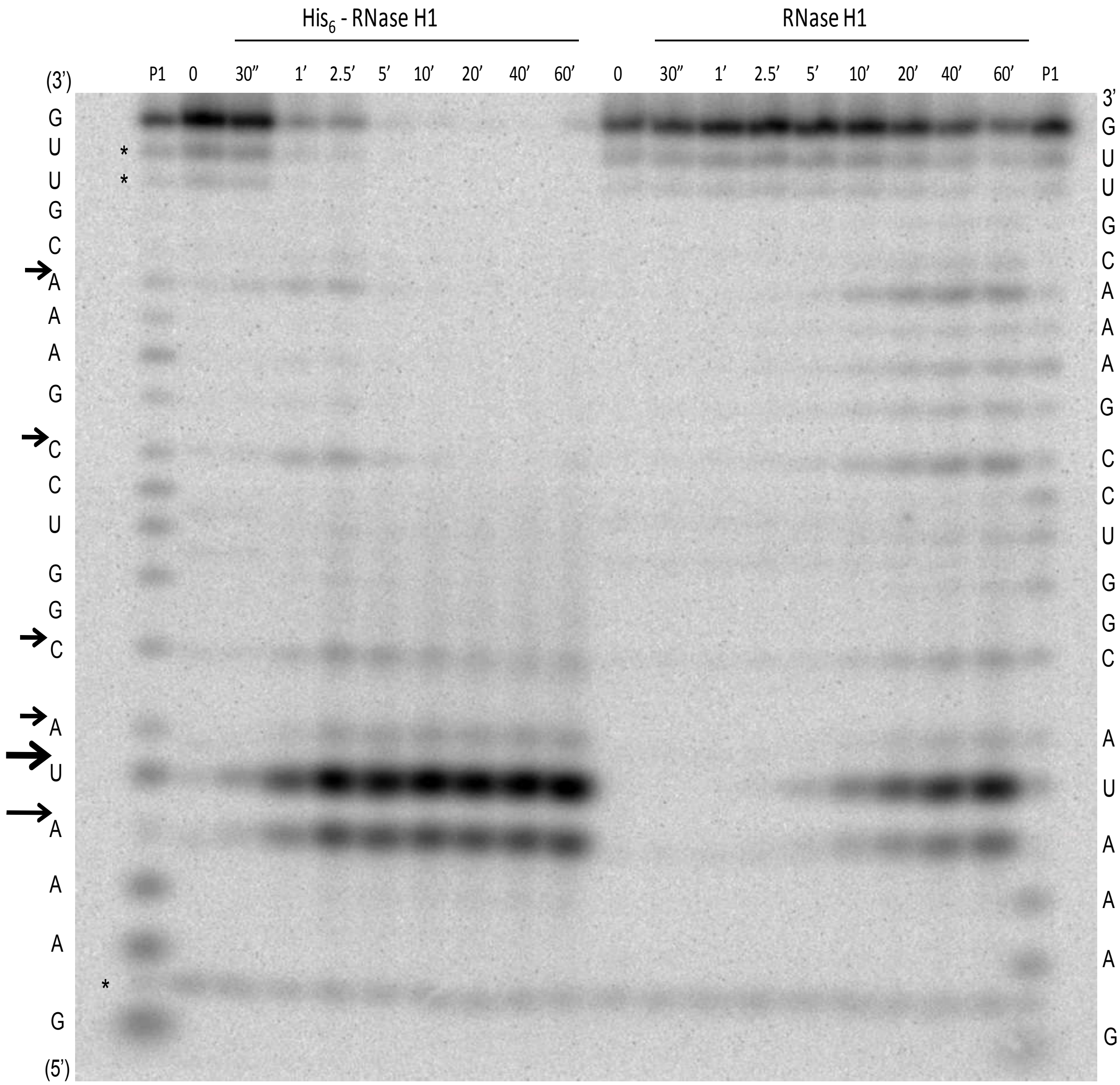
His6 - RNase H1
RNase H1
P1 0 30" 1' 2.5' 5' 10' 20' 40' 60' 0 30" 1' 2.5' 5' 10' 20' 40' 60' P1
(3')
G U U G C A A A G C C U G G C A U A A A G
(5')
3'
G U U G C A A A G C C U G G C A U A A A G
*
*
*

Figure 12. Divalent metal ion dependence of Hs-RNase H1 catalytic activity. The fraction of RNA cleaved was plotted as a function of divalent metal ion type and concentration. The enzymatic activity of Hs-RNase H1(histidine tagged) was determined at 30^0C in 150 mM KCl, 10 mM DTT and 20 mM HEPES (pH 7.5), and various concentrations of $MgCl_2$ (closed squares), $MnCl_2$ (open squares), $CoCl_2$ (closed diamonds), $NiSO_4$ (open diamonds), or $ZnCl_2$ (open triangles) using the 21bp c-Myb RNA•DNA hybrid as substrate. Experiments were carried out in duplicate, and the average values are shown along with error bars.

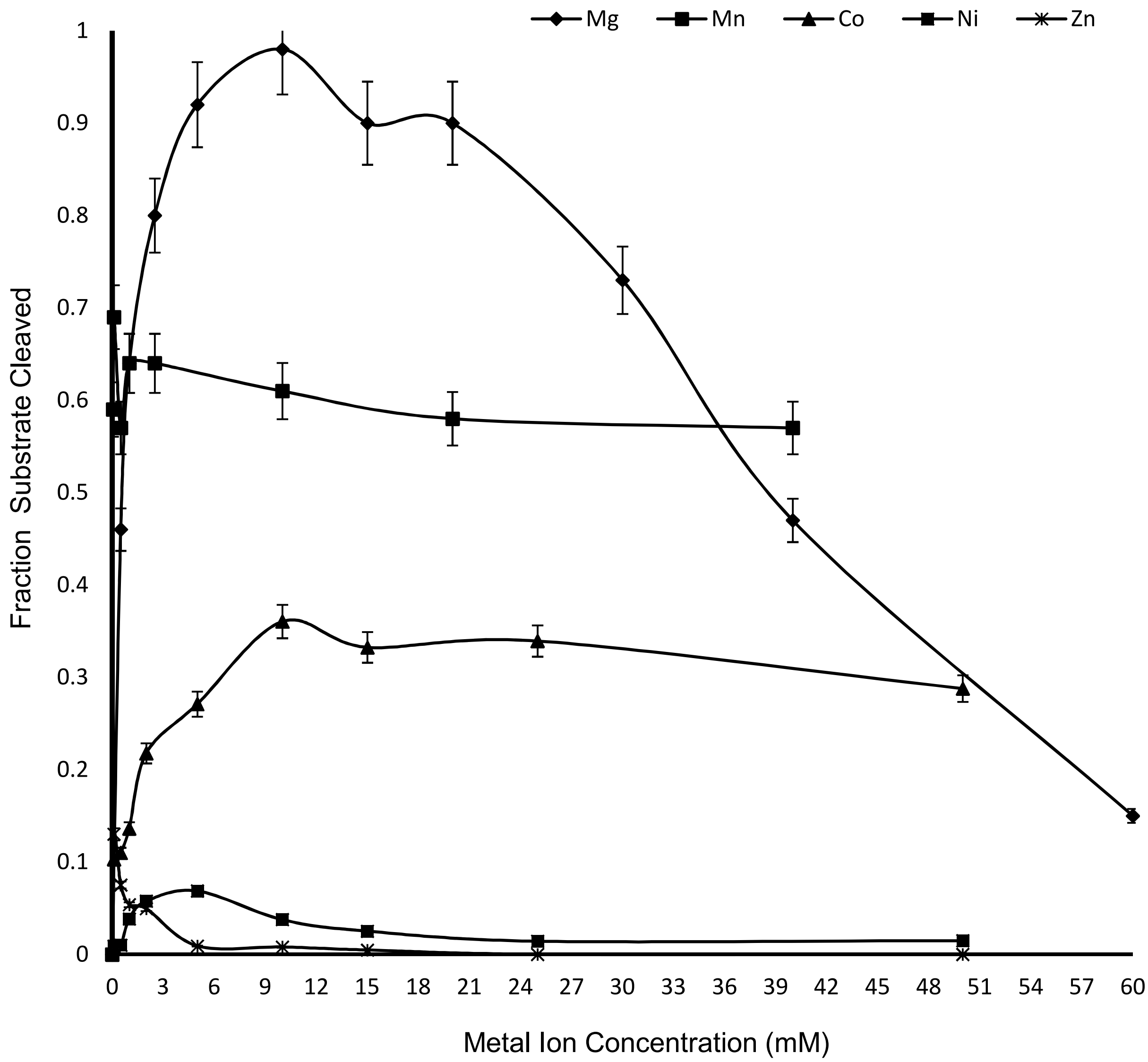

Mg
Mn
Co
Ni
Zn
Fraction Substrate Cleaved
Metal Ion Concentration (mM)
1
0.9
0.8
0.7
0.6
0.5
0.4
0.3
0.2
0.1
0
0
3
6
9
12
15
18
21
24
27
30
33
36
39
42
45
48
51
54
57
60

Figure 13. Salt and pH dependence of Hs-RNase H1 catalytic activity.

The catalytic activity of Hs-RNase H1 was determined at 30^{o}C in 20 mM Tris-HCl (pH 7.5) containing 10 mM $MgCl_2$, 10 mM DTT, at various concentrations of KCl (A) or pH at (150 mM KCl) (B), using the 21 bp c-myb RNA heteroduplex as substrate and 40nM Hs-RNase H1. Experiments were carried out in duplicate, and average values of the fraction of substrate cleaved are shown with error bars.

A

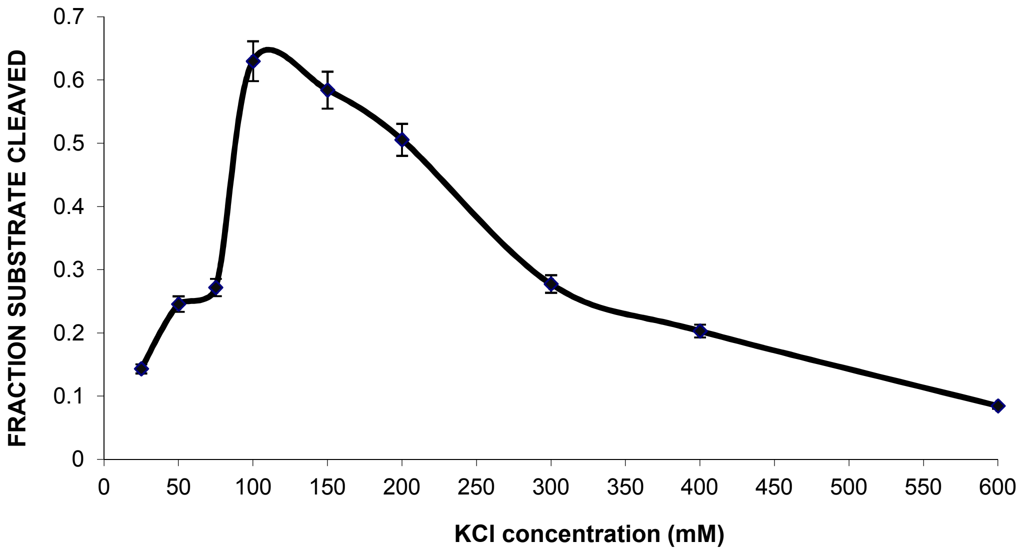

0.7
0.6
0.5
0.4
0.3
0.2
0.1
0
FRACTION SUBSTRATE CLEAVED
0
50
100
150
200
250
300
350
400
450
500
550
600
KCl concentration (mM)

B

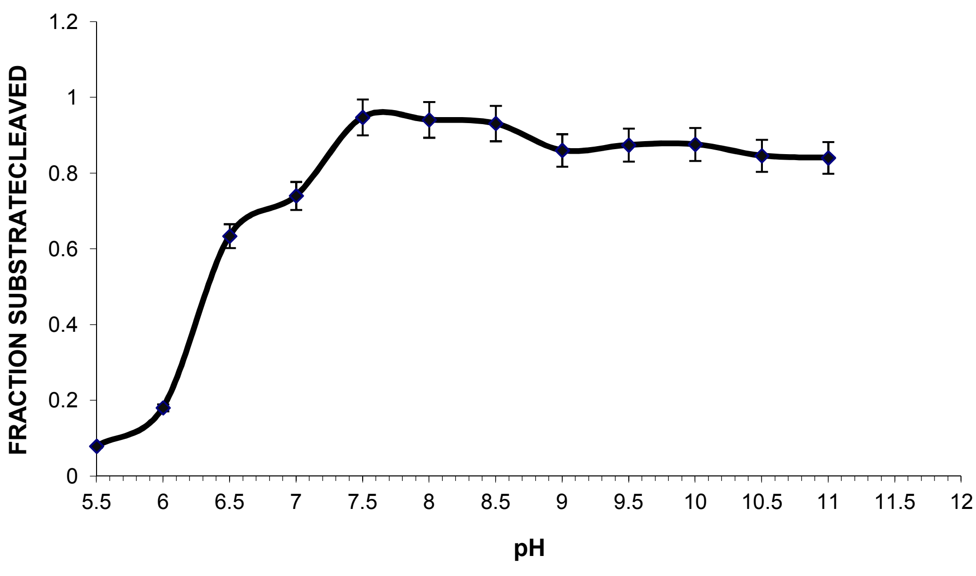

1.2
1
0.8
0.6
0.4
0.2
0
FRACTION SUBSTRATECLEAVED
5.5
6
6.5
7
7.5
8
8.5
9
9.5
10
10.5
11
11.5
12
pH

Table 1. Sustained action of antisense deoxyoligonucleotide in sub-stochiometric concentrations.

$\frac{\text{Moles of RNA}}{\text{Moles of DNA}}$	Fraction RNA Cleaved (30min)	No. of turnovers by the Antisense oligo
1	0.90	1
10	0.90	9
25	0.24	8
50	0.56	28
75	0.13	10
100	0.29	29

Figure 14. Conserved Histidine 264 is important for substrate cleavage by Hs-RNase H1.

A. Time-course assay of substrate cleavage by Hs-RNase H1 under steady-state (substrate excess) conditions. Hs-RNase H1 (10 nM) was combined with 5’-^{32}P-labeled, 21bp RNA•DNA hybrid (150 nM), then incubated at 30^{o}C in a buffer containing 150 mM NaCl, 10 mM $MgCl_2$, 25 mM HEPES (pH 7), and 10 mM DTT. Aliquots were combined with excess EDTA at the specified times, and the samples analyzed by electrophoresis in a 15% denaturing polyacrylamide gel as described in Materials and Methods. Lanes 1-6 represent 0, 1, 2.5, 5, 10 and 30 min time points, respectively.

B. Time-course assay with H264A mutant. The H264A Hs-RNase H1 mutant (10 nM) was combined with 5’-^{32}P labeled RNA•DNA hybrid (150 nM) in 150 mM NaCl, 10 mM $MgCl_2$, 25 mM HEPES (pH 7), and 10 mM DTT, and incubated at 30^{o}C. Aliquots were combined with excess EDTA at the specified times and analyzed by electrophoresis in a 15% denaturing polyacrylamide gel. Lanes 1-6 represent 0, 2.5, 5, 10, 30 and 60 min reaction times respectively.

C. Michaelis-Menten kinetic analysis. The initial rates (V_o) of substrate cleavage were obtained as a function of substrate concentration. Shown is a best-fit curve to a Michaelis-Menten kinetic scheme, with each point representing the average of two experiments. The K_m values are 107 ± 34 nM and 98 ± 21 nM, and the k_{cat} is 3.5 min^{-1} and 0.025 min^{-1} for Hs-RNase H1 and the H264A mutant, respectively.

D. The best-fit curve for a Michaelis-Menten kinetic scheme for the H264A mutant, This is an expanded graph of that for the H264A mutant in pane C. The K_m 98 ± 21 nM and the k_{cat} is 0.025 min^{-1} for H264A mutant.

A

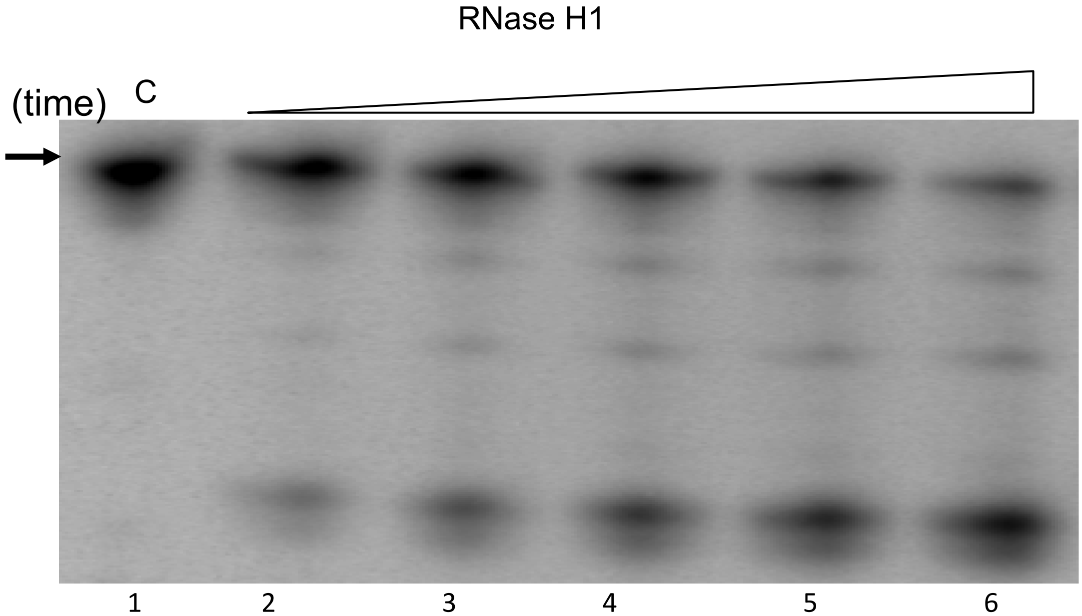

B

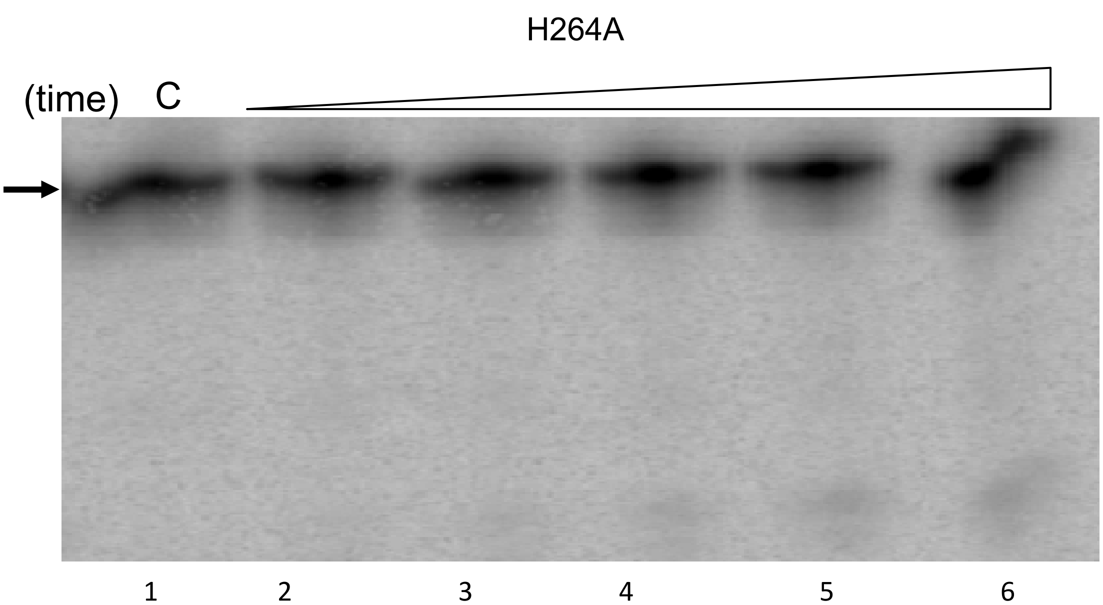

C

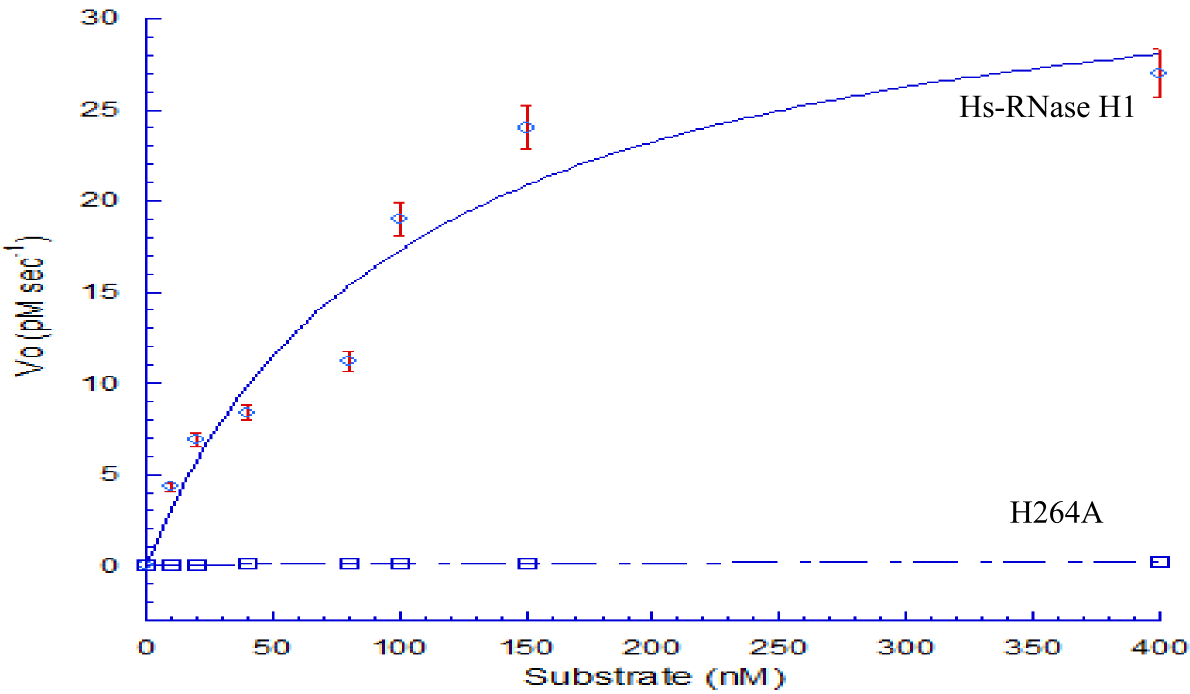
30
25
20
15
10
5
0
Vo (pM sec^{-1})
0
50
100
150
200
250
300
350
400
Substrate (nM)
Hs-RNase H1
H264A

D

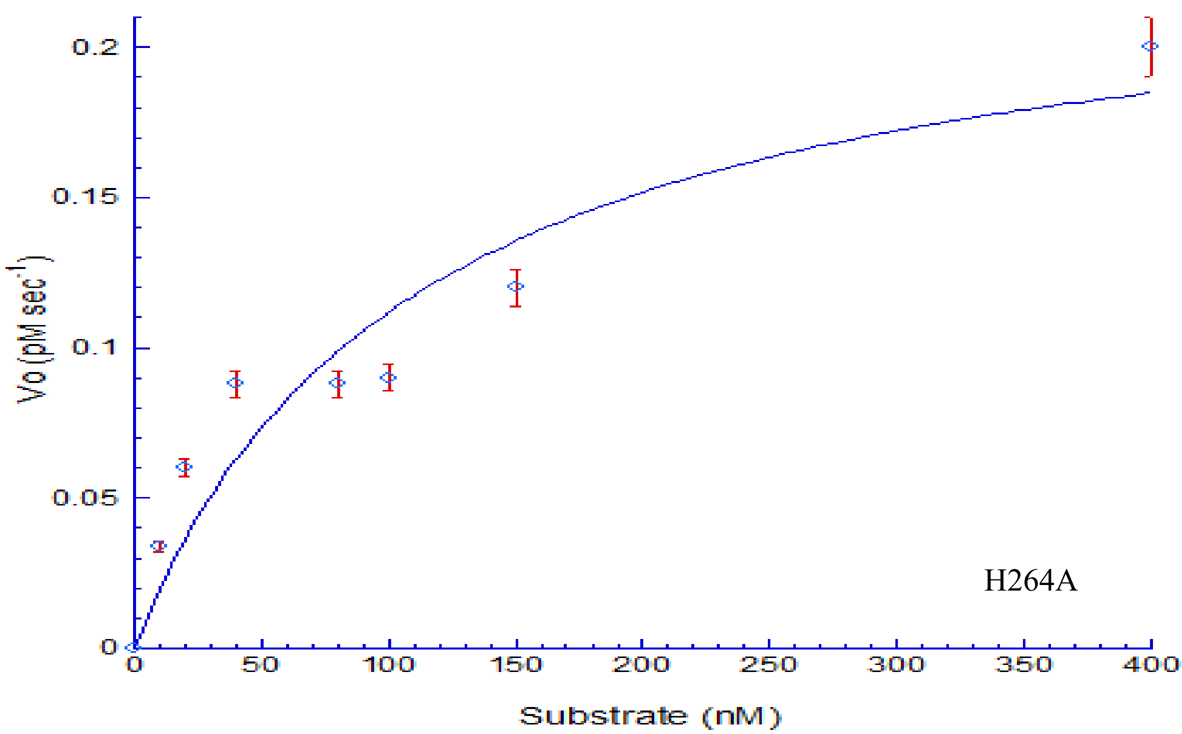
0.2
0.15
0.1
0.05
0
Vo (pM sec^{-1})
0
50
100
150
200
250
300
350
400
Substrate (nM)
H264A

Figure 15. Kinetic behavior of Hs-RNase H1 and the H264A mutant under single-turnover (enzyme excess) reaction conditions.

A. Hs-RNase H1 or H264A mutant (50 nM) was incubated at 30^{o}C with 5'-^{32}P-labeled, 21bp, c-myb RNA.DNA hybrid (5 nM) in a buffer containing 150 mM NaCl, 10 mM $MgCl_2$ 25 mM Tris-HCl (pH 7.5), and 10 mM DTT. Aliquots were combined with excess EDTA at the specified times. Lanes 1-7 display 0, 0.25, 0.5, 1, 2.5, 5 and 10 min time points for Hs-RNase H1, and lanes 8-14 display 0, 0.25, 0.5, 1, 2.5, 5 and 10 min time points for the H264A mutant, respectively. **B.** Graph showing the fraction of substrate cleaved as a function of reaction time (min). The best-fit curves to an exponential rise equation are shown.

A

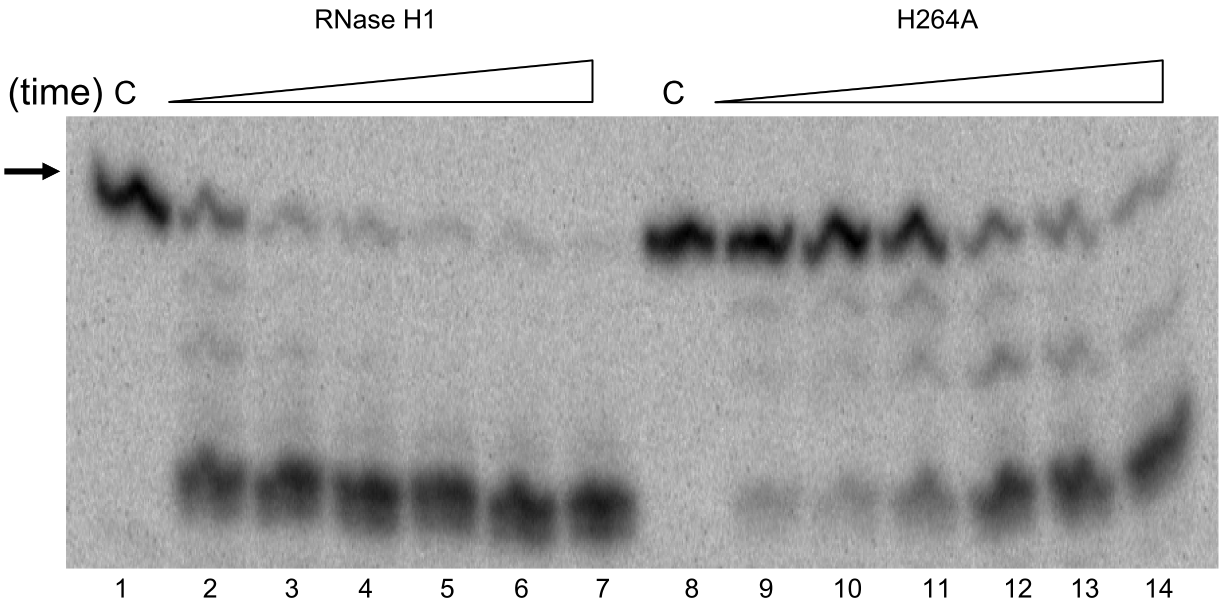
RNase H1
H264A
(time) C
C
1
2
3
4
5
6
7
8
9
10
11
12
13
14

B

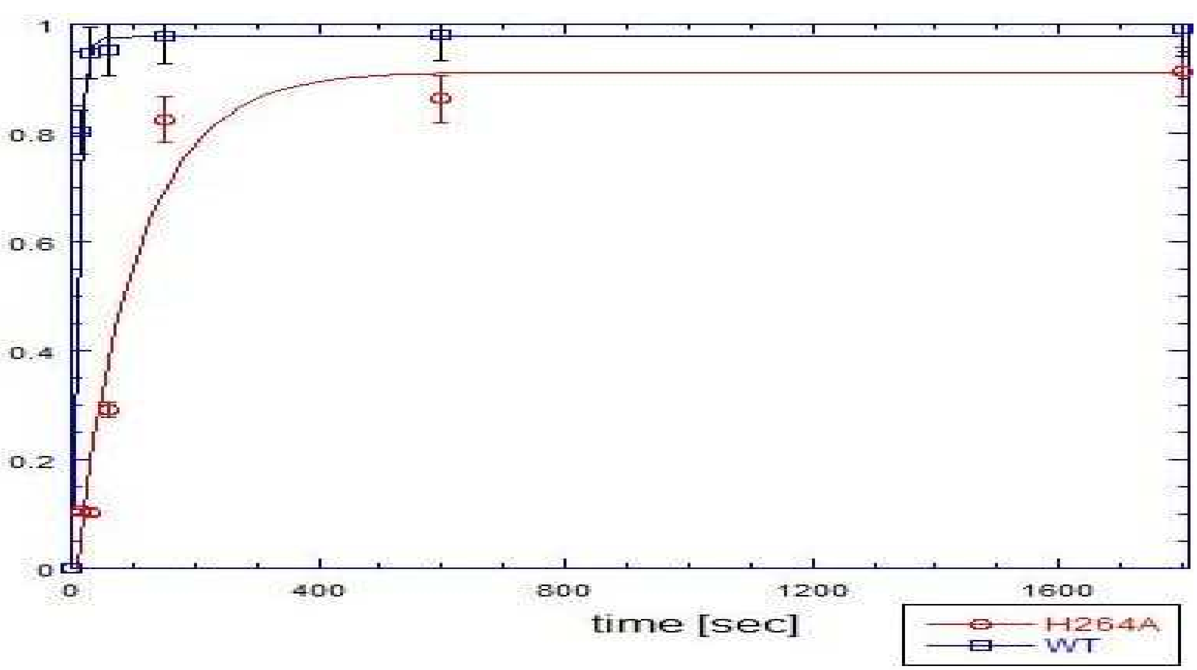
1
0.8
0.6
0.4
0.2
0
0
400
800
1200
1600
time [sec]
H264A
WT

CHAPTER 4

STRUCTURE-FUNCTION CORRELATES OF 2'-FLUOROARABINOSE (2'-FANA) OLIGONUCLEOTIDES IN RNase H1-DPENDENT OLIGO•RNA DUPLEX CLEAVAGE

4.1 Abstract and Project Overview

The gene-silencing action of antisense oligonucleotides can be significantly enhanced by specific modification of the sugar-phosphate backbone. 2'-deoxy-2'-fluoroarabinose (2'-FANA). For example, substituted AONs exhibit enhanced intracellular stability and higher affinities for their complementary RNA targets, compared to the corresponding unmodified AON (Wilds *et al*., 2000). Furthermore, the 2'-FANA-AON•RNA hybrids exhibiting specific patterns of substitutions are substrates for RNase H1. However, fully substituted 2'-FANA-AON•RNA hybrids are less reactive towards RNase H1 than as the corresponding 2'-deoxyribose AON•RNA hybrid. Mixed 2'-FANA/2'-deoxyribose AONs have been prepared, with the expectation that the mixed backbone would maintain RNase H1 reactivity of the hybrid, while preserving stability and persistence of action (Kalota *et al*., 2006). To provide an initial assessment of the functionality of 2'-FANA-substituted AONs we determined the reactivities of the corresponding hybrid towards Hs-RNase H1. RNA cleavage assays employed purified recombinant human RNase H1 and a model substrate consisting of a 21 nt RNA target sequence bound to the complementary 21 nt phosphorothioate (PS) AON exhibiting specific patterns of 2'-FANA ('F') substitutions, either at the "wings" of the molecule ("7-gapmer"; each wing=7 nt: FFFFFFF-DDDDDDD-FFFFFFF), or alternating with 3 nt segments of 2'-deoxyribose ('D') ("3-altimer": FFF-DDD-FFF-DDD-FFF-DDD-FFF). The initial rates of cleavage of hybrids containing the gapmer or altimer AON were compared to that of the all-2'-deoxyribose AON hybrid. The hybrid containing the fully 2'-FANA-substituted AON was the least reactive, and exhibited a relative initial cleavage rate (0.02) that was ~2% of the unmodified hybrid. In contrast, hybrids containing the gapmer or altimer AON exhibited relative initial rates of 0.26 and 0.88, respectively. Moreover, the processivity of Hs-RNase H1,

as measured by the amount of shorter RNA products relative to longer RNA products, increased as a function of 2'-deoxyribose substitution. We also assessed the effect of 2'-FANA substitution on binding by the RNase H1 hybrid-binding domain (HBD) and cleavage by the isolated catalytic domain, respectively.

The effectiveness of the 2'-FANA-substituted AONs in silencing gene expression in leukemia cells also was examined. Specifically, two separate sequences within the coding region of the c-myb mRNA are accessible targets for RNase H1 cleavage, mediated by either the 3-altimer or 7-gapmer. This was revealed by a decrease in both mRNA and protein levels in transfected K562 cells. It is also shown that an all-2'-FANA AON targeted to either sequence causes a significant reduction in c-myb protein levels, but in contrast to the corresponding 3-altimer or 7-gapmer AON, does not appreciably reduce the c-myb mRNA level. The insensitivity of c-myb mRNA levels to the all-2'-FANA AON is consistent with the negligible RNase H1 reactivity *in vitro* of the all-FANA·AON RNA hybrid. However, the strong reduction in c-myb protein level indicates a potent selective inhibition of translation. Given the high thermodynamic stability of all-2'-FANA AON·RNA hybrids, the mechanism of inhibition may involve a steric block to ribosome progression past the position of all-2'-FANA AON binding in the c-myb mRNA sequence.

4.2 Introduction

An antisense oligonucleotide (AON) can bind to a complementary sequence in an mRNA and block production of the encoded protein by several mechanisms: In one mechanism, AON binding creates a steric block to ribosome movement and/or codon recognition. In another mechanism, AON binding leads to RNase H1 cleavage of the mRNA at the AON binding

(Walder *et al*., 1988). Elicitation of RNase H1 cleavage of the target mRNA has been considered to be the more efficient of the two mechanisms for gene silencing, since the AON can act in a catalytic manner by directing the cleavage of many copies of the mRNA, even including newly-synthesized transcripts. Initial studies with unmodified oligodeoxynucleotides revealed limited antisense activity since they were rapidly degraded by nucleases *in vivo* (Wang *et al*., 1994; Wang *et al*., 1995). Replacement of the phosphodiester linkage with phosphorothioate (PS) linkages improved resistance to nuclease degradation, but decreased the affinity for the target RNA sequence. Subsequently, many additional modifications have been made, with the goal of improving gene silencing by increasing AON affinity for the target, as well as retaining RNase H1 reactivity. The most favored of these are 2'-*O*-alkyl modifications such as 2'-O-Methyl and 2'-O-Methoxyethyl (MOE) groups (Agarwal *et al*., 1997; Monia *et al*., 1993). These modifications favor the $C_{3'}$-endo sugar conformation in the AON, which in turn increases the stability of the corresponding RNA·DNA hybrid. While an enhanced stability of the heteroduplex may be advantageous, it is often associated with a drop in reactivity towards RNase H1, which is important for efficient gene silencing (Lok *et al*., 2002). To date there are only several types of modification that allow cleavage of the hybrid by RNase H1, with varying levels of efficiency. These include modified sugars such as arabinonucleic acids (ANAs), cyclohexene nucleic acids (CeNAs), and 2'-FANA (Damha *et al*., 1998; Noronha *et al*., 2000; Wilds *et al*., 2002). 2'-FANA AONs are of particular interest, due to the high stability of the corresponding heteroduplexes, compared to the ANA or CeNA-containing heteroduplexes. The 2'-FANA nucleotide conformation more closely mimics that of 2'-deoxyribose in the heteroduplex structure (Ikeda *et al*., 2002).

The cellular proto-oncogene c-myb is the target of somatic mutations and translocations in human cancers (Clappier *et al.,* 2007; Persson *et al.*, 2009). The c-Myb protein functions as an important transcription regulator in normal stem cells and progenitor compartments (Gifford *et al*., 2005; Opalinska *et al*., 2004), and also is required for the maintenance of leukemia stem cells (Min *et al*., 2002). The inhibition of c-Myb function is known to prevent initiation of leukemogenesis by eleven Mixed-lineage leukemia-eleven nineteen leukemia MLL-ENL (Hess *et al*., 2006) and also has antiproliferative effects in certain types of leukemic cells (Luger *et al*., 2002). Since suppression of c-Myb function does not have significantly adverse effects on normal hematopoiesis, a potential therapeutic strategy opens up for treating leukemia. The results presented below include both *in vitro* and cell-based studies that compare the ability to direct Hs-RNase H1 action on a model hybrid, and gene silencing efficiency of different types of 2'-FANA oligonucleotides targeted to an accessible 21 nt sequence in the c-Myb RNA. AONs with alternating stretches of three or seven 2'-FANA residues exhibit better potency than AONs fully-substituted by 2'-FANA, or in addition containing an alkyl linker.

4.3 Results

4.3.1 Dependence of hybrid reactivity on the pattern of 2'-FANA substitution in the AON.

Oligodeoxynucleotides containing specific patterns of 2'-FANA substitution (Table 2) were prepared and tested for their ability to direct Hs-RNase H1 cleavage of RNA in vitro. This analysis was informed by a previous demonstration of the ability of 2'-FANA-substituted AONs to support RNase H1-mediated cleavage of other RNA targets (Damha *et al*., 1998; Damha *et al*., 2001). Each AON (in P(S) form) was hybridized to the 21nt, 5'-^{32}P-labeled RNA (Table 2) to form the corresponding heteroduplex substrate. Each substrates was incubated with purified Hs-RNase H1, and aliquots were removed at specific times and quenched with excess EDTA, followed by gel electrophoretic separation. Phosphorimaging (Fig. 17, 18 and 19) and quantitation allowed determination of the relative reactivities as well as the specific sites of cleavage. The order of hybrid reactivity is as follows: All-2-deoxy > 3-Altimer > 7-Gapmer > All-2'-FANA (11-9-linker) > All-2'-FANA) (Fig. 17, 18 and 19). These results show that the ability of an AON to direct Hs-RNase H1 cleavage of the RNA is dependent upon the pattern of 2'-FANA substitution. The presence of phosphorothioate linkages has a modest effect on hybrid substrate reactivity: under conditions of substrate excess, the initial rate of cleavage of the substrate with P(S) AON was ~3-fold less than the reaction with the P(O) AON. The hybrid with the All-2'-Deoxy AON was 4-fold more reactive than the corresponding 3-altimer substrate; ~5-fold greater than the 7-gapmer substrate; and ~40-fold greater than the All-2'-FANA and All-2'-FANA [9,10 linker] substrates (Table 2). Analysis of the reaction products on sequencing gels showed the predominant 5'-end-containing cleavage products to be 5 to 6 nucleotides in length, but that longer cleavage products are observed in reactions involving AONs with a higher level of 2'-FANA substitution (Fig. 16). The accumulation of longer products may be explained by a reduction in processivity of RNase H1 when the hybrid contains a 2'-FANA AON. Interestingly, the All-2'-FANA hybrid substrate appears as if it has under gone only one round of cleavage. Perhaps the cleaved product remains tightly bound to the enzyme, interfering with the product release step. It also is noteworthy that the reactivity of the substrate containing the All-2'-FANA is only modestly increased when a (9,10) alkyl linker is introduced (Fig. 17, 18 and 19). The slow rate of cleavage of the All-2'-FANA and All-2'-FANA[9,10 alkyl linker] substrates may reflect the rigidity of the hybrid structures, consistent with the their higher Tm values (Watts *et al*., 2007). The modest increase in the rate of cleavage afforded by the ethyl linker may reflect the increased flexibility provided by the 9, 10 alkyl linker.

4.3.2 RNase H1 binding affinities of 2'-FANA hybrids substrates

Hybrids containing 2'-FANA-substituted AONs were examined for their affinities for the N-terminal hybrid-binding domain (HBD) of Hs-RNase H1. The K'_D values were determined by quantitation of gel mobility shift assays (Fig. 20 and 21). The HBD-binding affinities of the hybrids follow the order: (all-2'deoxy) P(O) > 3-Altimer (P(S)) > 7-gapmer (P(S)) > P(S) AON (Fig. 21). The K'_D values for All-2'-FANA and All-2'-FANA [9,10 linker]-containing hybrids could not be determined by the gel shift assay (Fig. 20 and 21), since the complexes were too weak to survive electrophoresis. The low binding affinity of the latter hybrids may reflect the lack of flexibility conferred by full 2'-FANA substitution, or through steric clash of the fluorine atoms with HBD functional groups. The comparable affinities of the P(S) 3-altimer and the All-2'-Deoxy hybrid substrates P(O) suggests that the slightly lower cleavage reactivity of the 3-altimer and 7-gapmer hybrid substrates compared to the P(O) AON, reflects an inhibition of the catalytic step, not the HBD-binding step. A second complex of lesser mobility is observed at higher HBD concentrations for the All-2'-Deoxy P(O) and P(S) AON hybrid substrates (Fig. 20 and 21). These complexes may consist of two HBDs binding to the hybrid.

4.3.3 Assessing the gene-silencing action of 2'-FANA antisense oligonucleotides

The K562 line of human leukemia cells expresses high levels of c-Myb protein, and has been used in analyses of antisense oligonucleotide efficacy in gene silencing (Kalota *et al*., 2006). This cell line was used as a model system to evaluate the efficiency of 2'-FANA-containing antisense oligonucleotides in reducing c-Myb levels. The oligonucleotides were targeted to a 21-nt segment of c-Myb mRNA that was previously shown to be accessible to oligonucleotide hybridization (Gifford *et al*., 2005). The efficiency of silencing was compared with a previously-characterized P(S)-DNA that is able to significantly reduce c-Myb levels (Opalinska *et al*., 2004). Table 2 provides the sequences and compositions of the four examined P(S)-2'-FANA-containing oligonucleotides. The AONs include the 2'-FANA 3-altimer, the 2'-FANA 7-gapmer, the All-2'-FANA oligonucleotide, and the All-2'-FANA[9,10 alkyl linker] oligonucleotide. A control oligonucleotide with a "scrambled" sequence (with the original sequence randomly reassorted) was included in each assay. Each AON (5 μg) was separately transfected into K562 leukemia cells by nucleofection. After 48 h, cells were harvested, and levels of c-myb RNA and protein were measured using qRT-PCR and western blotting, respectively. The results were compared with untreated cells, or mock treated cells (Fig. 22 A, B and C) whose RNA and protein levels were arbitrarily set at 100%. The 3-altimer AON inhibited c-Myb mRNA expression by 67%. The 7-gapmer, All-2'-FANA and All-2'-FANA[9,10 linker] oligonucleotides caused 65%, 53%, 24% and 15% reduction in c-Myb mRNA levels, respectively (Fig. 22 A, B and C). Neither mock transfection nor treatment with any of the scrambled sequence AONs caused a reduction in mRNA levels greater than 16%. Western analysis revealed that cells treated with the P(S), 3-altimer, 7-gapmer and All-2'-FANA AONs decreased c-myb protein levels by 95%. Notably, unlike the P(S) DNA, 3-altimer and 7-gapmer, the All-2'-FANA AON had no effect on c-myb mRNA levels over and above the control reactions, but decreased the c-Myb protein level. This could be explained if All-2'-FANA AON acts by blocking mRNA translation, rather than directing mRNA cleavage by RNase H1. Therefore, the All-2'-FANA AON exerts silencing of c-Myb expression by a distinctly different mechanism, perhaps through a translational block.

4.4 Discussion

In ongoing efforts to develop AONs with highly effective gene silencing abilities, there is continuing interest in understanding the substrate preferences of the RNase H family enzymes, and the structural features or modifications of antisense oligonucleotides that affect hybrid stability and reactivity. One highly promising modification is the 2'-FANA sugar. First, 2'-FANA nucleotides are more resistant to hydrolytic cleavage of the N-glycosidic bond, due to electronic effects of adjacent fluorine atom, which is highly electronegative (Maryam *et al*., 2010). Second, 2'-FANA AONs exhibit greater resistance to endonucleases and exonucleases, and this resistance is significantly enhanced if the 2'-FANA oligonucleotides also contain phosphorothioate internucleotide linkages (Watts *et al*., 2009). Third, substitution with 2'-FANA sugars increases the stability of the hybrid. In this regard it has been shown that the T_m increases by ~1.5°C per 2'-FANA nt substitution (Damha *et al*., 1998; Wild *et al*., 2000). Fourth, 2'-FANA AONs are the first examples of RNase H1-competent AONs that are not based on 2'-deoxy-D-ribofuranose residues. Although the stability of the hybrid structure at the mRNA target site is important for effective gene silencing, the additional ability of the hybrid to be cleaved by RNase H1 also is critical for this action (Lok *et al*., 2002; Wilds *et al*., 2002). Substitution by 2'-FANA does not significantly perturb the helical structure of the hybrid, and therefore retains significant structural similarity to the unmodified (native) DNA·RNA hybrids (Damha *et al*., 2001; Denisov *et al*., 2001; Tempe *et al*., 2001). Since 2'-FANA can be regarded as a structural mimic of 2'-deoxyribose (Denisov *et al*., 2001; Tempe *et al*., 2001), RNase H1 can recognize and cleave at both 2'-FANA·RNA and DNA·RNA segments in the hybrid substrate. In contrast, RNase H1 cleavage occurs only across the DNA gap in 2'-O-alkyl gapmer hybrid substrates. The greater stability of 2'-FANA·RNA hybrids may reflect a conformational pre-organization of the oligonucleotide, that reduces the entropic penalty for heteroduplex formation. Crystallographic data (Berger *et al*., 1998; Fedorff *et al*., 1993) indicates the adoption of an O4'-endo (East) sugar pucker by 2'F-ANA residues, which is a conformation that lies between C2'-endo (South) and C3'-endo (North) puckers. It was subsequently demonstrated that RNase H1 recognizes the East conformation of the sugar in the DNA strand of DNA·RNA duplexes (Salazar *et al*., 1993). Also, the optimal conformation includes the bases in the anti conformation about the glycosidic bond. The presence of 2'-F atoms provides a network of pseudohydrogen bonds that stabilizes this conformation.

For the reasons summarized above was surmised that 2'-FANA-modified AONs would provide more potent therapeutic action. The ability of the AONs to serve as antisense-based drugs was assessed by (i) testing the ability to elicit RNase H1 action in vitro, and (ii) gene silencing in a leukemia cell line. The data show that the 2'-FANA 3-altimer and 7-gapmer AONs have comparable ability to elicit RNase H1 in that they decrease mRNA and protein levels compatible with the corresponding unmodified DNA. In contrast to the 3-altimer or 7-gapmer, the All-2'-FANA AON decreases c-Myb protein levels, but not c-Myb mRNA levels, suggesting a block to c-myb mRNA translation, rather than mRNA cleavage, as the mechanism of inhibition. Gene silencing by AONs with these modification is superior, as the dose needed is lower, and the effects are more persistent as compared to the corresponding (phosphorothioate) DNA oligonucleotide.

In summary, this study supports the continued examination of the potential therapeutic utilization of the 2'-FANA modification in AONs. The highly efficient inhibition of protein expression is the primary goal of all antisense therapeutic strategies, and the data suggest that the 2'-FANA modification supports sustained silencing after a single administration, either by mRNA cleavage or by a translational block, and at substantially lower concentrations compared to the unmodified AON. These findings underscore the proposal that 2'-FANA modified AONs will ultimately be an important addition to the repertoire of rational antisense strategies for effective treatment of disease.

TABLE 2. Sequences, and designations and reactivities of AONs, and reactivities of the corresponding substrate.

	SEQUENCE	DESIGNATION	INITIAL VELOCITY(Vo) of cleavage of hybrid (nmol/sec)
1	5'-caacgtttcggaccgtatttc-3'	P(O)	0.93
2	5'-caacgtttcggaccgtatttc-3'	P(S)	0.37
3	5'-CAAcgtTTCggaCCGtatTTC-3'	3-Altimer	0.29
4	5'-CAACGTTtcggaccGTATTTC-3'	7-Gapmer	0.16
5	5'-CAACGTTTCGGACCGTATTTC-3'	All FANA	0.02
6	5'-CAACGTTTCEGACCGTATTTC-3'	9,11 linker	0.02

All nucleotides are linked by phosphorothioate bridges except for P(O) which contains phosphodiester linkages. Upper case letters indicate 2'-FANA modified nucleotides. Lower case letters indicate unmodified nucleotides. 'E' indicates an ethyl alcohol 9,10 anucleosidic (alkyl) linkage (Mangos *et al*., 2003).

Figure 16. Time course for cleavage of substituted hybrid substrates in vitro by Hs-RNase H1. Shown is a phosphorimage of a sequencing gel, displaying cleavage of specific RNA•DNA hybrids by Hs-RNase H1. Reactions were carried out essentially as described in Materials and Methods, 40 nM Hs-RNase H1 and 100 nM hybrid substrate. Reaction times are given at the top of the gel image. "P1" refers to P1 nuclease reaction. Arrows indicate the main (and also final) products of cleavage (5 and 6 nt in length) in the 2'-deoxy P(O) and P(S) AON reactions. "0" indicates a control where RNA was combined with enzyme in the absence of Mg^{2+}, then 95% formamide/20 mM EDTA immediately added, and the samples analyzed as described. The star at the lower left indicates the position of a nonenzymatic cleavage product of the 5'-^{32}P-labeled RNA.

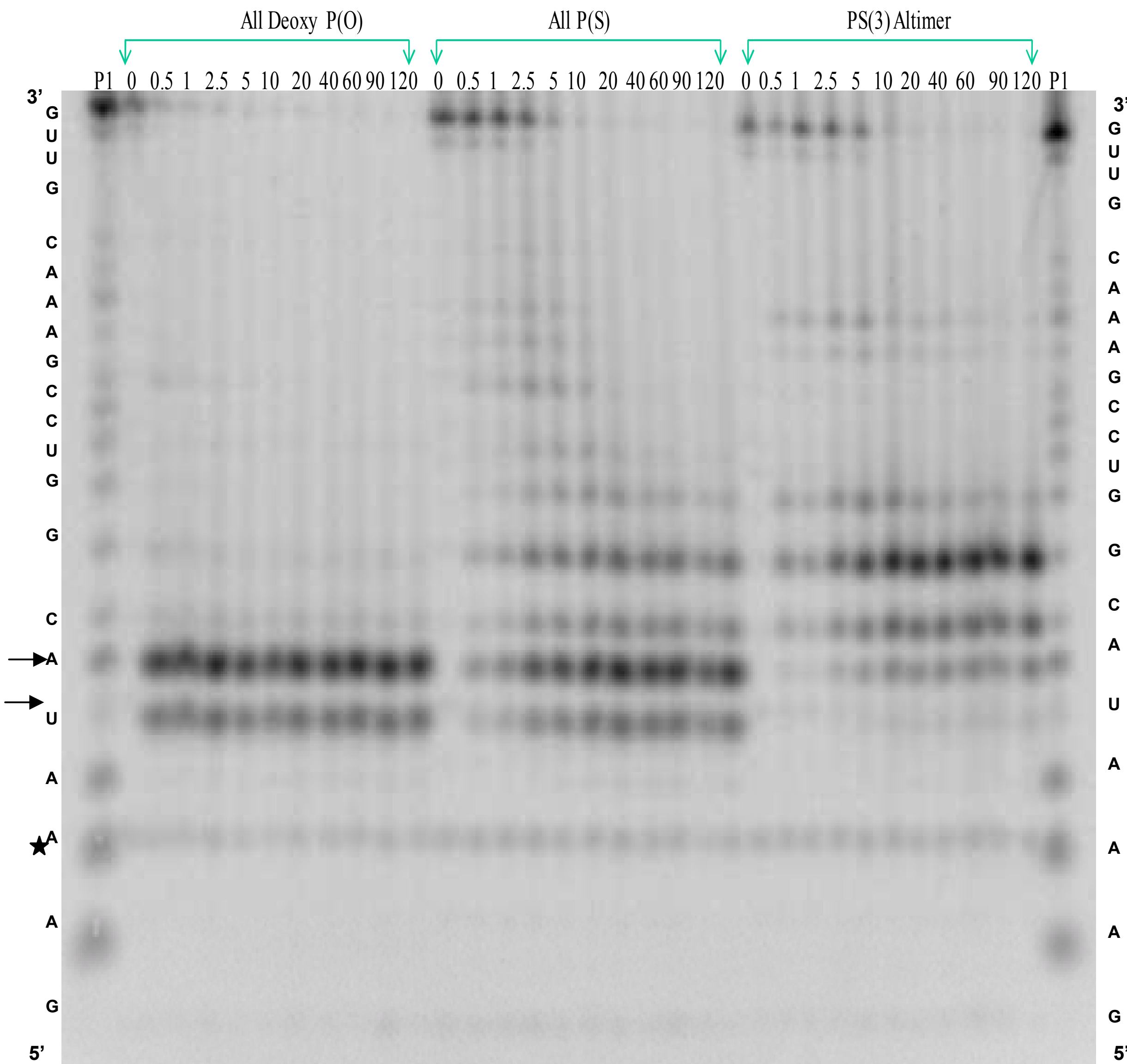
All Deoxy P(O)
All P(S)
PS(3) Altimer
P1 0 0.5 1 2.5 5 10 20 40 60 90 120 0 0.5 1 2.5 5 10 20 40 60 90 120 0 0.5 1 2.5 5 10 20 40 60 90 120 P1
3'
G U U G C A A A G C C U G G C A U A A A G
5'
3'
G U U G C A A A G C C U G G C A U A A A G
5'

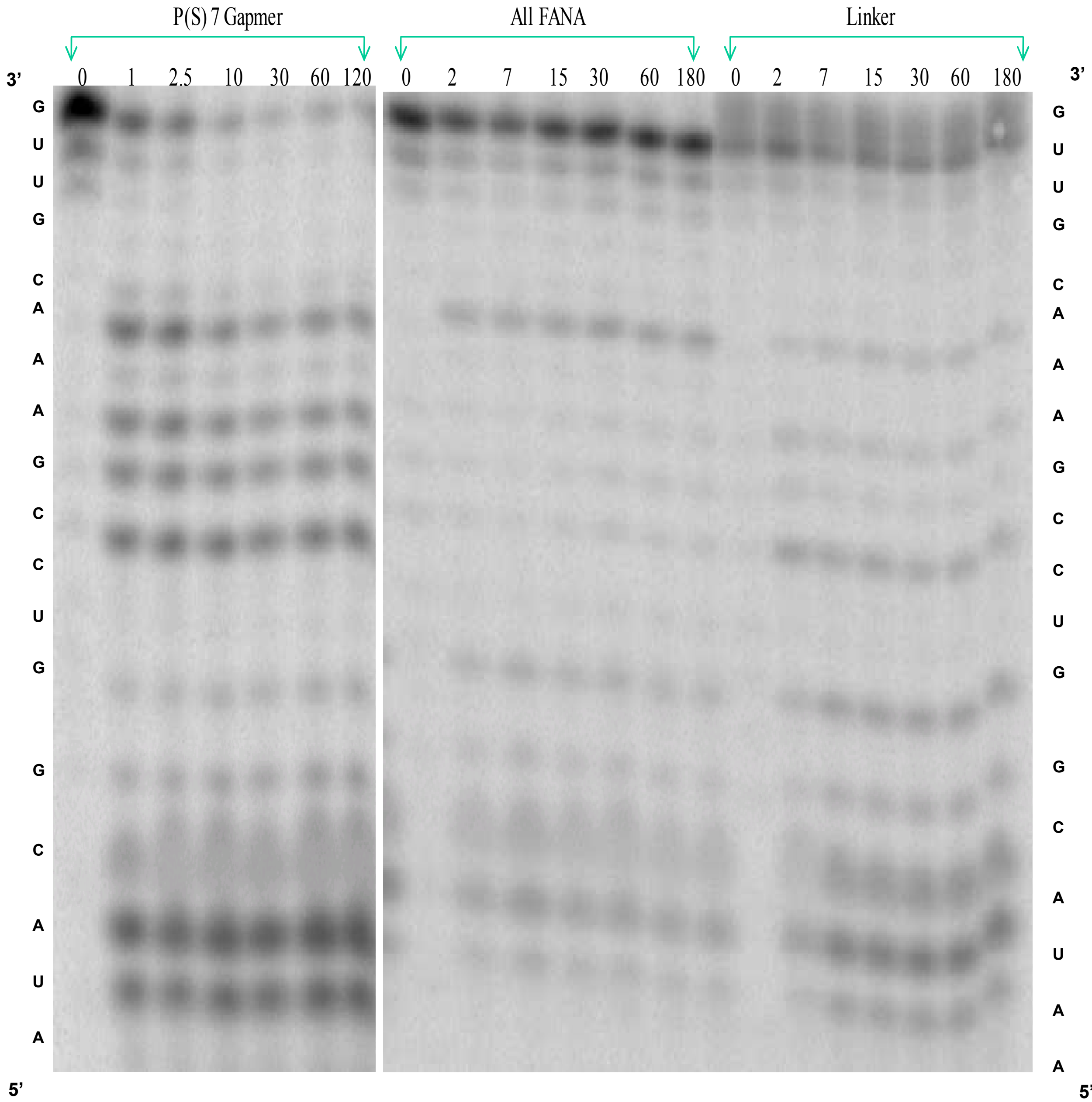

P(S) 7 Gapmer
All FANA
Linker
3'
0 1 2.5 10 30 60 120
0 2 7 15 30 60 180
0 2 7 15 30 60 180
3'
G
U
U
G
C
A
A
A
G
C
C
U
G
G
C
A
U
A
5'
G
U
U
G
C
A
A
A
G
C
C
U
G
G
C
A
U
A
A
5'

Figure 17. Denaturing polyacrylamide gel analysis of Hs-RNase H1 of hybrid substrate. Time course substrate cleavage reactions were performed as described in Materials and Methods. The 15 cm long gels were used to quantitate rates and extent of substrate cleavage. Lanes 1 and 8 in each set of experiments (A, B, C) represent a control reaction that was assembled in the absence of Mg^{2+}, then immediately added to 95% formamide, 20 mM EDTA. A. Cleavage assay carried out in the presence of 40 nM Hs-RNase H1 and all 2'-deoxy P(O)•RNA, all 2'-deoxy P(S) •RNA hybrid substrates. The reaction times for lanes 2-7 and 9-14 were: 30s, 1 min, 2.5 min, 10 min, 30 min, and 60 min respectively. B. Cleavage assay carried out in the presence of 30 nM Hs-RNase H1 and 3-Altimer P(S)•RNA, 7-Gapmer•RNA hybrid substrate. The reaction times for lanes 2-7 and 9-14 were: 30 s, 1 min, 2.5 min, 10 min, 30 min, and 60 min respectively. C. Cleavage assay carried out in the presence of 30 nM Hs-RNase H1 and 9, 10 linker•RNA and all FANA•RNA hybrid substrate. The reaction times for lanes 2-7 and 9-14 were: 2 min, 7 min, 15 min, 30 min, 60 min, and 180 min respectively.

DNA: Denoted as green spheres

2'-FANA: Denoted as shaded white spheres

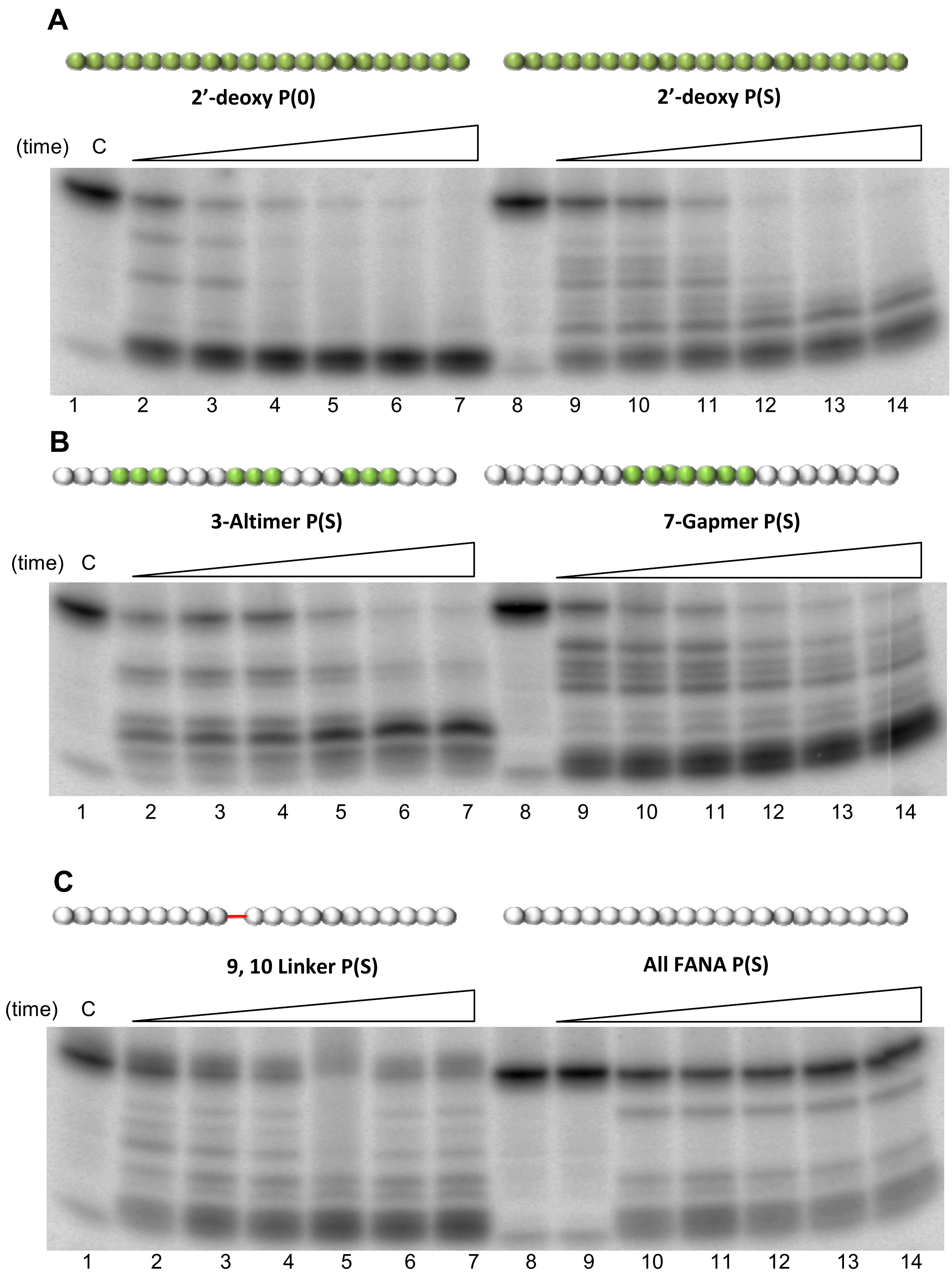
A
2’-deoxy P(0)
2’-deoxy P(S)
(time) C
1 2 3 4 5 6 7 8 9 10 11 12 13 14
B
3-Altimer P(S)
7-Gapmer P(S)
(time) C
1 2 3 4 5 6 7 8 9 10 11 12 13 14
C
9, 10 Linker P(S)
All FANA P(S)
(time) C
1 2 3 4 5 6 7 8 9 10 11 12 13 14

Figure 18. Time course assay of Hs-RNase H1 cleavage of 2'-FANA•RNA hybrid substrates.

The RNA.DNA hybrid substrate consisted of a 21 nt segment of the c-myb mRNA, and a complementary oligodeoxynucleotide containing phosphorothioate linkages, and with specific patterns of 2'-FANA substitution. Cleavage assays involved 100 nM hybrid (RNA 5'-^{32}P-labeled), and 40 nM Hs-RNase H1. The reaction temperature was 30˚C, and the buffer consisted of 150 mM KCl, 10 mM $MgCl_2$, and 20 mM Tris-HCl (pH 7.5). $MgCl_2$ was added to initiate the reaction. Aliquots were removed at the indicated times, and added to an equal volume of 95% deionized formamide containing 20 mM EDTA. Samples were heated at 95˚C for either 2 min (AON or 3-altimer hybrids) or for 5 min. (7-altimer, 9,10-Linker, or the all-2'-FANA hybrids) prior to electrophoresis in a 15% polyacrylamide gel (15 cm length) containing 7M urea in TBE. The 15 cm length gels facilitated the determination of cleavage rates. The gel lanes were visualized by phosphorimaging (Typhoon 9400 System), and evaluated using ImageQuant software. The amount of remaining (uncleaved) hybrid was determined along with the total amount of cleaved RNA. From these values the fraction of RNA cleaved was determined. This number includes any and all cleavage events that act on the full-length substrate to create shorter RNA products. The points on the graph represent the average of two experiments, with the maximum error $\leq$ 20%. "AON" (solid diamonds) refers to the hybrid containing the (unmodified) 21 nt P(O) oligodeoxynucleotide. "P(S)" (open squares) refers to the phosphorothioate-substituted [(P(S)] oligodeoxynucleotide. "3 ALT" (solid triangles) refers to 2'-FANA 3-altimer [P(S)]; "7 ALT" (X symbol) refers to the 2'-FANA 7-altimer[P(S)]; "linker" (asterisk) refers to the all-2'-FANA AON [P(S)] containing a single ethyl linker; and "All-FANA" (open circles) represents the P(S), All-2'-FANA AON. Note that the all the hybrids with the exception of the All-2'-FANA hybrid, are completely cleaved, with the most reactive hybrid cleaved within ~2.5 min. For the All-2'-FANA containing hybrid, the maximal extent of cleavage plateaus at ~30-40%, suggesting a qualitatively different kinetic behavior, compared to the hybrids with the other AONs.

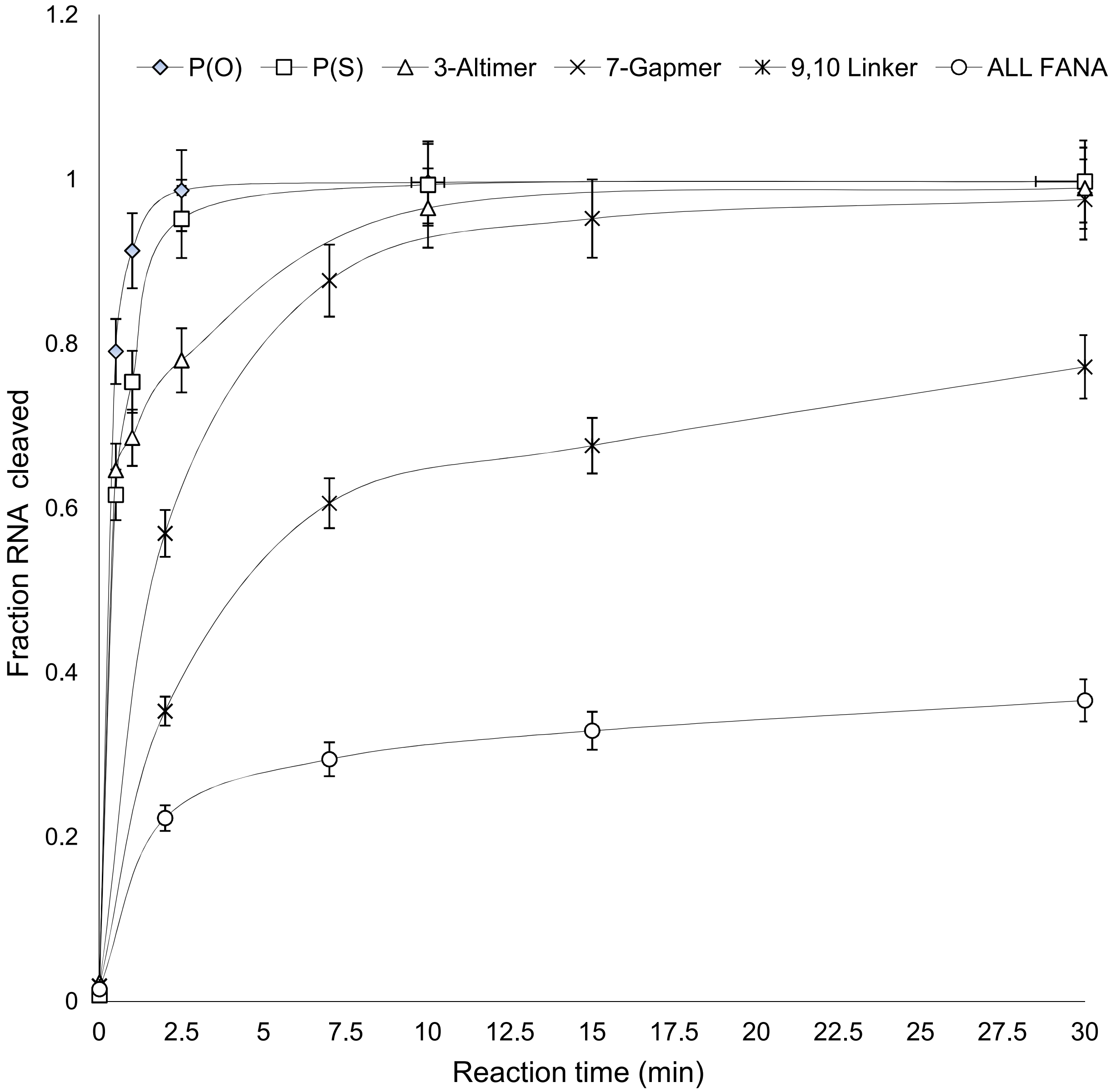

1.2
1
0.8
0.6
0.4
0.2
0
Fraction RNA cleaved
P(O)
P(S)
3-Altimer
7-Gapmer
9,10 Linker
ALL FANA
0
2.5
5
7.5
10
12.5
15
17.5
20
22.5
25
27.5
30
Reaction time (min)

Figure 19. **Initial velocities of cleavage of hybrids containing substituted AONs**. Initial velocities were determined by plotting the fraction of substrate cleaved as function of time (sec). The slope of the linear represents the initial velocities.

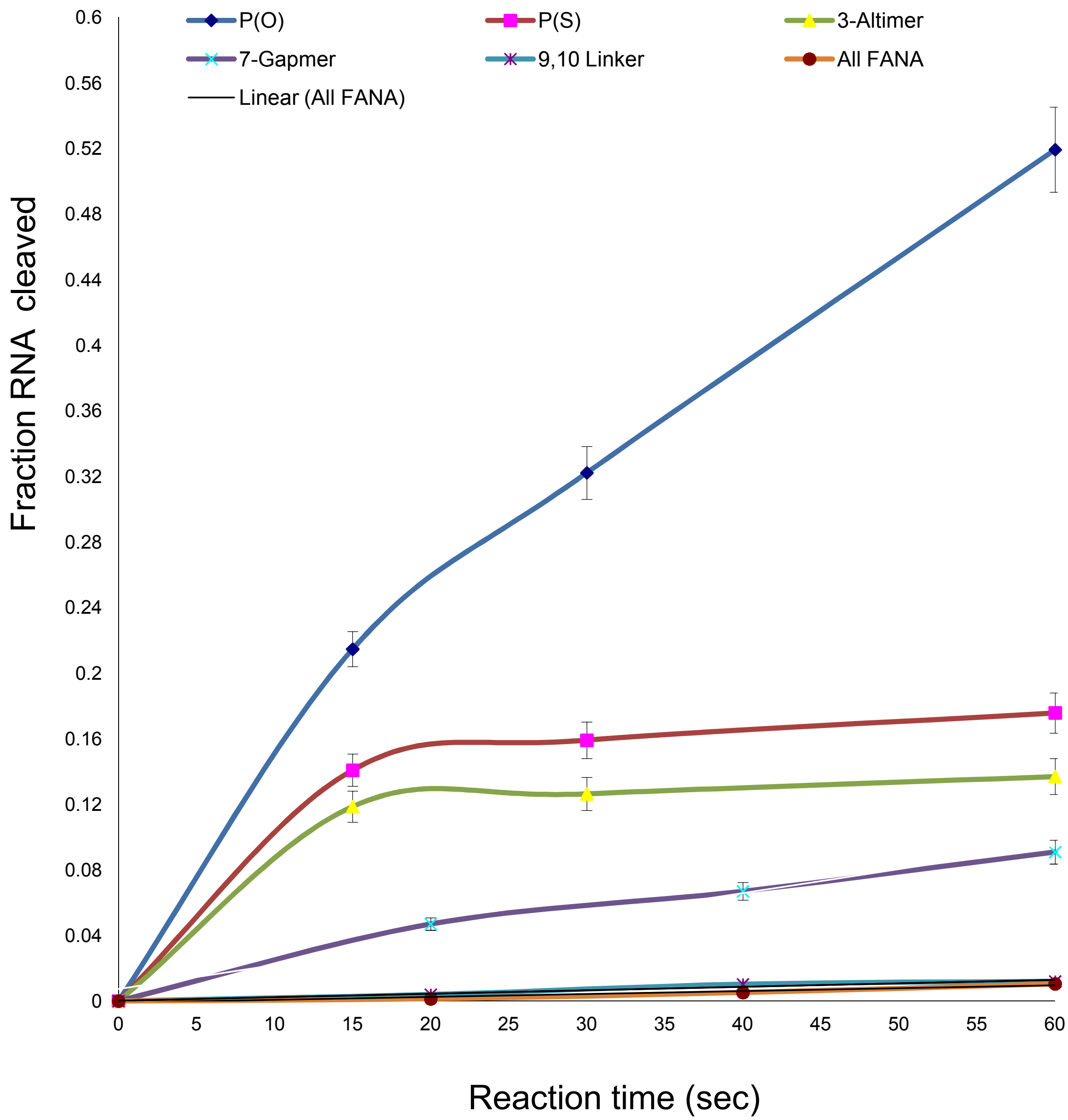

P(O)
P(S)
3-Altimer
7-Gapmer
9,10 Linker
All FANA
Linear (All FANA)
Fraction RNA cleaved
Reaction time (sec)
0
0.04
0.08
0.12
0.16
0.2
0.24
0.28
0.32
0.36
0.4
0.44
0.48
0.52
0.56
0.6
0
5
10
15
20
25
30
35
40
45
50
55
60

Figure 20. Binding affinities of P(S) 2'-FANA substituted hybrids for Hs-RNase H1. Binding isotherms of hybrid substrates DNA•RNA (A) 3- altimer•RNA (B) 7-Gapmer•RNA (C) 9,10 Linker•RNA (D) and All 2'-FANA•RNA . Gel mobility shift assay experiments were carried out in 150 mM KCl, 25 mM Tris-HCl (pH 7.5) and 10 mm DTT at increasing concentrations of the purified Hs-RNase H1. The values shown are an average of at least two experiments.

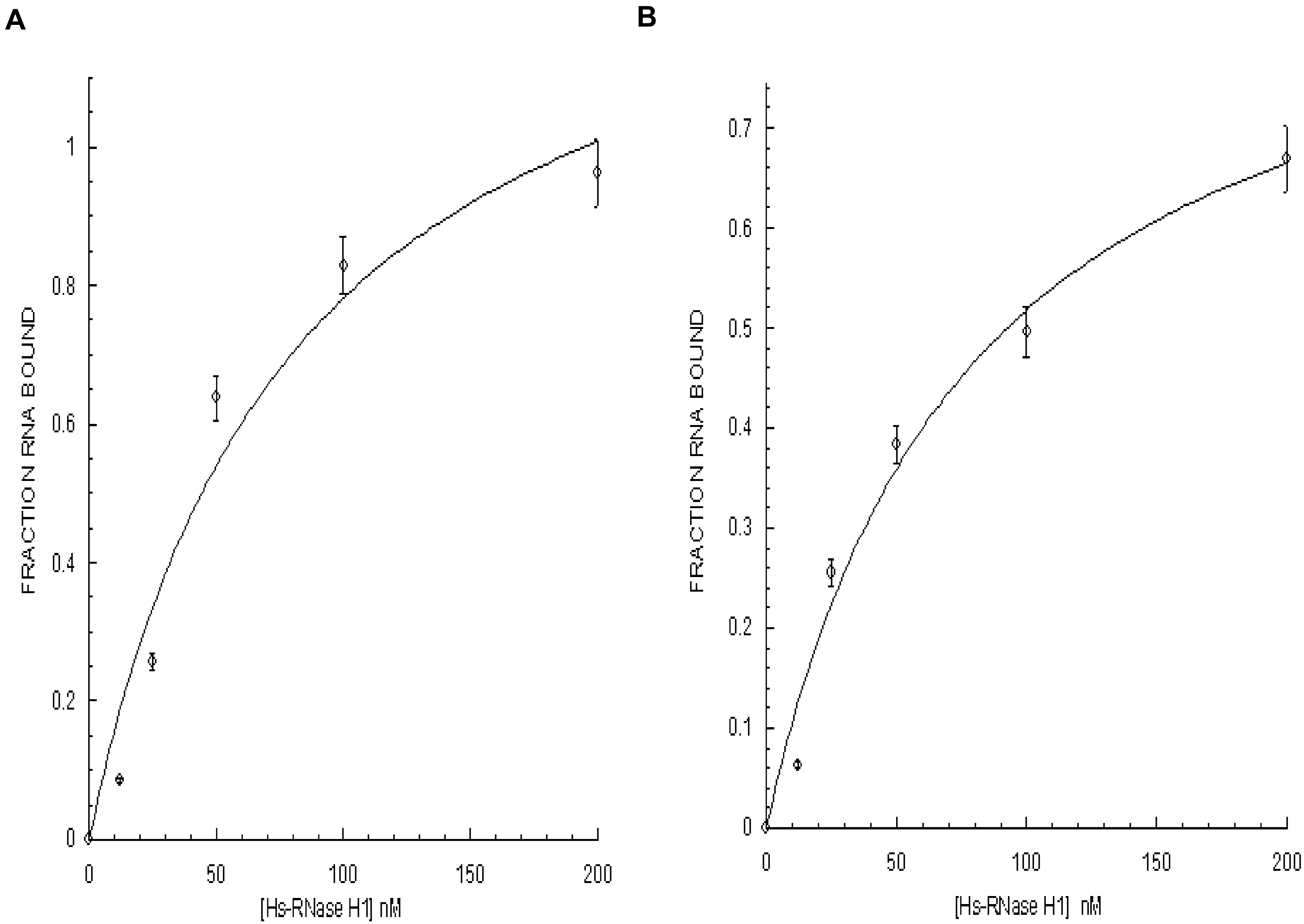
A
B
FRACTION RNA BOUND
[Hs-RNase H1] nM
0
0.2
0.4
0.6
0.8
1
50
100
150
200
0.1
0.3
0.5
0.7

C

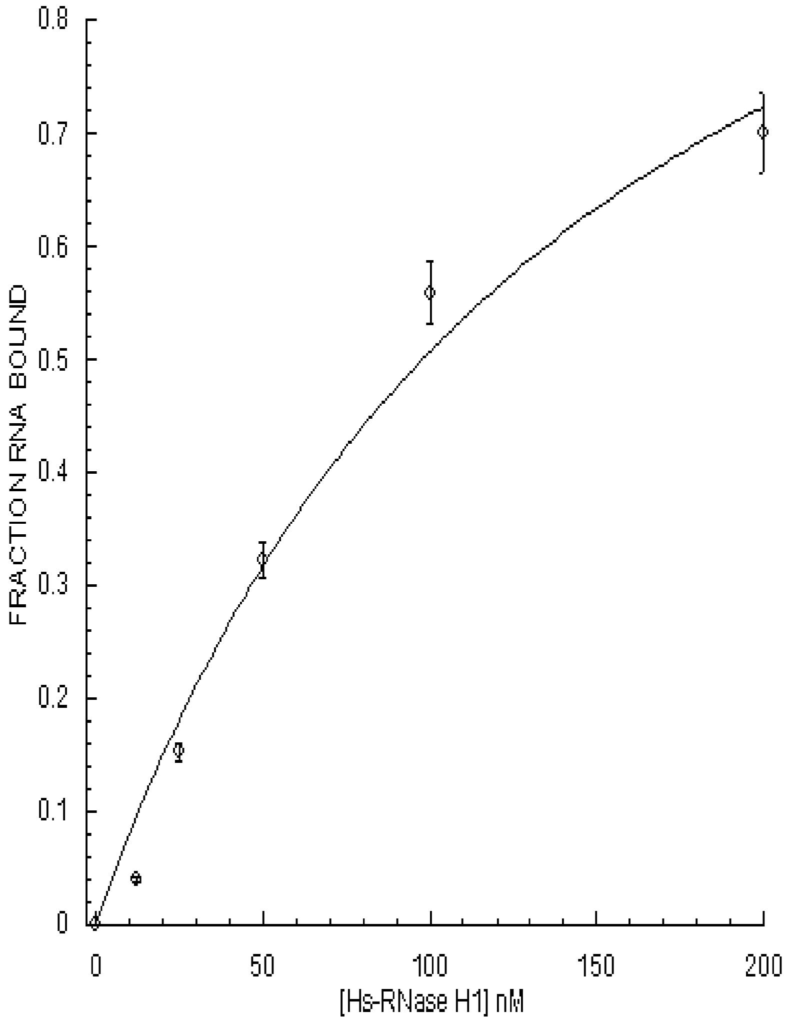

0.8
0.7
0.6
0.5
0.4
0.3
0.2
0.1
0
FRACTION RNA BOUND
0
50
100
150
200
[Hs-RNase H1] nM

D

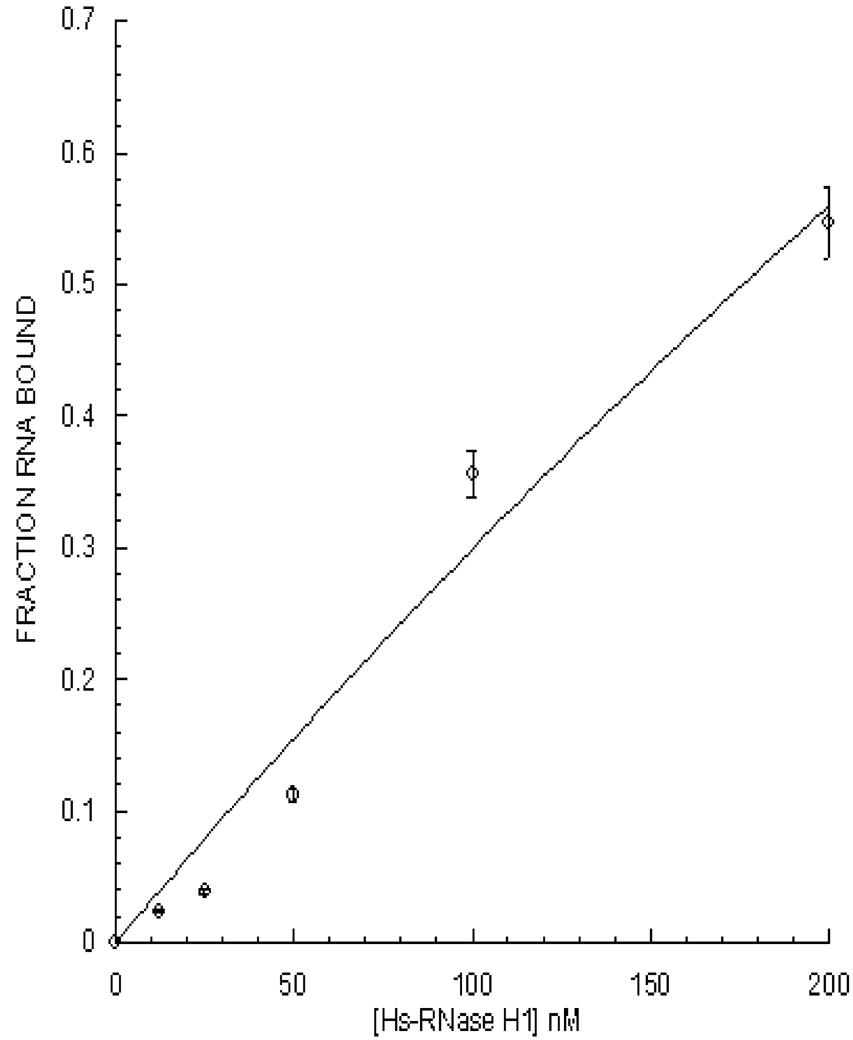

0.7
0.6
0.5
0.4
0.3
0.2
0.1
0
FRACTION RNA BOUND
0
50
100
150
200
[Hs-RNase H1] nM

E

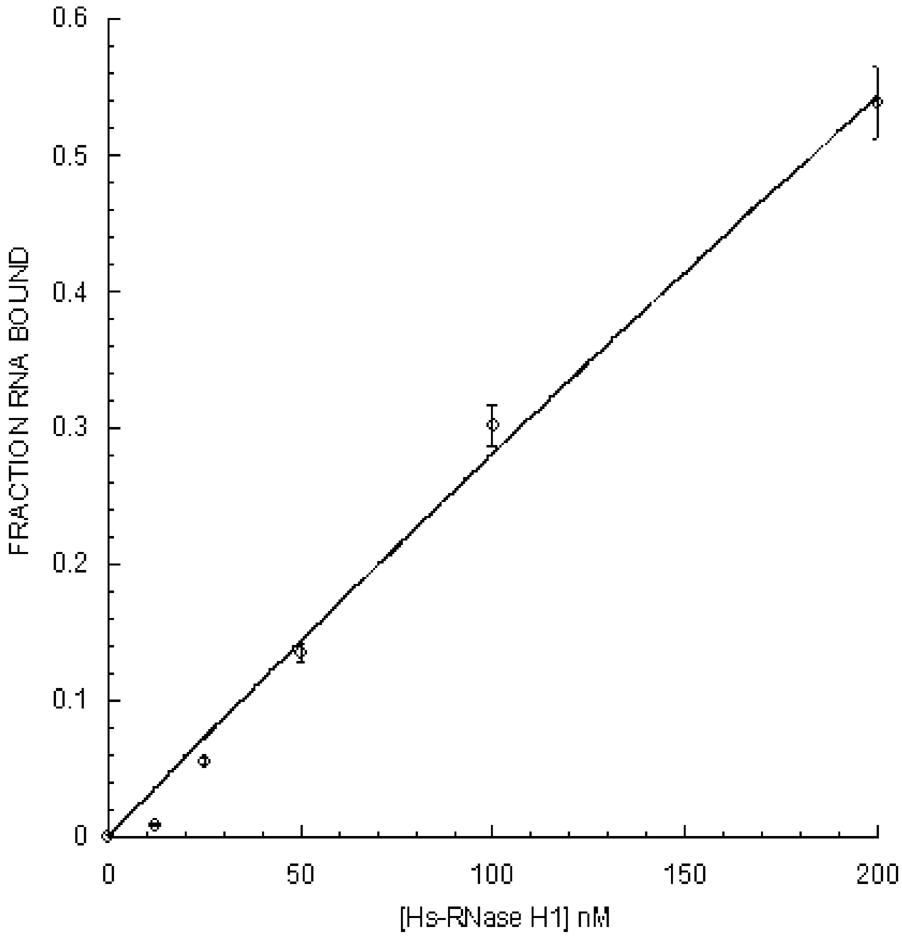

0.6
0.5
0.4
0.3
0.2
0.1
0
FRACTION RNA BOUND
0
50
100
150
200
[Hs-RNase H1] nM

Figure 21. Gel electrophoretic mobility shift analysis of Hs-RNase H1 binding to P(S) 2'-FANA substituted hybrids. A, DNA·RNA, B, 3-altimer·RNA C, 7-Gapmer·RNA, D, All-2'-FANA·RNA and E, 9,10 Linker·RNA P(S). Binding reactions were analyzed by electrophoresis in an 8% non-denaturing polycrylamide gel as described in Materials and Methods. Each experiment has the protein concentrations indicated in nM. The bound hybrid is indicated with arrows.

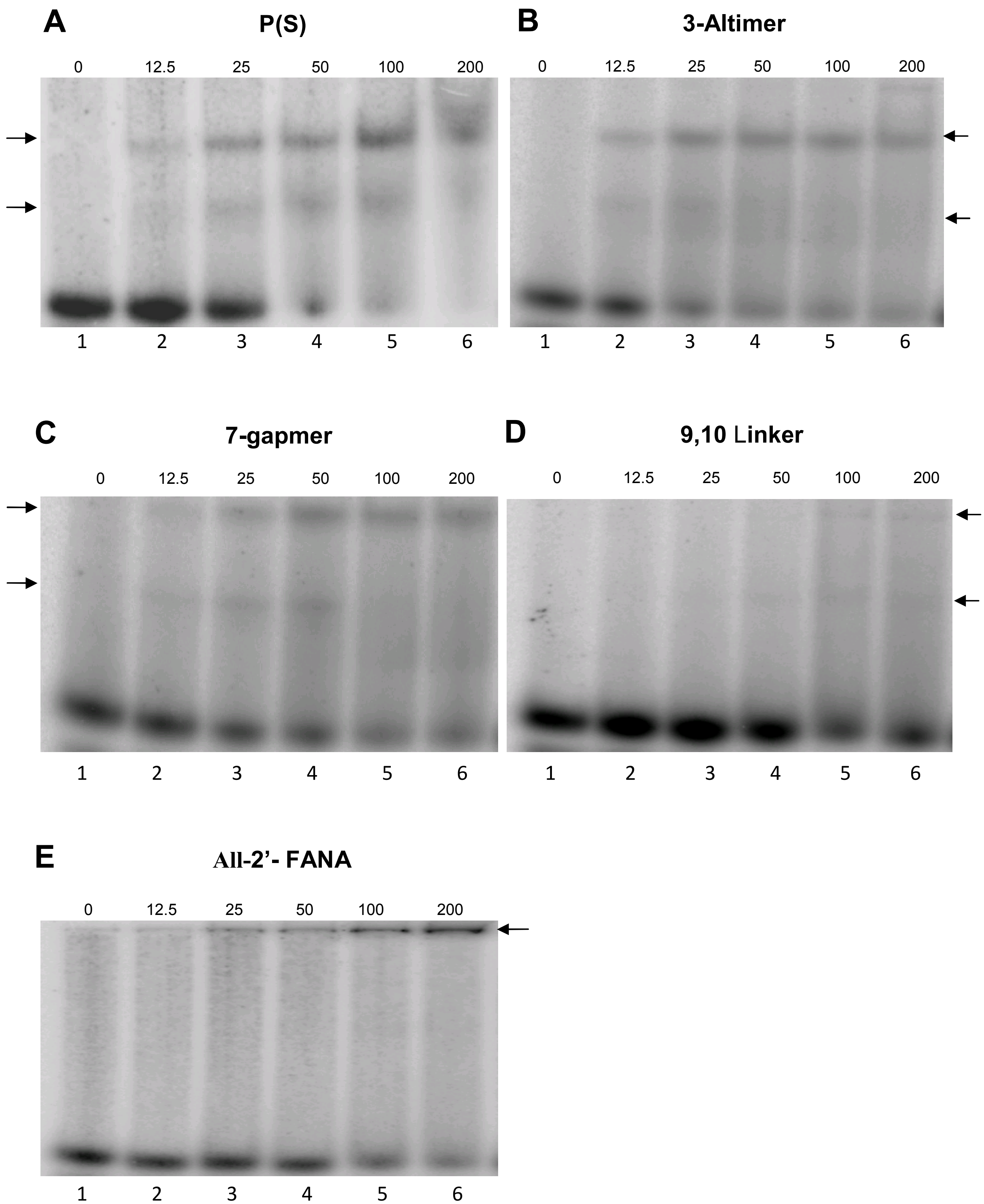
A
P(S)
0
12.5
25
50
100
200
1
2
3
4
5
6
B
3-Altimer
0
12.5
25
50
100
200
1
2
3
4
5
6
C
7-gapmer
0
12.5
25
50
100
200
1
2
3
4
5
6
D
9,10 Linker
0
12.5
25
50
100
200
1
2
3
4
5
6
E
All-2'- FANA
0
12.5
25
50
100
200
1
2
3
4
5
6

Figure 22. qRT-PCR and western blot analysis of c-MYB expression following antisense oligonucleotide transfection of K562 leukemia cells.

A. qRT-PCR assay performed on total RNA isolated from K562 cells transfected with 5 µg of different 2'-FANA or DNA AONs [P(S)]. Data are presented as a function of c-myb RNA copies, normalized to GAPDH RNA. Mock (control) cells were subjected to nucleoporation in the absence of an AON. qRT-PCR was performed 24 hours post nucleofection.

(B) c-Myb protein western analysis performed after 24 hours, using cell lysate obtained from K562 cells transfected with 2'-FANA and PS-DNA molecules.

(C) c-Myb western analysis performed after 48 hours on cell lysates obtained from K562 cells transfected with 2'-FANA and P(S)-DNA molecules.

Note: The experiments were performed by Anna Kalota from the Gewirtz lab.

A

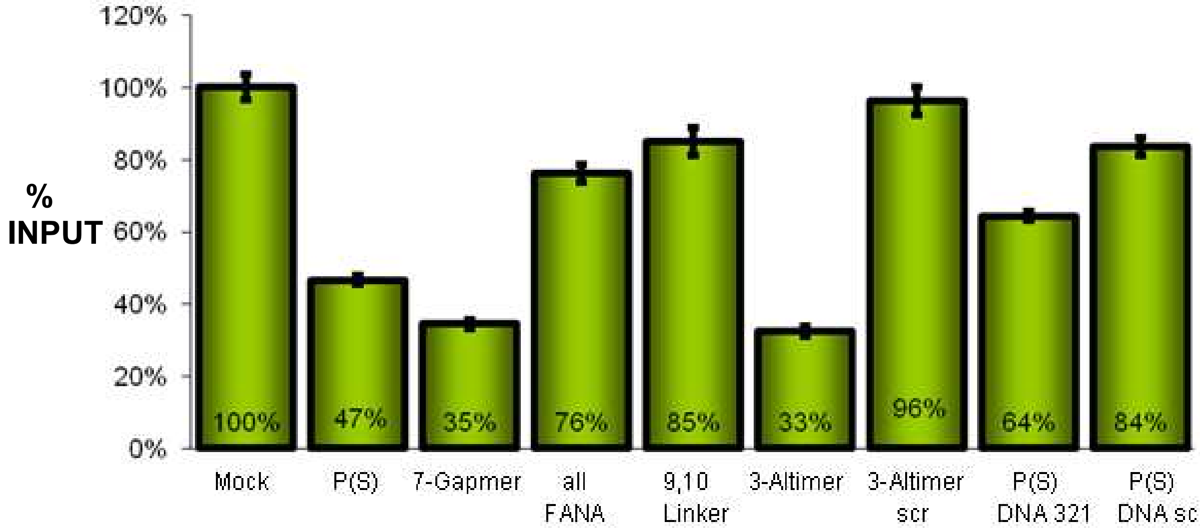
%
INPUT
120%
100%
80%
60%
40%
20%
0%
100%
47%
35%
76%
85%
33%
96%
64%
84%
Mock
P(S)
7-Gapmer
all FANA
9,10 Linker
3-Altimer
3-Altimer scr
P(S) DNA 321
P(S) DNA scr

B

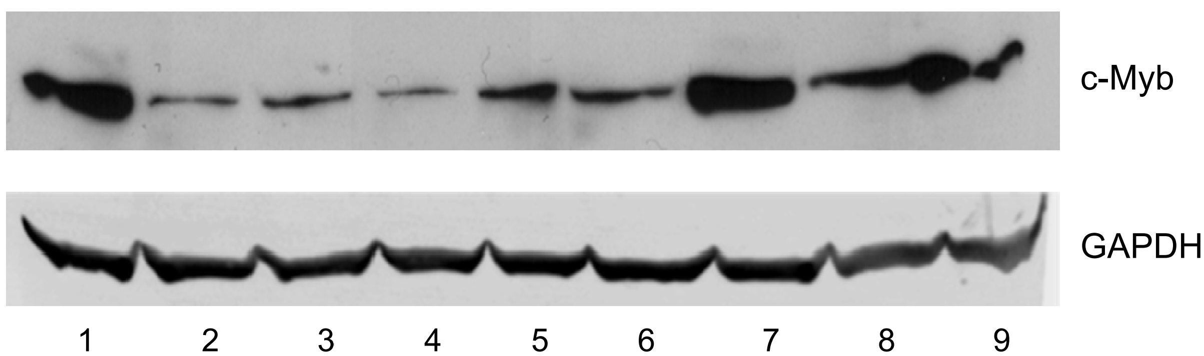
c-Myb
GAPDH
1
2
3
4
5
6
7
8
9

C

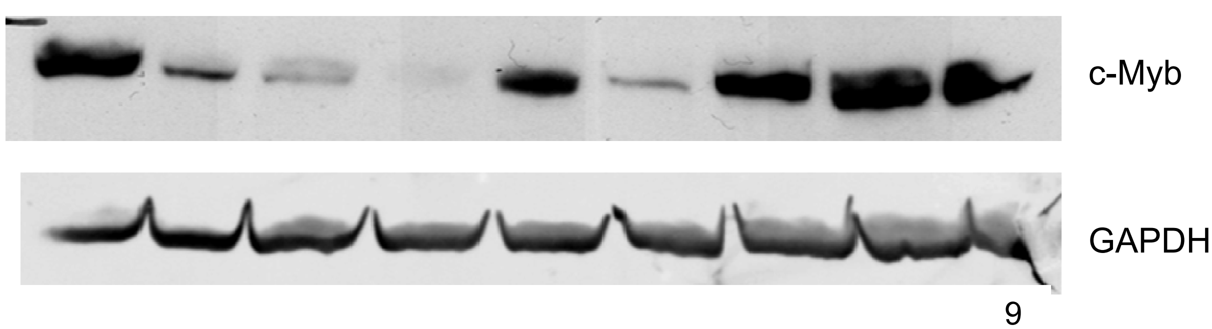
c-Myb
GAPDH
9

References Cited

Agarwal *et al.,* (1997) Mixed-backbone oligonucleotides as second generation antisense oligonucleotides: *in vitro* and *in vivo* studies. *Proc. Natl. Acad. Sci.* USA, 94: 2620-2625

Arudchandran *et al*., (2002). Multiple ribonuclease H-encoding genes in the *Caenorhabditis elegans* genome contrasts with the two typical ribonuclease H-encoding genes in the human genome. *Mol. Biol. Evol*, 19:1910–1919.

Arunachandran *et al*., (2000). The absence of Ribonuclease HI or H2 alters sensitivity of *S. cerevisiae* to hydroxyl urea caffeine: implications for roles of RNase H in DNA replication and repair. *Genes Cells.*5: 789-802.

Berger *et al*., (1998) Crystal structures of B-DNA with incorporated 2'-deoxy-2'fluoro-arabino-furanosyl thymines: implications of conformational preorganization for duplex stability. *Nucleic Acids Res*., 26: 2473-2480.

Cerritelli *et al.,* (2003) Failure to produce mitochondrial DNA results in embryonic lethality in RNase H1 null mice. *Mol. Cell* 11: 807-815.

Cerritelli *et al*., (2009) Ribonucleases H: the enzymes in eukaryotes*. FEBS J.* 27: 1494-1505.

Champoux *et al*., (1993) Roles of ribonuclease H in reverse transcription. In *Reverse Transcriptase*, Cold Spring Harbor Laboratory Press, Plainview, NY. pp. 103-118.

Chapados *et al.,* (2001) Structural biochemistry of a type 2 RNase H: RNA primer recognition and removal during DNA replication. *J. Mol. Biol*: 307, 541-556.

Chon *et al*., contributions of the two accessory subunits. RNASEH2B and RNASEH2C, to the activity and properties of the RNase H2 complex. *Nucleic Acids Res* 37: 96-110.

Clappier *et al*., (2007). The c-Myb locus is involved in chromosomal translocation and genomic duplications in human T-cell acute leukemia (T-ALL), the translocation defining a new T-ALL subtype in very young children*. Blood* 110: 1251-1261.

Crouch *et al.,* (2001). RNase H 1 of *Saccharomyces cerevisiae*: methods and nomenclature. *Methods Enzymol* 341: 395-413.

Crow *et al.,* (2006) Mutations in genes encoding ribonuclease H2 subunits cause Aicardi-Goutieres syndrome and mimic congenital viral brain infection. *Nat. Genetics* 38: 910-916.

Damha *et al*., (1998) Hybrids of RNA and arabinonucleic acids (ANA and 2'F-ANA) are substrates of ribonuclease H. *J. Am. Chem. Soc.* 120: 12976-12977..

Damha *et al*., (2001) Properties of arabinonucleic acids (ANA & 2'F-ANA): Implications for the design of antisense therapeutics that invoke RNase H cleavage of RNA. *Nucleosides Nucleotides Nucleic Acids*, 20: 429-440.

Dean *et al*., (2003) Antisense oligonucleotide-based therapeutics for cancer. *Oncogene* 22: 9087-9096.

Denisov *et al*., (2001) Solution structure of an arabinonucleic acid (ANA/RNA) and DNA/RNA hybrids. *Nucleic Acids Res*., 29: 4284-4293.

Eder *et al*., (1993). Substrate specificity of human RNase H1 and its role in excision repair of ribose residues misincorporated in DNA *Biochemie.* 75: 123-126.

Fedoroff *et al*., (1993) Structure of a DNA:RNA hybrid duplex. Why RNase H does not cleave pure RNA. *J. Mol. Biol*., 233, 509-523.

Frank *et al* (1994) Purification and characterization of human RNase HII. *Nucleic Acids Res*, 22: 5247-5254.

Gaidamakov *et al.,* (2005) Eukaryotic RNases H1 act processively by interactions through the duplex RNA-binding domain. *Nucleic Acids Res.* 33: 2166–2175.

Gao *et al*., (1992). Phosphorothioate oligonucleotides are inhibitors of Human DNA polymerases and RNase H: Implications for antisense technology. *Mol Pharmacol*, 41: 223-229

Gifford *et al*., (2005) Identification of antisense nucleic acid nucleic acid hybridization sites in mRNA molecules with self quenching fluorescent reporter molecules. *Nucleic Acids Res,* 33: e28.

Haruki *et al.,* (2002) Cleavage of DNA-RNA-DNA/DNA chimeric substrate containing single ribonucleotide at the DNA-RNA junction with prokaryotic RNases HII. *FEBS Lett,* 531:204-208.

Ikeda *et al*., (1998) The effect of two antipodal fluorine-induced sugar puckers on the conformation and stability of the Dickerson-Drew dodecamer duplex $[d(CGCGAATTCGCG)]_2$. *Nucleic Acids Res*. 26: 2337-2244.

Itaya *et al*., (1990) Isolation and characterization of a second RNase H (RNase HII) of *Escherichia coli* K-12 encoded by the rnhB gene. *Proc. Natl. Acad. Sci.* USA 87: 8587-8589.

Jongruja *et al*., (2010) The N-terminal hybrid binding domain of RNase HI from *Thermatoga maritima* is important for substrate binding and Mg^{2+}-dependent activity. *FEBS J, 277*: 4474-4489.

Kalota *et al*., (2006) 2'-Deoxy-2'fluoro-β-D-arabinonucleic acid (2'F-ANA) modified oligonucleotides (ON) effect highly efficient, and persistent, gene silencing. *Nucleic Acids Res*. 34: 451-461.

Kanaya *et al*., (1984) The rnh gene is essential for the growth of *Escherichia coli*. *Proc. Natl. Acad. Sci.* USA 81:3447-3451.

Kanaya *et al*., (1991) Importance of positive charge cluster in *Escherichia coli* ribonuclease H1 for the effective binding of the substrate. *J. Biol. Chem*. 266: 11621-11627.

Kanayagi K. *et al*., (1990). Three dimensional structure of ribonuclease H from *E.coli*. *Nature* 347: 306-309.

Keck *et al*., (1998) Activation/attenuation model for RNase H. A one metal mechanism with second metal inhibition. *J. Biol. Chem*. 273: 34128-34133.

Kochiwa *et al*., (2006) Stage-specific expression of *Caenorhabditis elegans* ribonuclease H1 enzymes with different substrate specificities and bivalent cation requirements. *FEBS J.* 273: 420–429.

Kogma *et al*., (1998) Physiological functions of *E. coli* RNase HI INSERM, Paris.

Lima *et al*. (2004). Structural requirements at the catalytic site of the heteroduplex substrate for human RNase H1 catalysis. *J. Biol. Chem.* 279: 36317-36326.

Lima *et al*., (2007). Human RNase H discriminates between subtle variations in the structure of the heteroduplex substrate. *Mol. Pharmacol.* 71: 83-91

Lima *et al*., (2007). The positional influence of the helical geometry of the heteroduplex substrate on human RNase H1 catalysis*. Mol. Pharmacol* . 71: 73-82.

Lin *et al*., (2010) R loops stimulate genetic instability of CTG.CTG repeats. *Pro.c Natl. Acad. Sci.* USA 107: 692-697.

Lok *et al.,* (2000). Synthesis and biophysical properties of arabinonucleic acids (ANA): circular dichroic spectra, melting temperatures and ribonuclease H susceptibility of ANA:RNA hybrid duplexes. *Biochemistry* 39: 7050-7062.

Lok *et al*., (2002) Potent gene-specific inhibitory properties of mixed-backbone antisense oligonucleotides comprised of 2'-deoxy-2'-fluoro-β-D-arabinose and 2'-deoxyribose nucleotides. *Biochemistry*. 41: 3457-3467.

Luger *et al*., (2002) Oligonucleotide-mediated inhibition of c-myb gene expression in autografted bone marrow: a pilot study. *Blood* 99: 1150-1158.

Mangos *et al*., (2003) Efficient RNase H-directed cleavage of RNA promoted by antisense DNA or 2'F-ANA constructs containing acyclic nucleotide inserts. *J. Am. Chem. Soc*., 125: 654-661.

Marayam et al., (2011) Energetically important C-H···F-C pseudohydrogen bonding in water: evidence and application to rational design of oligonucleotides with high binding affinity. *J. Am.. Chem. Soc*. 133(4): 728-31

Min *et al*., (2002) Oligonucleotides comprised of alternating 2'-deoxy-2'-fluoro-β-D-arabinonucleosides and D-2'-deoxyribonucleosides (2'F-ANA/DNA 'altimers') induce efficient RNA cleavage mediated by RNase H. *Bioorg. Med. Chem*. Lett. 12: 2651-2654.

Monia *et al*., (1993) Evaluation of 2'-Modified oligonucleotides containing 2'-deoxy gaps as antisense inhibitors of gene expression. *J. Biol. Chem*. 268: 14514-14522.

Noronha *et al*., (2000) Synthesis and biophysical properties of arabinonucleic acids (ANA): circular dichroic spectra, melting temperatures, and ribonuclease H susceptibility of ANA.RNA hybrid duplexes. *Biochemistry*, 39: 7050-7062.

Nowotny *et al.,* (2005) Crystal structure of RNase H bound to an RNA/DNA hybrid: substrate specificity and metal dependent catalysis. *Cell.* 121: 1005-1016.

Nowotny *et al*., (2006). Stepwise analysis of metal ions in RNase H catalysis: from substrate destabilization to product release. *EMBO J.* 25: 1924-1933.

Nowotny *et al*., (2007) Structure of human RNase H1 complexed with an RNA/DNA hybrid: Insight into HIV reverse transcription. *Mol. Cell.* 28: 264-276.

Nowotny *et al.,* (2008) Specific recognition of RNA/DNA hybrid and enhancement of human RNase H1 activity by HBD. *EMBO J.* 27: 1172–1181.

Ohtani *et al*., (1999) Molecular diversities of RNase H. *J. Biosci. Bioeng.* 88: 12-19.

Ohtani *et al.,* (1999) Identification of the genes encoding Mn^{2+}-dependent RNase HII and Mg^{2+}-dependent RNase HIII from *Bacillus subtilis*. Classification of RNase H into three families. *Biochemistry* 38: 605-618.

Opalinska *et al*., 2002 Nucleic acid therapeutics: basic principles and recent applications. *Nature Rev. Drug Discov*. 1: 503-514.

Opalinska *et al*., (2004) oxetane modified, conformationally constrained, antisense oligodeoxyribonucleotides function efficiently as gene silencing molecules. *Nucleic Acids Res*. 32: 5791-5799.

Persson *et al*., (2009). Recurrent fusion of MYB and NFIB transcription factor genes in carcinomas of the breast and head and neck. *Proc. Natl. Acad. Sci.* 106: 18740-18744.

Pileur *et al*., (2000) Eukaryotic RNase HI and RNase HII generate characteristic hydrolytic patterns on DNA-RNA hybrids: further evidence that mitochondrial RNaseH is an RNase HII. *Nucleic acids Res.* 28: 3674-3683.

Qui *et al*., (1999) *Saccharomyces cerevisiae* RNase H (35) functions in RNA primer removal during lagging-strand DNA synthesis, most efficiently in cooperation with Rad27 nuclease. *Mol. Cell. Biol.* 19: 8361-8371.

Rosta *et al*., (2011). Catalytic mechanism of RNA backbone cleavage by Ribonuclease H from quantum mechanics/molecular mechanics simulations. *J. Am. Chem. Soc*. 133: 8934-8941.

Salazar *et al*., (1993) The DNA strand in DNA•RNA hybrid duplexes is neither B-form nor A-form in solution. *Biochemistry*. 32: 4207-4215.

Shultz *et al*., (2007) Genome-wide analysis of the core DNA replication machinery in the higher plants Arabidopsis and rice. *Plant Physiol.* 144: 1697-1714.

Stein *et al*., (1969) Enzyme from calf thymus degrading the RNA moiety of the DNA-RNA hybrids: effect on DNA dependant RNA polymerase. *Science.* 166: 393-395.

Todokoro *et al*., (2007) identification of the gene encoding a type 1 RNase H with and N-terminal double-stranded RNA binding domain from a psychrophillic bacterium. *FEBS* J. 274: 3715-3727.

Todokoro *et al*., (2009) Ribonuclease H: Molecular diversities, substrate binding domains, and catalytic mechanism of prokaryotic enzymes. *FEBS J.* 276: 2837-2853.

Tramontano *et al*., (2010) HIV-1 RT-associated RNase H function inhibitors: recent advances in drug development. *Curr. Med. Chem*. 17: 2837-2857.

Trempe *et al*., (2001) NMR solution structure of an olignucleotide hairpin with a 2'F-ANA/RNA stem: Implications for RNase H specificity toward DNA/RNA hybrid duplexes. *J. Am. Chem. Soc*. 123: 4896-4903.

Yang *et al*. (1990). Structure of ribonuclease H phased at 2Å resolution by MAD analysis of the selenomethionyl protein. *Science.* 249: 1398-1405.

Wagner, R. W. (1994) Gene inhibition using antisense oligodeoxynucleotides, *Nature*. 372: 333.

Walder *et al*., (1988) Role of RNase H in hybrid-arrested translation by antisense oligonucleotides. *Proc. Natl. Acad. Sci*. *USA*. 85: 5011.

Wang *et al*. (1998) A comparison of guanosine-quartet inhibitory effects versus cytidine homopolymer inhibitory effects on rat neointimal formation. *Antisense Nucleic Acid Drug Dev.* 8: 227–236.

Wang *et al*., (2000) Cyclohexene nucleic acids (CeNA): Serum stable oligonucleotides that activate RNase H and increase duplex stability with complementary RNA. *J. Am. Chem. Soc*. 122: 8595-8602.

Wilds and Damha (2002) 2'-deoxy-2'-fluoro-β-D-arabinonucleosides and oligonucleotides (2'F-ANA): synthesis and physiochemical studies. *Nucleic Acids Res*. 28: 3625-3635.

Wu *et al*. (2001) Investigating the structure of human RNase H1 by site-directed mutagenesis. *J. Biol. Chem.* 276: 23547-23553.